U.S. Department
of Transportation

**Federal Railroad
Administration**

Correlation of Concrete Tie Track Performance in Revenue Service and at the Facility for Accelerated Service Testing

Office of Research and
Development
Washington, DC 20590

Volume II   Predictions And Evaluations of Track Settlement

1. Report No.	2. Government Accession No.	3. Recipient's Catalog No.
FRA/ORD-82/44.2		

4. Title and Subtitle	5. Report Date
Correlation of Concrete Tie Track Performance in Revenue Service and at the Facility for Accelerated Service Testing – Volume II	August 1984
	6. Performing Organization Code
	8. Performing Organization Report No.

7. Author's)
Harry E. Stewart and Ernest T. Selig

9. Performing Organization Name and Address	10. Work Unit No. (TRAIS)
Department of Civil Engineering University of Massachusetts Amherst, Massachusetts 01003	
	11. Contract or Grant No.
	R-4146(7187)-090
	13. Type of Report and Period Covered

12. Sponsoring Agency Name and Address	
U.S. Department of Transportation Federal Railroad Administration Washington, D.C. 20590	Final Report
	14. Sponsoring Agency Code
	RRD-10

16. Abstract   Predictions and evaluations of settlement were made for revenue and the Facility for Accelerated Service Testing (FAST) track, both containing concrete and wood tie sections. The ballast physical states were investigated by field tests done before and after track maintenance. Borings were also taken to identify the subgrade conditions. The stress-dependent elastic and inelastic ballast behaviors were derived from repeated load triaxial tests and a ballast box device. Triaxial tests were also performed on the subgrade soils.

A computer model, GEOTRACK, was used to estimate the stresses and deformations in the track foundations. In addition, revenue site track modulus values predicted with GEOTRACK were compared to measured values. Predictions of track settlement were then made based upon the laboratory test results and stresses estimated using the computer model. The predicted values were compared to field measurements obtained using ballast instrumentation and surveying from benchmarks. The predicted settlements were of the same order as the measured values, however, some differences in trends were observed. A discussion of the factors that were not included in the methodology is presented, along with the implications of these factors on track performance.

17. Key Words Ballast, computer model, cyclic properties, elastic deformation, FAST, permanent deformation, subgrade, track structures, track performance, track loading, concrete ties.	18. Distribution Statement This document is available to the public through the National Technical Information Service, Springfield, VA. 22161.

19. Security Classif. (of this report)	20. Security Classif. (of this page)	21. No. of Pages	22. Price
Unclassified	Unclassified		

Form DOT F 1700.7 (8-72)   Reproduction of completed page authorized

PREFACE

TABLE OF CONTENTS

TABLE OF CONTENTS (completed)

LIST OF TABLES

LIST OF FIGURES

LIST OF FIGURES

CHAPTER 1. EXECUTIVE SUMMARY

The objective of this part of the FAST/revenue service correlation study was the development and application of the methodology for prediction of the geotechnical aspects of track performance. Track performance is defined in terms of vertical track settlement. The following field sites were evaluated: 1) in-service revenue track having concrete crossties at Streator (Leeds), Illinois, Richmond (Lorraine), Virginia, and Aberdeen, Maryland, 2) a revenue wood tie track section at Streator (Leeds), Illinois, and 3) wood and concrete tie sections at the Department of Transportation Facility for Accelerated Service Testing (FAST) test track in Pueblo, Colorado. The Streator site is owned by the Atchison, Topeka and Santa Fe Railroad. The Richmond section is owned by the Chessie System. The Aberdeen test section is owned by Amtrak.

A variety of field tests were conducted at these sites to assess the physical states of the ballast materials as they existed prior to a track maintenance (raising and tamping) operation. The ballast physical states were identified using the plate load test, ballast density test, and lateral tie push test. These physical state tests were repeated after the surfacing operation to determine the changes in the ballast physical properties caused by the maintenance. One of the primary effects of track maintenance was a loosening and disturbance of the traffic-compacted and stabilized ballast layer, both in the cribs and under the ties. The physical states of the ballast found immediately after the maintenance were approximately independent of ballast type and initial condition.

Ballast materials were recovered from the sites and subjected to repeated load triaxial testing to investigate the elastic and inelastic behavior. A granite ballast from FAST was also tested in a variety of repeated load conditions, including a mix of load levels.

The elastic behavior was defined in terms of the resilient modulus. The resilient moduli values from extension tests were smaller than the moduli values from compression tests under similar stress conditions. When the vertical stresses were cycled between extension and compression states, the total resilient moduli fell between the individual extension and compressive values. The resilient behavior of the field site ballasts was not significantly dependent upon ballast type.

The inelastic behavior of the ballast was found to be dependent upon the first cycle strain, ε_1, and a material constant, C. This constant was independent of stress conditions for a particular ballast, but was not the same for all ballasts. The total permanent or inelastic strain developed in a ballast sample with a mix of loads was controlled by the maximum past load and was independent of the loading sequence. Subsequent applications of reduced load as well as partial unloadings resulted in negligible increases in permanent strain. This means that the largest dynamic wheel loads cause most of the track settlement. A strain superposition method was developed to account for the deformations that result from repeated applications of the mixed loading conditions present at the field sites.

The inelastic behavior of ballast was also investigated using a box-type testing device, intended to simulate field behavior. The trends in ballast deformation from these box tests were similar to those observed from the triaxial tests. The box tests also showed that relatively large horizontal

9

residual stresses can develop in the ballast, both in the crib and under the ties, as a result of cyclic loadings.

Measurements of vertical track modulus at the revenue sites did not indicate that significant changes in the magnitude of track modulus occurred due to the maintenance. The major factors contributing to the magnitude of track modulus were ballast depth and subgrade stiffness. Also, the field measurements of track modulus showed that the uniformity of track support was not improved as a result of the surfacings.

Among the important differences between the sites was the train loading imposed on the track systems. The dynamic wheel loads at each site were measured by BCL to characterize the mixed loading conditions. The static wheel load distributions for each site were obtained from consist data. Although the average static and dynamic wheel loads were about equal for a particular site, the static wheel load distributions for the revenue sites were quite different from the dynamic distributions. One out of one thousand (0.1 percent exceedance level) dynamic wheel loads at Aberdeen was measured at 75 kips. At the 0.1 percent exceedance level at Leeds, Lorraine, and FAST, the dynamic wheel loads were about 46 kips. These very high dynamic loads at Aberdeen were a result of a combined effect of wheel tread irregularities and the high speeds of passenger trains. The loading environment at FAST was much more uniform than at the revenue sites, because of the controlled nature of the FAST experiments. The average static and dynamic wheel loads at FAST, however, were about 1.5 to 2 times larger than the average values measured at the revenue sites.

Survey measurements were made at each of the field sites by BCL to determine cumulative vertical track settlements. The survey data from Aberdeen and FAST were supplemented by inductance coil strain gauges embedded in the ballast layer. The strain gauge instrumentation of the ballast layers lead to the conclusion that the zone of ballast disturbed by the maintenance operation was the primary source of track settlement, and that over the relatively short experimental time period, the subgrade contributions to track deformation could be neglected for these sites.

The settlements at the Lorraine and Aberdeen sites continued to develop at what appeared to be a steady rate throughout the period of the measurements, after the initial traffic following maintenance. Although the total vertical settlements at all of the revenue sites continued to increase as tonnage accumulated, the roughness of the track profiles did not increase.

The ballast deformations at FAST were found to be similar for both wood and concrete tie sections. This was true for the ballast measurements obtained during the initial FAST experiments and for the ballast deformations following the 1979 rebuild.

A three-dimensional, nonlinear, elastic, multilayer model, GEOTRACK, was used to predict track deflections and track moduli for the revenue sites. The model predictions of vertical track deflection agreed well with field measurements, although the model tended to underestimate the field values.

The methodology to predict the inelastic or permanent settlement of the field track sections used GEOTRACK nonlinear stress analyses of the field site track sections with stress-dependent ballast properties, representative subgrade moduli, and multiple-axle combinations of the measured dynamic wheel loads. The predicted stresses from the computer analyses for each particular field site and loading condition were used, along with the permanent deformation behavior of the ballasts from laboratory tests to estimate the resulting ballast strains.

The general magnitudes of the predicted deformations agreed with the measured values. The shapes of the deformation versus million gross tons predicted results did not agree as well. The predicted rate of deformation accumulation for the revenue sites was less than the survey measurements indicated, particularly for the Aberdeen and Lorraine sites. The settlement predictions made for FAST Section 22 agreed best with the field measurements. This was probably a result of the more controlled track loading and test conditions present at FAST.

Uncertainties in both the first cycle strains and the representative stress paths could account for some of the differences between measured and predicted settlements. Deviations between measured and predicted track settlements could have resulted from other factors not considered in the methodology. One of the most important factors not included is thought to be settlement induced by vibrations transmitted through the track superstructure to the ballast. Other factors that can have varying degrees of influence on track settlement and performance include ballast degradation, environmental effects and subgrade responses. Although these last three factors did not appear significant for the monitoring periods at the field sites investigated during this study, they could be significant at other sites.

CHAPTER 2. INTRODUCTION

In order to improve current track design methods and quantify track main-
tenance life, research is necessary to understand the behavior of the track
foundation under dynamic traffic loading. The repetitive loading and unload-
ing of track structures due to the passage of train traffic causes settlement
in the supporting ballast and subgrade. As the traffic history accumulates,
these deformations continue to increase until the track has deteriorated to a
state at which it can no longer perform at a desired service level. At this
point, the track is surfaced (raised and tamped) to reestablish the necessary
profile, and the deformation process starts again.

The forcus of this report is on the prediction of track performance at
four field sites. Track performance is assessed in terms of vertical track
settlement and the factors that contribute to settlement. The sites consist
of concrete tie revenue service track at Leeds, near Streator, Illinois; Lor-
raine, near Richmond, Virginia; a site south of Aberdeen, Maryland; and wood
tie track at Leeds. Wood and concrete tie track at FAST is included for com-
parison.

Differences in track structural characteristics and track foundation
among the sites were identified. A variety of field tests were conducted to
assess the physical states of the ballast materials as they existed prior to
track maintenance. These physical state tests were repeated after a surfac-
ing operation to determine the changes in the ballast properties that occur-
red due to track maintenance. To complete the site characterization, stan-
dard penetration and Dutch cone penetration tests were used to investigate
the subgrade support characteristics of the revenue sites. These tests were
done using a drill rig specially equipped with rail wheels so that the borings
could be taken directly under the track structure. The results of these sub-
surface explorations were used to help identify variations in strength and
composition of the foundation layers over the depths influenced by train load-
ings. Moisture changes in the top of subgrade were also monitored and corre-
lated with weather conditions. A summary evaluation of these test results
has been given in a companion Volume I [1]* to this report. The results of
these tests will be explained further where necessary to support conclusions
made within this report.

Among the important differences between the revenue sites are the train
loadings imposed on the track systems. To determine these, the dynamic wheel
load distributions were measured by the prime contractor, Battelle-Columbus
Laboratories (BCL), for representative traffic at each of the sites. Since
each site was subjected to a significant range of wheel loads rather than
constant repetition of the same magnitude loading, a method was developed
that can be used to account for the real mix of wheel loads.

The ballast and subgrade soils from each of the field sites were tested
to determine both the resilient and inelastic behavior of these materials
under representative loading conditions. Both cyclic and repeated load tri-
axial tests were used to determine the resilient modulus of the ballast ma-
terial under full unloading, partial unloading, and shear stress reversal
conditions. Undisturbed subgrade samples were also subjected to repeated
load tests under anticipated field stress conditions to determine the

---

*Numbers in brackets [ ] denote references.

resilient modulus. The final estimates of the elastic properties of the track substructure were based on the results of the physical state, triaxial, standard penetration and cone penetration tests.

The development of an analytical model that incorporates the fundamental track structural components and foundation characteristics is a necessary tool for assessing track performance. The model used in this study, GEOTRACK, is a three-dimensional, nonlinear, elastic, multi-layer track analysis program that emphasizes the geotechnical aspects of track. The GEOTRACK model is conceptually similar to the MULTA model developed by BCL, as explained in Ref. [40].

Measurements of vertical track modulus were taken before and after maintenance at the field sites by BCL during the initial site visits. The track structural and foundation properties determined for the field sites were used with the GEOTRACK model to predict values of track modulus. The comparisons between measured and predicted elastic track moduli served as an additional validation of the model's elastic capabilities.

The prediction of the vertical track settlement at each of the field sites was based upon inelastic behavior of the foundation soils, as measured in the laboratory under representative loading conditions. The inelastic behavior of the foundation soils has been investigated using repeated load triaxial tests and a ballast box device developed for this program for simulating field conditions. A method was developed that can be used to account for the deformations that occur from repeated applications of the mixed loading conditions present at the field sites. Predicted values of track settlement were then compared with the track settlements measured at the field sites. These field measurements were obtained using inductance coils that measure ballast strain and optical surveying from benchmarks.

The report will conclude with a discussion of the various factors that have not been accounted for in the deformation prediction model, and the implications of these factors on track performance.

CHAPTER 3.   SITE DESCRIPTIONS

3.1   General Background

Four revenue service track locations and the experimental FAST track in Pueblo, Colorado were selected as test areas for this research project. The revenue service sites included three locations that contained concrete cross ties and a control section having wood cross ties. The wood tie control section and one concrete tie section are located at Leeds near Streator, Illinois, in the north-central section of the state. The remaining two concrete tie test sections are located at Aberdeen, Maryland and Lorraine near Richmond, Virginia. A more detailed description of each of these four sites was given in Refs. [1,2,3,4,5]. The FAST track contained both wood and concrete tie test sections.

The FAST track sections 17, 18 and 19 were instrumented in 1976, when the track was originally constructed, in order to monitor track foundation deformations and stresses. The track conditions for these sections are given in Table 1a. The measurements made in these track sections are used in portions of the correlation study.

Part of the FAST track was reconstructed after 400 million gross tons (MGT) traffic had accumulated over the original track at the site. The general rebuild procedure for these test sections consisted of:

a) Undercutting the existing track.
b) Removal of the existing track structure.
c) Subgrade preparation, including grading and compaction where necessary.
d) Building new skeletonized track on the subgrade.
e) Dumping and tamping ballast and raising the track.
f) Regulating the ballast, followed by surfacing and lining operations.

Further details regarding the rebuild procedures can be found in Ref. [6].

Data for certain ballast physical state tests were available from the rebuilt sections 3 and 22. The track conditions for these sections are given in Table 1b. The concrete ties used in section 22 were the RT7-SS2 type.

3.2   Track Structure·

The track structure for railroads has several mechanical components, the most obvious of which are the cross ties and rails. Rails are generally fastened to the wood ties using the conventional tie plate and cut spike system. Rails are attached to the concrete ties using a spring-type clip fastener system. Tie pads support the rail on concrete ties, and electrical insulators separate the steel rail from the steel rail clips. Table 2 lists the main track structural parameters for FAST and the revenue service test sections. Some of the structural characteristics which differ among the test sections are: a) tie type and dimensions, b) tie spacing, c) tie weight, d) rail section, e) rail fastener, and f) pad type.

3.3   Ballast Materials and Physical States

A description of the ballast materials, along with the results of the

14

Table 1. FAST Track Section Conditions

a) Original Track

Track Section	Track Geometry	Ballast Type	Ballast Depth (in.)	Tie Type	Tie Spacing (in.)
17C	Curved	Granite	15	Concrete	24.0
17E	Tangent	Granite	15	Concrete	24.0
18A	Tangent	Granite	21	Wood	19.5
18B	Tangent	Granite	15	Wood	19.5
20B	Tangent	Limestone	15	Wood	19.5
20G	Tangent	Traprock	15	Wood	19.5

b) Reconstructed Track

Track Section	Track Geometry	Ballast Type	Ballast Depth (in.)	Tie Type	Tie Spacing (in.)
3	Curved	Granite*	20	Wood	19.5
17ABCDE	Curved	Granite	16	Concrete	24.0
22A	Tangent	Traprock	15	Wood	19.5
22B	Tangent	Traprock	15	Concrete	24.0

*Several types of granite were used.

Table 2. Track Structural Properties for All Sites

Parameter	FAST		Leeds		Aberdeen	Lorraine
	Wood	Concrete	Wood	Concrete		
Tie Type	Hardwood	RT7-SS2	Hardwood	CC244C	RT7-SS2	CC244
Tie Spacing (in.)	19.5	24.0	19.5	24.0	24.0	25.0
Tie Length (in.)	102	102	102	102	102	102
Tie Bottom Width (in.)	9.00	10.75	9.00	10.75	10.75	10.75
Tie Weight (lb)	$\approx$250	$\approx$825	$\approx$250	$\approx$750	$\approx$825	$\approx$750
Tie Bending Stiffness, EI(lb-in^2 x 10^6)	386	2360	386	2360	2360	2360
Rail Section	136RE	136RE	136RE	136RE	140RE	122RE
Rail Weight (lb/yard)	136.2	136.2	136.2	136.2	140.6	122.1
Rail Bending Stiffness, EI(lb-in^2 x 10^6)	2742.6	2742.6	2742.6	2742.6	2797.5	2138.6
Rail Fastener Type	Cut Spikes	Pandrol	Cut Spikes	Pandrol	Pandrol	Pandrol
Rail Fastener Stiffness (lb per in. x 10^6)	> 6	5-6	> 6	2-6	5-6	2-6

ballast physical state tests was presented in Ref. [1]. A summary of the results and conclusions will be presented here where relevant to the prediction methodology.

The physical state tests used to characterize the ballast materials were ballast density, plate load, and lateral tie push. These tests were done before and after the track was raised and tamped so that quantitative assessments of the change in ballast physical state could be made.

The ballast density tests were done in the cribs and under the ties as close to the rail seat as possible. The plate load tests were done at similar locations. The lateral tie push tests were done on single ties located away from the density and plate load test areas.

The ballast density test procedure has been described in Refs. [7 and 8]. The test results showed that the maintenance operation decreased the relative compaction of the ballast under the ties by 10-12% at the sites where a large raise was applied. Large raises of 1-1/2 to 2 in. were given to the Lorraine and Leeds wood tie section. The pre- and post-maintenance ballast densities were the same at the Aberdeen site, where the raise was only about 0.1 in.

Plate load tests on the ballasts were done before and after maintenance at selected locations in the cribs and under the ties. Descriptions of the plate load test procedures and apparatus can be found in Refs. [8,9,10]. The test results showed that the largest plate bearing resistances were under the ties near the rail seat areas. The pre-maintenance values were greatest at the Lorraine site, possibly because of the high degree of fouling and the greatest accumulation of tonnage since previous maintenance.

The post-maintenance values of plate bearing index were very similar for all of the sites, with the exception of Aberdeen. The Aberdeen site showed the smallest change in plate bearing index at the under-tie location as a result of the small raise. The largest decrease in plate bearing index due to maintenance was also at the Lorraine site. This site had the largest raise, about 2 in., which would significantly disturb the ballast structure, particularly when the ballast is fouled. This was consistent with the observation that the Lorraine site also showed the largest decrease in relative compaction at the under-tie location. For all of the sites where significant trackbed disturbance under the ties resulted from raising and tamping, the plate load tests showed no significant difference in ballast stiffness, independent of ballast type.

Values of the plate bearing index were also measured under the center of the tie. Again, the Lorraine site had the highest average value before the maintenance. The Aberdeen values at this location showed no change resulting from maintenance, but do show that the values under the center of the ties prior to maintenance were only 1/3 of the value measured under the tie at the rail seat. The plate load tests for all of the revenue sites showed that the ballast stiffnesses were always greater under the tie at the rail seat than under the tie center prior to maintenance. After the maintenance operations, the ballast stiffnesses under the tie were about the same at both locations, although still slightly greater near the rail seat areas.

3.4 Ballast Resilient Behavior

General Concepts

The behavior of a granular material under repeated loading conditions has generally been recognized as being nonlinearly stress-dependent, and very different from the behavior of the same soil under monotonic loading conditions.

17

This type of behavior is shown in Fig. 1. During the primary loading of a granular soil such as ballast, the strain develops rapidly and is only partially recovered upon unloading. Each additional cycle contributes another increment of plastic or permanent strain. The magnitude of the increment generally decreases with the number of cycles. The difference between the maximum strain under peak load and the permanent strain after unloading for each cycle is the resilient or recoverable strain. The resilient modulus of materials is defined as the repeated deviator stress divided by the recoverable strain. The amount of resilient recoverable strain generally decreases with number of cycles.

Research has shown that under moderate levels of repeated load, the resilient strains become approximately constant after some number of cycles, and the material behaves elastically. Kalcheff and Hicks [11] have indicated that only a few hundred cycles are necessary for this stabilization to occur. However, Brown [12] and Morgan [13] have shown that several thousand load repetitions are necessary to reach constant values of resilient modulus.

The magnitude of the resilient modulus is very much stress-state dependent. Several studies [14,15,16] have shown that the resilient response of unbound granular materials greatly increases as the confining pressure increases and is affected to a much smaller extent by the magnitude of repeated deviator stress. This has led to the conclusion that the resilient modulus can be related to the bulk stress state using the relationship

$$E_r = K_1 \overline{\theta}^{K_2} \quad , \tag{1}$$

where E_r = resilient modulus,

K_1, K_2 = soil constants determined from laboratory test results, and

$\overline{\theta}$ = bulk stress or the first invariant of stress.
The bulk effective stress is defined by

$$\overline{\theta} = \overline{\sigma}_1 + \overline{\sigma}_2 + \overline{\sigma}_3$$

$$= \overline{\sigma}_1 + 2\overline{\sigma}_3 \text{ for triaxial compression tests,}$$

where $\overline{\sigma}_1$, $\overline{\sigma}_2$, $\overline{\sigma}_3$ = major, intermediate and minor effective principal stresses, respectively.
This formulation has been widely used [17,18,19] to characterize the resilient modulus of granular materials.

The bulk stress formulation (Eq. 1) has been preferred for ballast material by Robnett, et al. [20] and Knutson [21]. Alva-Hurtado [22] has investigated the resilient response of a granite railroad ballast and determined that an arithmetic relationship was equally valid when relating bulk stress to resilient modulus. The relationship developed by Alva-Hurtado also showed that the initial compaction state affected the resilient modulus.

Although it has been shown that granular materials exhibit high values of resilient modulus even when the applied deviator stress level is near failure [23], the use of bulk stress cannot allow any distinction to be made between the effects of deviator stress or cell pressure. Various combinations

18
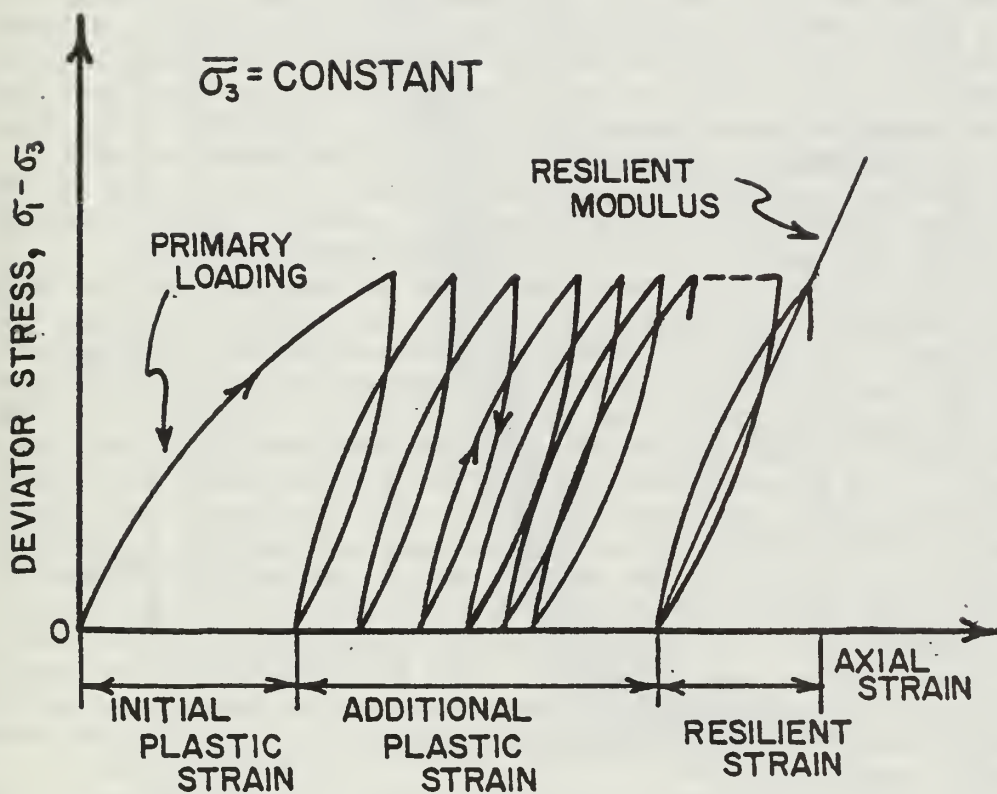
Figure 1.   Representation of Stress-Strain Curve from a Triaxial
             Sample Under Repeated Load

of cell pressure and deviator stress are assumed to achieve the same bulk stress, i.e., low cell pressure - high deviator stress or high cell pressure - low deviator stress or medium cell pressure - medium deviator stress combinations, all can result in the same bulk stress.

Staged Testing

In order to study the resilient behavior of railroad ballast under more general loading conditions that would include partial unloading and shear stress reversal, two triaxial test series were performed. The first series of triaxial tests did not involve shear stress reversal so the major principal stress was always the vertical stress. These tests were called staged tests, since a sample was subjected to several stress paths involving full and partial unloadings and various combinations of maximum and minimum positive shear stress. Previous research by Hicks [14] and Allen [24] has indicated that one specimen can be used to measure the resilient response of granular materials over a range of stress levels, and that the sequence of applied stresses did not significantly affect the measured resilient response.

The ballast material used for both test series was the Wyoming granite originally used at FAST in sections 17 and 18. This material was chosen for several reasons. The static compression stress-strain behavior was well documented [22,25], data and bulk stress formulations for the resilient response had been generated by other researchers [17,22], and reproduceable sample preparation and compaction procedures had been established.

The gradation curve for the granite ballast is shown in Fig. 2. This ballast can be classified as an AREA Number 5 material. The specification ranges for the AREA Number 5 ballast are shown in Fig. 2.

All of the staged cyclic tests were done on compacted samples of ballast. The rubber-tipped impact hammer compaction method developed by Yoo, et al. [7] was chosen to prepare the laboratory triaxial samples. The method consisted of placing layers of ballast into a specially designed split compaction mold that was clamped together and placed around the triaxial cell base pedestal. The layer was then subjected to twenty blows from the rubber-tipped impact hammer. This compactive effort resulted in reproduceable density states.

After each sample was compacted in the mold, the sample was aligned with the triaxial system loading piston and the mold was removed. A small vacuum was applied to the inside of the sample prior to removal of the mold in order to give the sample enough strength so that it would not collapse during further test preparation. The ballast was tested dry to provide for more rapid sample preparation and ease of testing. The effective isotropic consolidation pressures were achieved by increasing the vacuum applied to the inside of the sample, eliminating the need for an exterior fluid pressure surrounding the triaxial sample cylinder.

The specific initial test conditions, sample dimensions, and dry densities for the staged tests are given in Table 3, along with the results from tests involving shear stress reversal. As can be seen from the results given in Table 3, the compaction procedures gave reproduceable densities. The average dry density was 100.3 pounds per cubic foot (pcf) and had a coefficient of variation of only 0.7%. The average initial void ratio, e_o, was 0.66.

As previously stated, the purpose of the staged cyclic tests was to investigate the relationship between the applied stress level and resilient modulus for both full unloading and partial unloading. Full unloading for these tests will result from complete removal of any applied deviator stress, $\sigma_1 - \sigma_3$. Partial unloading will result from cycling between two levels of deviator stress without allowing complete unloading.
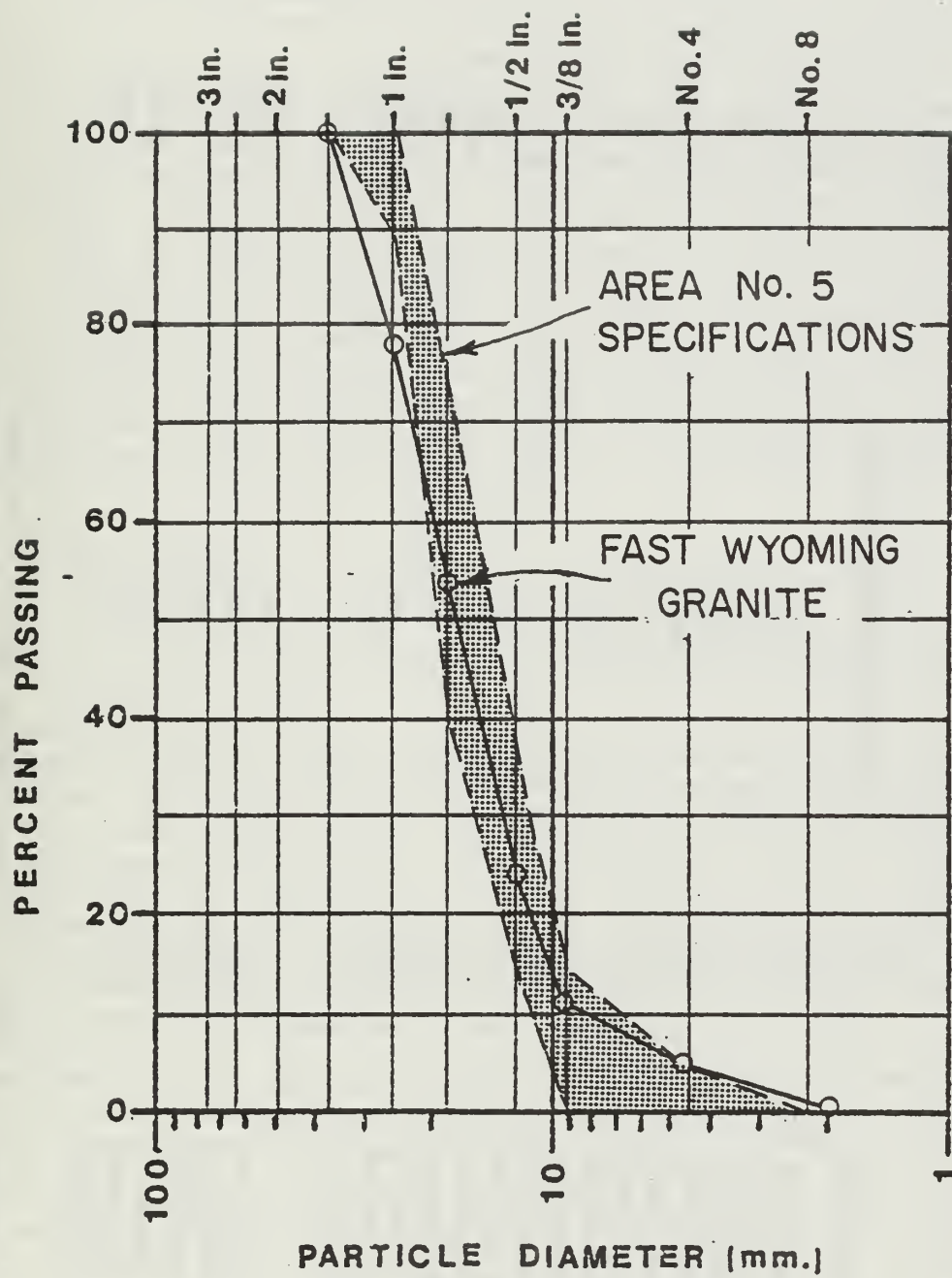
Figure 2. FAST Wyoming Granite Gradation

21

Table 3. Initial Test Conditions for Ballast Staged and Stress Reversal Tests

Test No.	Condition	$\bar{\sigma}_3$ (psi)	γ_d Dry Unit Weight (pcf)	$e_o = \dfrac{G_s \gamma_w - \gamma_d}{\gamma_d}$
S-1	Compacted	3.0	99.3	0.68
S-2	Compacted	6.0	100.7	0.65
S-3	Compacted	6.0	99.1	0.68
S-4	Compacted	6.0	100.2	0.66
S-5	Compacted	6.0	100.4	0.66
S-6	Compacted	6.0	101.6	0.64
S-7	Compacted	6.0	100.4	0.66
S-8	Compacted	3.0	100.1	0.66
S-9	Compacted	3.0	99.7	0.67
S-10	Compacted	3.0	101.1	0.65
S-11	Compacted	3.0	100.1	0.65
S-12	Compacted	12.0	100.1	0.65
S-13	Compacted	12.0	98.9	0.68
S-14	Compacted	12.0	100.9	0.65
S-15	Compacted	12.0	100.4	0.66
CK-1	Compacted	6.0	100.5	0.66
CK-2	Compacted	9.0	100.7	0.65
CK-3	Compacted	12.0	99.8	0.67
CK-4	Compacted	12.0	100.2	0.66
CK-5	Compacted	12.0	100.6	0.66
CK-6	Compacted	15.0	101.4	0.64

Average initial height = 14.79 in.; average initial area = 27.81 in.^{2}

e_o = initial void ratio; G_s = specific gravity = 2.67; γ_w = unit weight of water.

Confining pressures of 3, 6 and 12 psi were selected for these staged tests. For each confining pressure, four levels of applied shear stress (q) were used. The various combinations of cell pressure, maximum shear stress, and minimum shear stress used for the test stress paths are given in Table 4. Table 4 also gives the maximum bulk stress, $\bar{\theta}$, for each test, along with the stress ratio, q_{max}/q_f, where q_f is the static compressive strength of the ballast for a given effective cell pressure.

Four individual staged tests were done at each confining stress. In each test, the order of stress application was varied to investigate any changes in resilient modulus that might result from variations in stress sequence. Permanent deformation characteristics for each stress level and sequence were also analyzed. These results will be discussed in another section.

The order of applied stress paths for each of the tests is given in Table 5. Each stress path was repeated for 1000 cycles of loading and unloading and the recoverable strain between the maximum and minimum applied shear stress was measured. The recoverable strains during cycling along any of the stress paths tended to decrease as the number of cycles increased, but had generally reached an equilibrium value after about 500 cycles of the stress path had been applied. The resilient modulus, E_r, resulting from any of the stress paths was calculated by dividing the resilient strain into twice the cyclic shear stress, Δq, according to

$$E_r = \frac{2\Delta q}{\varepsilon_r} \quad , \tag{2}$$

where Δq = difference between maximum and minimum applied shear stress, and

ε_r = resilient strain.

The averaged results of the resilient moduli for each of the individual stress paths are given in Table 6, along with the corresponding average resilient strains. The resilient moduli values given in Table 6 are plotted against the maximum bulk stress for each stress path in Fig. 3. There is no distinct relationship between bulk stress and resilient modulus evident when moduli values measured from partial unloading stress paths are included. A check was also made to see if the data fit the common log-log formulation. Again, there was good correlation between log of E_r and log of $\bar{\theta}$ if only the results from fully unloaded stress paths were used.

Figure 4 shows the comparison between resilient moduli values obtained by Alva-Hurtado [22] and those obtained in this study. The arithmetic regression equations for these two sets of data are given in Table 7a. Although both sets of moduli measurements were made on the same granite material at the same density state, the results obtained by Alva-Hurtado are higher than those obtained in this study. The reason for this is not known, but it could be from differences in detailed test conditions or from changes in ballast gradation and angularity caused by repeated use of the same material. However, the slopes of the two E_r vs $\bar{\theta}$ curves shown in Fig. 4 are the same. The coefficients for the log-log regression equations for the resilient moduli-bulk stress formulation from these sets of data are also given in Table 7b for comparison.

Shear Stress Reversal Testing

The resilient behavior of ballast under one-way repeated loading in which the full deviator stress was removed was shown to be related to the maximum bulk stress on the material. Partial unloading resilient moduli are not

Table 4. Stress Levels for Staged Tests

Stress Path	$\bar{\sigma}_{3c}$ (psi)	$\bar{\sigma}_1$ Min (psi)	$\bar{\sigma}_1$ Max (psi)	q Min (psi)	q Max (psi)	Δq (psi)	$\bar{\theta}$ Max (psi)	$\dfrac{q_{max}}{q_f}$
OA	3.00	3.00	6.12	0.00	1.56	1.56	12.12	0.150
OB		3.00	9.26	0.00	3.13	3.13	15.26	0.301
OC		3.00	12.38	0.00	4.69	4.69	18.38	0.451
OD		3.00	15.51	0.00	6.26	6.26	21.51	0.602
AB		6.12	9.26	1.56	3.13	1.56	15.26	0.301
AC		6.12	12.38	1.56	4.69	3.13	18.38	0.451
AD		6.12	15.51	1.56	6.26	4.69	21.51	0.602
BC		9.26	12.38	3.13	4.69	1.56	18.38	0.451
BD		9.26	15.51	3.13	6.26	3.13	21.51	0.602
CD		12.38	15.51	4.69	6.26	1.56	21.51	0.602
O´A´	6.00	6.00	12.00	0.00	3.00	3.00	24.00	0.150
O´B´		6.00	18.00	0.00	6.00	6.00	30.00	0.301
O´C´		6.00	24.00	0.00	9.00	9.00	36.00	0.451
O´D´		6.00	30.00	0.00	12.00	12.00	42.00	0.602
A´B´		12.00	18.00	3.00	6.00	3.00	30.00	0.301
A´C´		12.00	24.00	3.00	9.00	6.00	36.00	0.451
A´D´		12.00	30.00	3.00	12.00	9.00	42.00	0.602
B´C´		18.00	24.00	6.00	9.00	3.00	36.00	0.451
B´D´		18.00	30.00	6.00	12.00	6.00	42.00	0.602
C´D´		24.00	30.00	9.00	12.00	3.00	42.00	0.602
O´´A´´	12.00	12.00	18.00	0.00	3.00	3.00	42.00	0.084
O´´B´´		12.00	24.00	0.00	6.00	6.00	48.00	0.168
O´´C´´		12.00	30.00	0.00	9.00	9.00	54.00	0.252
O´´D´´		12.00	36.00	0.00	12.00	12.00	60.00	0.335
A´´B´´		18.00	24.00	3.00	6.00	3.00	48.00	0.168
A´´C´´		18.00	30.00	3.00	9.00	6.00	54.00	0.252
A´´D´´		18.00	36.00	3.00	12.00	9.00	60.00	0.335
B´´C´´		24.00	30.00	6.00	9.00	3.00	54.00	0.252
B´´D´´		24.00	36.00	6.00	12.00	6.00	60.00	0.335
C´´D´´		30.00	36.00	9.00	12.00	3.00	60.00	0.335

Table 5. Order of Applied Stress Paths for Staged Tests

					Staged Test Number						
S-8	S-9	S-10	S-11	S-3	S-5	S-6	S-7	S-12	S-13	S-14	S-15
3.0	3.0	3.0	3.0	6.0	6.0	6.0	6.0	12.0	12.0	12.0	12.0
OA	OB	OC	OD	O'A'	O'B'	O'C'	O'D'	O''A''	O''B''	O''C''	O''D''
OB	OC	OD	OA	O'B'	O'C'	O'D'	O'A'	O''B''	O''C''	O''D''	O''A''
OC	OD	OA	OB	O'C'	O'D'	O'A'	O'B'	O''C''	O''D''	O''A''	O''B''
OD	OA	OB	OC	O'D'	O'A'	O'B'	O'C'	O''D''	O''A''	O''B''	O''C''
AB	AB	AB	AB	A'B'	A'B'	A'B'	A'B'	A''B''	A''B''	A''B''	A''B''
AC	AC	AC	AC	A'C'	A'C'	A'C'	A'C'	A''C''	A''C''	A''C''	A''C''
AD	AD	AD	AD	A'D'	A'D'	A'D'	A'D'	A''D''	A''D''	A''D''	A''D''
BC	BC	BC	BC	B'C'	B'C'	B'C'	B'C'	B''C''	B''C''	B''C''	B''C''
BD	BD	BD	BD	B'D'	B'D'	B'D'	B'D'	B''D''	B''D''	B''D''	B''D''
CD	CD	CD	CD	C'D'	C'D'	C'D'	C'D'	C''D''	C''D''	C''D''	C''D''
OC	OD	OA	OB	O'C'	O'D'	O'A'	O'B'	O''C''	O''D''	O''A''	O''B''
OB	OC	OD	OA	O'B'	O'C'	O'D'	O'A'	O''B''	O''C''	O''D''	O''A''
OA	OB	OC	OD	O'A'	O'B'	O'C'	O'D'	O''A''	O''B''	O''C''	O''D''
OD	OA	OB	OC	O'D'	O'A'	O'B'	O'C'	O''D''	O''A''	O''B''	O''C''
	OD										

$\bar{\sigma}_{3c}$ (psi) →

25

Table 6.   Average Resilient Moduli and Strains for Staged Tests

$\bar{\sigma}_{3c}$ (psi)	Stress Path	Δq (psi)	Avg. E_r (ksi)	$2\Delta q/E_r$ = Avg. ε_r ($\mu\varepsilon$)
3.0	OA	1.56	14.4	217
	OB	3.13	15.7	399
	OC	4.69	16.8	559
	OD	6.26	17.7	709
	AB	1.56	25.4	123
	AC	3.13	24.3	252
	AD	4.69	24.6	381
	BC	1.56	33.1	94
	BD	3.13	30.5	206
	CD	1.56	40.8	76
6.0	O´A´	3.00	23.2	259
	O´B´	6.00	24.0	500
	O´C´	9.00	25.6	704
	O´D´	12.00	27.0	888
	A´B´	3.00	38.8	154
	A´C´	6.00	37.8	318
	A´D´	9.00	37.9	475
	B´C´	3.00	53.3	113
	B´D´	6.00	45.1	266
	C´D´	3.00	57.5	104
12.0	O´´A´´	3.00	33.0	182
	O´´B´´	6.00	32.8	366
	O´´C´´	9.00	33.3	540
	O´´D´´	12.00	33.9	707
	A´´B´´	3.00	50.3	119
	A´´C´´	6.00	43.6	275
	A´´D´´	9.00	44.0	409
	B´´C´´	3.00	68.1	88
	B´´D´´	6.00	58.0	207
	C´´D´´	3.00	84.9	71
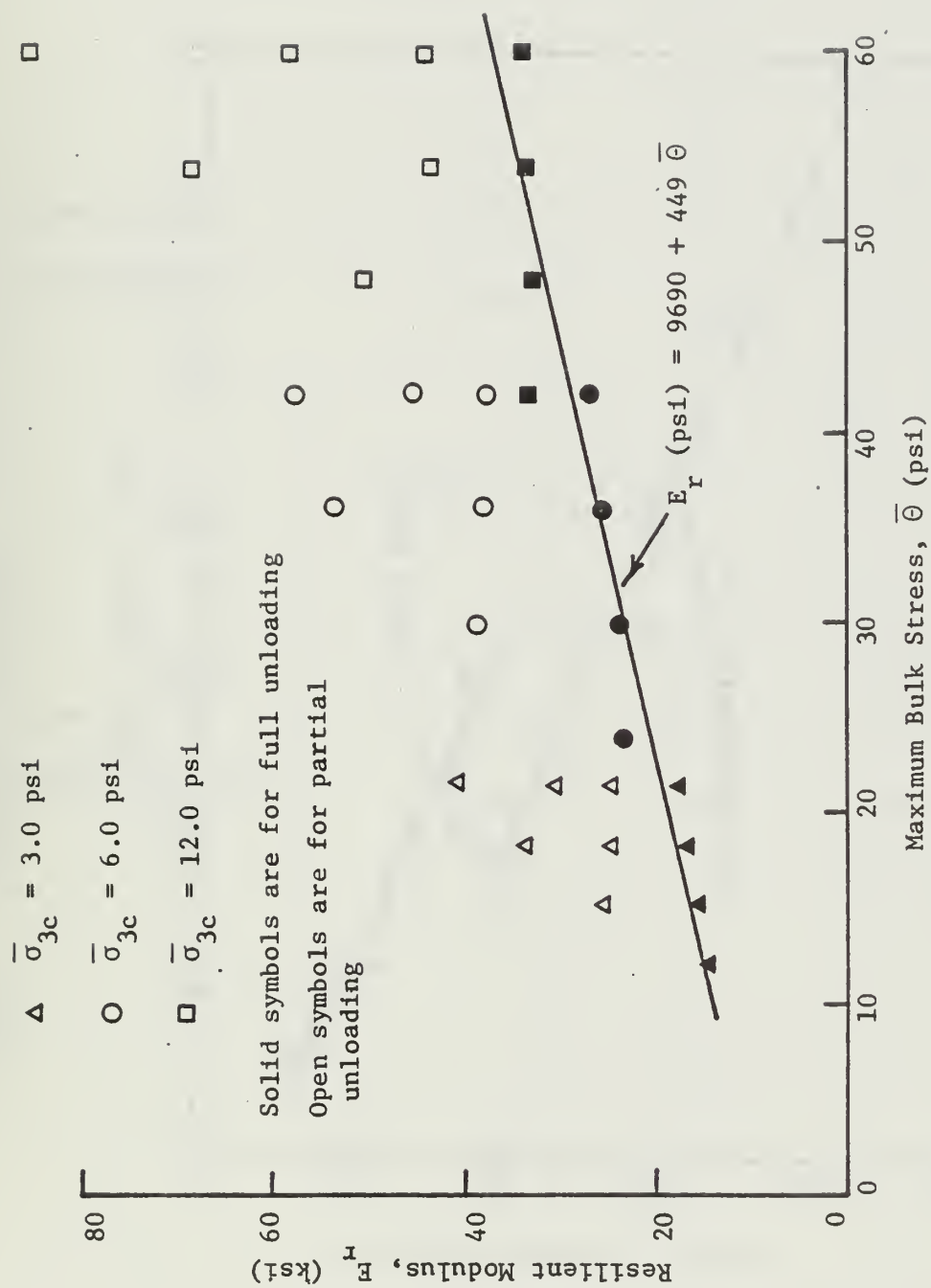
Figure 3. Resilient Modulus versus Maximum Bulk Stress from Staged Tests

27
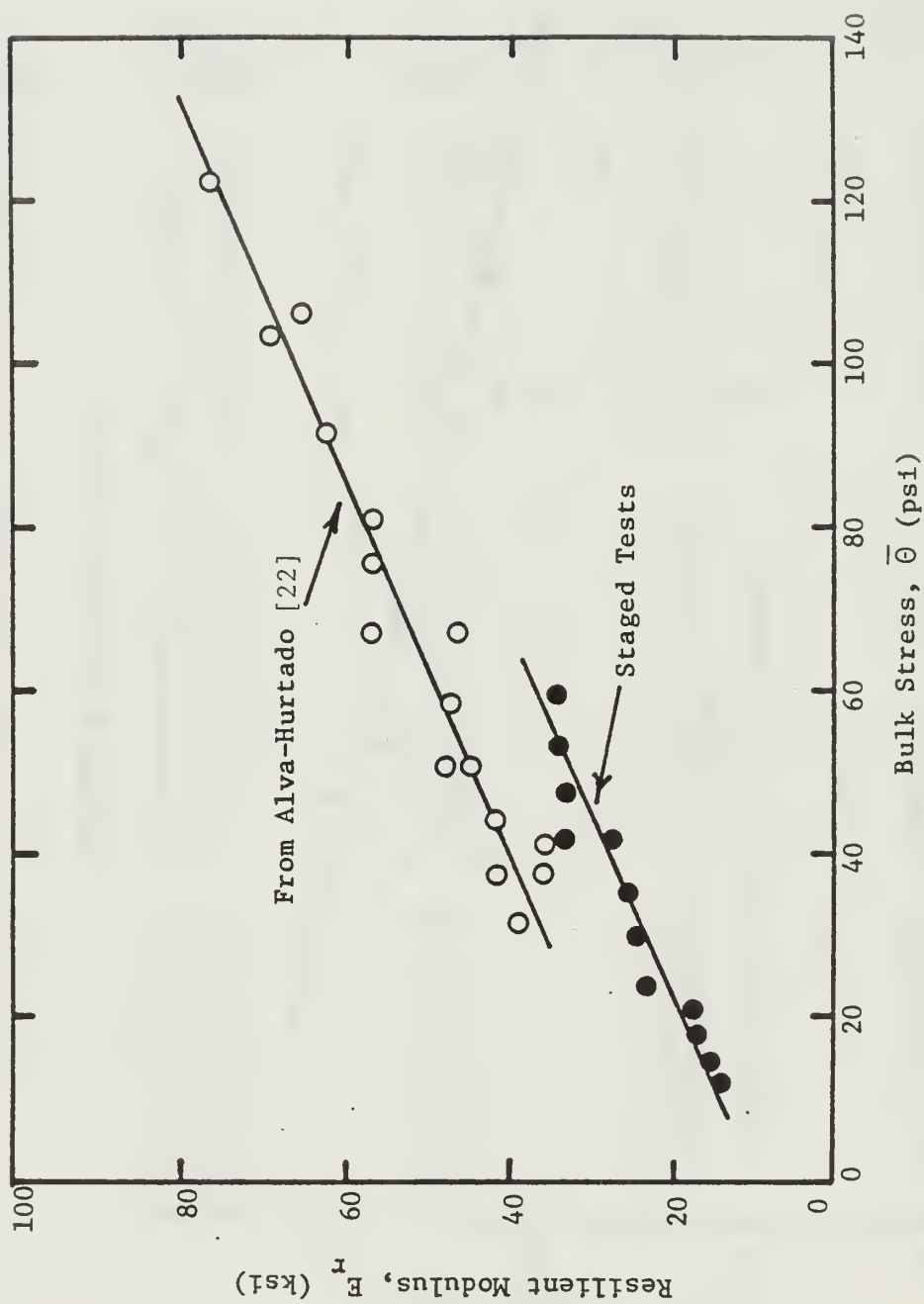
Figure 4. Arithmetic Relationship of E_r as a Function of Θ

28

Table 7.   Regression Equations for E_r as a Function of $\bar{\theta}$

a) Model: $E_r = K_1 + K_2\bar{\theta}$

	K_1	K_2	r^2
Staged Tests	9690	449	0.92
Alva-Hurtado [22] (N = 10,000)	22685	425	0.94

b) Model: $E_r = K_3\bar{\theta}^{K_4}$

	K_3	K_4	r^2
Staged Tests	3160	0.593	0.95
Alva-Hurtado [22] (N = 10,000)	5477	0.535	0.91

related to the bulk stress alone, and thus must be influenced by a combination of stress parameters. When triaxial samples are subjected to both positive and negative cyclic shear stresses, the resilient behavior is even more complicated. Cycling between positive and negative shear stresses causes a continual reversal of the principal stress directions in a triaxial sample. For triaxial compression, the final stress state is such that the major principal stress acts in the vertical direction on a horizontal plane. For triaxial extension, the final major principal stress acts in the horizontal direction on a vertical plane.

A "positive" shear stress, $q = (\sigma_1 - \sigma_3)/2$, will be defined as the shear stress resulting from a major principal stress acting within ±45° from the vertical. Likewise, a "negative" shear stress occurs when the major principal stress is acting within ±45° from the horizontal. Thus, these triaxial compressional stresses produce positive shear stresses and these extensional stresses produce negative shear stresses. When the shear stresses are cycled from positive to negative, the orientation of the major principal stress and plane is abruptly rotated by 90° as the stresses pass through the isotropic condition.

The sample initial dimensions, densities and void ratios for the stress reversal tests have been given in Table 3. The test conditions for these tests are given in Table 8. For these tests, $\overline{\sigma}_v$ will mean the vertical stress acting on the sample, which can be the major principal stress, $\overline{\sigma}_1$, or the minor principal stress, $\overline{\sigma}_3$, depending on the overall stress condition. Similarly, $\overline{\sigma}_h$ will refer to the horizontal stress acting on the sample. All test samples were isotropically consolidated prior to shear application. For the isotropic condition, $\overline{\sigma}_v = \overline{\sigma}_h = \overline{\sigma}_1 = \overline{\sigma}_3 = \overline{\sigma}_c$, where $\overline{\sigma}_c$ is the isotropic consolidation pressure. Also given in Table 8 are the stress ratios, q/q_f, for both the compressional and extensional portions of the applied stress paths, and the mean stress, $\overline{p}$, applied to the sample.

For triaxial extension tests, the static shear strength is defined by

$$q_f = \frac{\overline{c}\,\cos\overline{\phi} - \overline{\sigma}_{1f}\,\sin\overline{\phi}}{1 + \sin\overline{\phi}}\,,$$ (3)

where $\overline{\sigma}_{1f}$ is the major principal stress at failure. For these triaxial extension tests, $\overline{\sigma}_{1f} = \overline{\sigma}_{hf} = \overline{\sigma}_c$, since the cell pressure was maintained constant throughout the test.

A cycle of loading for the stress reversal tests consisted of first applying the axial compressive stress followed by unloading to the extensional stress, and then reloading to isotropic conditions. Loading is defined as any change of stress state where the mean stress increases, that is, $\overline{p} = (\overline{\sigma}_v + \overline{\sigma}_h)/2$ increases. Unloading is defined as a decrease in $\overline{p}$. During testing, the resilient strains resulting from loading to q_{max} and unloading to q_{min} were monitored. The resilient moduli calculations were based on

$$E_{re} = \frac{2\,q_{min}}{\varepsilon_{re}}\,,$$ (4)

$$E_{rc} = \frac{2\,q_{max}}{\varepsilon_{rc}}\,,$$ (5)

30

Table 8. Test Conditions for Stress Reversal Cyclic Tests

Test	$\bar{\sigma}_c$ (psi)	$\bar{\sigma}_h$ (psi) Max	Min	$\bar{\sigma}_v$ (psi) Max	Min	$\bar{p}$ (psi) Max	Min	q^* (psi) Max	Min	Cyclic Δq (psi)	Bulk Stress,** $\bar{\theta}$ (psi) Max	Min
CK-1	6.0	6.0	6.0	12.0	2.34	9.0	4.17	3.0	-1.83	4.83	24.0	14.34
CK-2	9.0	9.0	9.0	27.0	3.00	18.0	6.00	9.0	-3.00	12.00	45.0	21.00
CK-3	12.0	12.0	12:0	18.0	6.00	15.0	9.00	3.0	-3.00	6.00	42.0	30.00
CK-4	12.0	12.0	12.0	24.0	6.00	18.0	9.00	6.0	-3.00	9.00	48.0	30.00
CK-5	12.0	12.0	12.0	30.0	6.00	21.0	9.00	9.0	-3.00	12.00	54.0	30.00
CK-6	15.0	15.0	15.0	33.0	9.00	24.0	12.00	9.0	-3.00	12.00	63.0	39.00

$*q = (\bar{\sigma}_v - \bar{\sigma}_h)/2$

$**\bar{\theta} = \bar{\sigma}_v + 2\bar{\sigma}_h$; thus Compression $\bar{\theta} = \bar{\sigma}_1 + 2\bar{\sigma}_3$, and Extension $\bar{\theta} = \bar{\sigma}_3 + 2\bar{\sigma}_1$

(q/q_f)

Test	Compression	Extension
CK-1	0.150	0.712
CK-2	0.321	0.812
CK-3	0.084	0.631
CK-4	0.168	0.631
CK-5	0.252	0.631
CK-6	0.206	0.520

31

$$E_{rt} = \frac{2(q_{max} - q_{min})}{\varepsilon_{rc} - \varepsilon_{re}} \quad , \tag{6}$$

where E_{re}, E_{rc} and E_{rt} are the extension, compression and total resilient moduli,

ε_{re} and ε_{rc} are the resilient strains resulting from extension and compression, and

q_{max} and q_{min} are the maximum and minimum shear stresses.

The measured resilient moduli for these tests are listed in Table 9 for various cycle numbers. These tabulated values show that the extensional resilient modulus is always less than the compressional modulus, which results in the total resilient modulus having a value intermediate to the compressional and extensional moduli. The general trend for these tests is that the moduli increase as number of cycles increases. In contrast, the results from the staged tests showed that the moduli reached approximately constant values after a fewer number of cycles.

Resilient Modulus Formulation

After many load-unload cycles, the behavior of railroad ballast becomes relatively elastic, in that the resilient strains become approximately constant. The elastic behavior is nonlinear, however.

The resilient strains from the loading portions of the staged tests and the peak points of the shear stress reversal tests are given in Table 10. These points will be used to determine the resilient modulus formulation for situations involving full unloading and with shear stress reversal. The results from the stress reversal test at 9 psi effective confining pressure are not included because equipment malfunction during testing invalidated some of the test results.

Figure 5 shows the relationships between the applied shear stress levels and the vertical resilient strains. The resilient strains increase as cell pressure decreases, for a given shear stress level, for both extension and compression.

The compressional resilient strains in Fig. 5 for each cell pressure were fit to an equation of the form

$$q = A(\mu \varepsilon_r)^B \quad , \tag{7}$$

using the data listed in Table 10. Since intermediate data were not available for the extensional resilient strain curves, straight lines from the origin through the peak extensional resilient strains were assumed. The resilient extensional strains were related to the negative shear stress by

$$q = \alpha(\mu \varepsilon) \quad . \tag{8}$$

The coefficients A, B and α for each cell pressure were subsequently fit to a log-log relationship as a function of cell pressure. Good agreement between the observed data and the assumed forms of the regression equations was found for the fitted data. The solid lines shown on Fig. 5 were based on the regression equations, and are in close agreement with the observations.

Table 11 lists the assumed form of each regression equation and the derived coefficients and coefficients of determination for the regressions. The resilient strain relationships given in Table 11 were used to define contours

Table 9. Measured Resilient Moduli from Stress Reversal Tests

| | | | | Resilient Moduli (ksi) | | | | | | | | | | | |
| | $\bar{\sigma}_c$ (psi) | q (psi) Max | q (psi) Min | Δq (psi) | N = 100 E_{re} | E_{rc} | E_{rt} | N = 1000 E_{re} | E_{rc} | E_{rt} | N = 10000 E_{re} | E_{rc} | E_{rt} | Static Loading After Cycles E_{re} | E_{rc} | E_{rt} |
Test																
CK-1	6.0	3.0	-1.8	4.83	9.7	17.9	13.6	8.2	25.6	14.0				7.8	24.7	13.6
CK-2	9.0	9.0	-3.0	12.00	7.4	15.2	12.0	17.9	20.5	19.8						
CK-3	12.0	3.0	-3.0	6.00	16.5	19.7	17.9	15.0	30.6	20.2	22.2	34.1	26.9	18.9	32.8	24.0
CK-4	12.0	6.0	-3.0	9.00	12.9	33.5	21.8	14.3	37.0	24.2	19.7	55.4	34.5	22.7	37.4	30.7
CK-5	12.0	9.0	-3.0	12.00	17.7	29.8	25.4	12.4	37.8	25.0	17.3	42.6	31.2	20.4	38.2	31.4
CK-6	15.0	9.0	-3.0	12.00	15.5	35.8	27.0	17.6	45.6	32.7	24.5	55.1	42.0	32.8	43.3	40.1

E_{re} = resilient modulus in extension,

E_{rc} = resilient modulus in compression, and

E_{rt} = total resilient modulus.

33

Table 10. Resilient Strains for Staged Tests and Stress
Reversal Tests

a) Staged Tests

$\bar{\sigma}_3$ (psi)	q (psi)	ϵ_r ($\mu\epsilon$)
3.0	1.56	217
	3.13	399
	4.69	560
	6.26	709
6.0	3.00	259
	6.00	500
	9.00	704
	12.00	888
12.0	3.00	182
	6.00	366
	9.00	540
	12.00	707

b) Stress Reversal Tests

$\bar{\sigma}_3$ (psi)	q (psi)	ϵ_r ($\mu\epsilon$)
6.0	−1.83	−467
	2.99	242
12.0	−3.01	−318
	−2.99	−264
	−2.99	−293
	2.99	182
	5.98	320
	9.11	477
15.0	−3.01	−184
	8.99	415
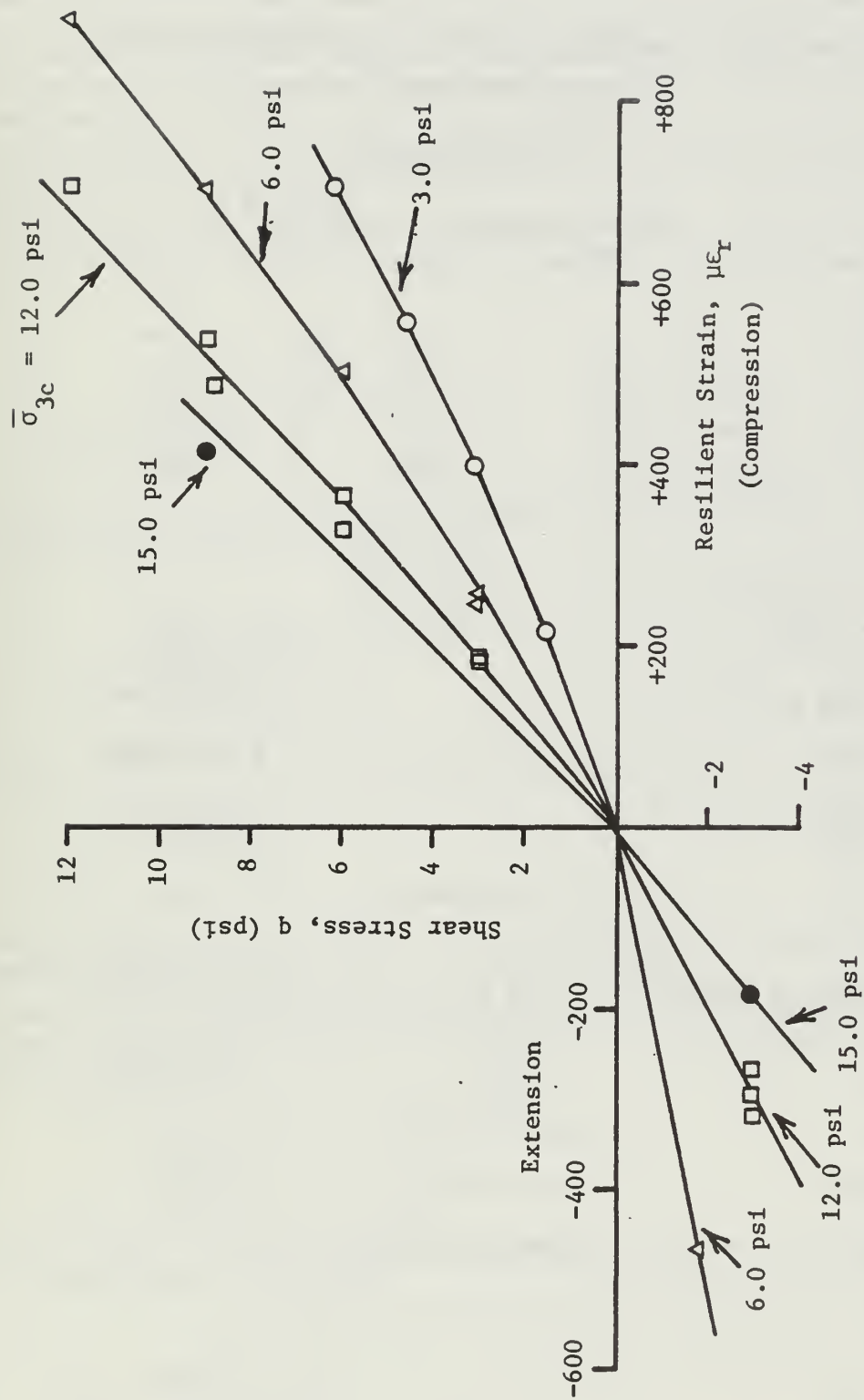
Figure 5.   Shear Stress versus Resilient Strain for Compression and Extension

Table 11. Regression Results for Compression and
Extension Resilient Strains

a) Compression

Form of Equation: $q = A(\mu\varepsilon_r)^B$

$\overline{\sigma}_3$ (psi)	A	B	r^2
3.0	2.486×10^{-3}	1.171	1.00
6.0	7.680×10^{-3}	1.079	1.00
12.0	13.914×10^{-3}	1.036	0.99

Equations for Parameters A, B:

$A = C(\overline{\sigma}_3)^D$	$B = E(\overline{\sigma}_3)^F$
$C = 8.647 \times 10^{-4}$	$E = 1.2816$
$D = 1.145$	$F = -0.0883$
$r^2 = 0.98$	$r^2 = 0.96$

b) Extension

Form of Equation: $q = \alpha(\mu\varepsilon_r)$ Equation for α:

$\overline{\sigma}_3$ (psi)	α	$\alpha = \beta(\overline{\sigma}_3)^\gamma$
6.0	3.921×10^{-3}	$\beta = 2.535 \times 10^{-4}$
12.0	1.023×10^{-3}	$\gamma = 1.518$
15.0	1.639×10^{-3}	$r^2 = 0.99$

of equal resilient strain as related to $\bar{p} = \bar{\sigma}_v + \bar{\sigma}_h/2$ and $q = \sigma_v - \sigma_h/2$ for full unloading cases. These resilient strain contours are shown in Fig. 6. This figure shows that for a given effective confining pressure, a positive shear stress results in smaller resilient strains than the application of the same magnitude negative shear stress. This means that the compressional resilient modulus will be larger than the extensional resilient modulus for isotropic tests cycled between $\pm q$.

The procedure for calculating the resilient modulus, E_{rc}, for compression loading from $q = 0$ to a specified value of q_{max}, followed by full unloading to $q = 0$ is as follows:

1) The expression relating shear stress, q_{max}, to resilient strain, ε_{rc}, as a function of effective confining pressure, $\bar{\sigma}_3$, can be rearranged to

$$\mu\varepsilon_{rc} = \left(\frac{q_{max} \bar{\sigma}_3^{-D}}{C} \right)^{\left(\frac{\bar{\sigma}_3}{E} \right)^{-F}} , \qquad (9)$$

where C, D, E and F are the coefficients listed in Table 11. Substitution of the coefficients results in

$$\mu\varepsilon_{rc} = \left(\frac{q_{max} \bar{\sigma}_3^{-1.145}}{8.647 \times 10^{-4}} \right)^{\left(\frac{\bar{\sigma}_3^{0.088}}{1.282} \right)} . \qquad (10)$$

2) The compressional resilient modulus, E_{rc}, is then

$$E_{rc} = \frac{2 \, q_{max}}{\mu\varepsilon_{rc} \times 10^{-6}} . \qquad (11)$$

The procedure for calculation of the extensional resilient modulus, E_{re}, for repeated loadings from $q = 0$ to q_{min} is as follows:

1) The expressions relating shear stress, q_{min}, to resilient extensional strains, ε_{re}, as a function of effective confining pressure, $\bar{\sigma}_3$, can be rearranged to

$$\mu\varepsilon_{re} = \frac{q_{min} \bar{\sigma}_3^{-\gamma}}{\beta} , \qquad (12)$$

where β and γ are the coefficients listed in Table 11. Substitution of the coefficients results in

$$\mu\varepsilon_{re} = \frac{q_{min} \bar{\sigma}_3^{-1.518}}{2.535 \times 10^{-4}} . \qquad (13)$$

2) The extensional resilient modulus, E_{re}, is then
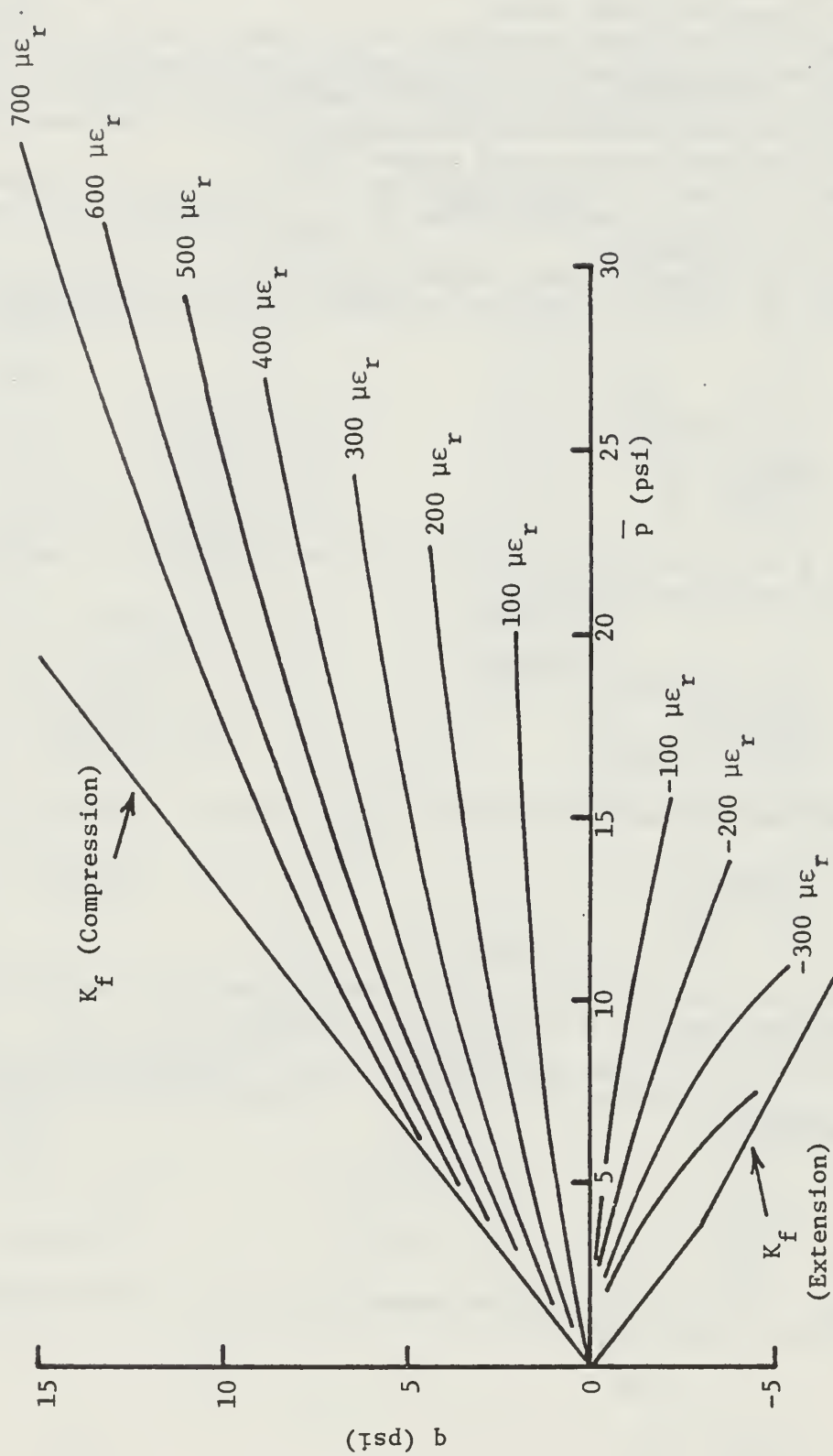
Figure 6. Resilient Strain Contours for Full Unloading

38

$$E_{re} = \frac{2 \, q_{min}}{\mu\varepsilon_{re} \times 10^{-6}} \quad . \tag{14}$$

For tests where the shear stress is reversed, the repeated stresses are cycled between q_{max} and q_{min}. The total resilient modulus, E_{rt}, would be calculated as follows:

1) Calculate $\mu\varepsilon_{rc}$ for q_{max} as given in Eq. 9.

2) Calculate $\mu\varepsilon_{re}$ for q_{min} as given in Eq. 13.

3) Calculate E_{rt} by

$$E_{rt} = \frac{2(q_{max}-q_{min})}{(\mu\varepsilon_{rc}-\mu\varepsilon_{re}) \times 10^{-6}} \quad . \tag{15}$$

Resilient Modulus Validation

The formulation presented for full unloading, with and without shear stress reversal, will be used for characterization of the resilient behavior of the ballast materials.

This method for calculation of resilient moduli was used to compute the full unloading moduli from the staged and stress reversal tests on the compacted granite ballast. The predicted and measured resilient moduli values for these tests are given in Table 12.

Repeated load tests were performed on compacted samples of ballast recovered from the Leeds, Illinois, wood and concrete tie sections and the Lorraine, Virginia, and Aberdeen, Maryland, concrete tie sections. These ballasts and their properties were previously described in Volume 1 [1]. Details regarding the test procedure can be found in Ref. [26]. The measured and predicted resilient moduli for the field site ballasts after about 10,000 load cycles are given in Table 13.

The comparisons between all the predicted and measured resilient moduli given in Tables 12 and 13 are shown in Fig. 7. Agreement is good for the staged and shear stress reversal tests. The limited data on resilient moduli from the field sites show that the field site ballasts have resilient moduli similar to the granite ballast moduli measured in the staged and stress reversal tests. This suggests that ballast type is not an important consideration with respect to resilient modulus.

3.5 Ballast Inelastic Behavior

Introduction

Repeated load triaxial tests were done on compacted ballast samples to investigate the amount of permanent deformation that accumulated as a function of stress level and number of constant-amplitude load applications. Variable-amplitude repeated load tests with both full and partial unloading (staged tests), and constant-amplitude repeated load tests with shear stress reversal were also done on the FAST granite ballast.

The stress conditions for the constant-amplitude repeated load tests have been given in Table 13. The stress conditions and load sequences for the staged tests on the granite ballast have been given in Tables 4 and 5. The

39

Table 12. Resilient Moduli for Granite Ballast

Staged and Stress Reversal Comparisons

$\overline{\sigma}_3$ (psi)	q_{min} (psi)	q_{max} (psi)	Resilient Modulus, E_r (ksi)	
			Measured	Predicted
3.0	0.0	1.56	14.4	14.6
3.0	0.0	3.13	15.7	16.2
3.0	0.0	4.69	16.8	17.1
3.0	0.0	6.26	16.7	17.8
6.0	0.0	3.00	23.2	22.8
6.0	0.0	6.00	24.0	24.3
6.0	0.0	9.00	25.6	25.1
6.0	0.0	12.00	27.0	25.8
12.0	0.0	3.00	33.0	34.8
12.0	0.0	6.00	32.8	35.5
12.0	0.0	9.00	33.0	35.9
12.0	0.0	12.00	33.9	36.2
6.0	-1.8	3.00	13.6	13.1
9.0	-3.0	9.00	19.8	23.8
12.0	-3.0	3.00	24.0	27.0
12.0	-3.0	6.00	30.7	29.5
12.0	-3.0	9.00	31.4	31.0
15.0	-3.0	9.00	40.1	37.8

Table 13. Resilient Moduli for Field Site Ballasts

Site	$\overline{\sigma}_3$ (psi)	q_{min} (psi)	q_{max} (psi)	Resilient Modulus E_r (ksi)	
				Measured	Predicted
Leeds, Wood (slag)	3.0	0.0	7.50	23.0	18.3
	12.0	0.0	7.50	42.8	35.7
Leeds, Concrete (granite)	3.0	0.0	3.55	17.7	16.4
	3.0	0.0	7.50	20.8	18.3
	3.0	0.0	14.15	17.0	20.0
	12.0	0.0	3.75	53.6	35.0
	12.0	0.0	7.50	38.8	35.7
	12.0	0.0	15.00	38.8	36.4
Lorraine (limestone)	3.0	0.0	5.70	27.6	17.6
	3.0	0.0	7.50	19.1	18.3
	7.0	0.0	7.50	27.8	26.7
	12.0	0.0	7.50	40.9	35.7
	12.0	0.0	15.00	43.1	36.4
Aberdeen (traprock)	3.0	0.0	3.00	28.6	16.1
	3.0	0.0	6.00	33.8	17.7
	12.0	0.0	3.75	36.3	35.0
	12.0	0.0	7.50	41.3	35.7
	12.0	0.0	15.00	34.6	36.4
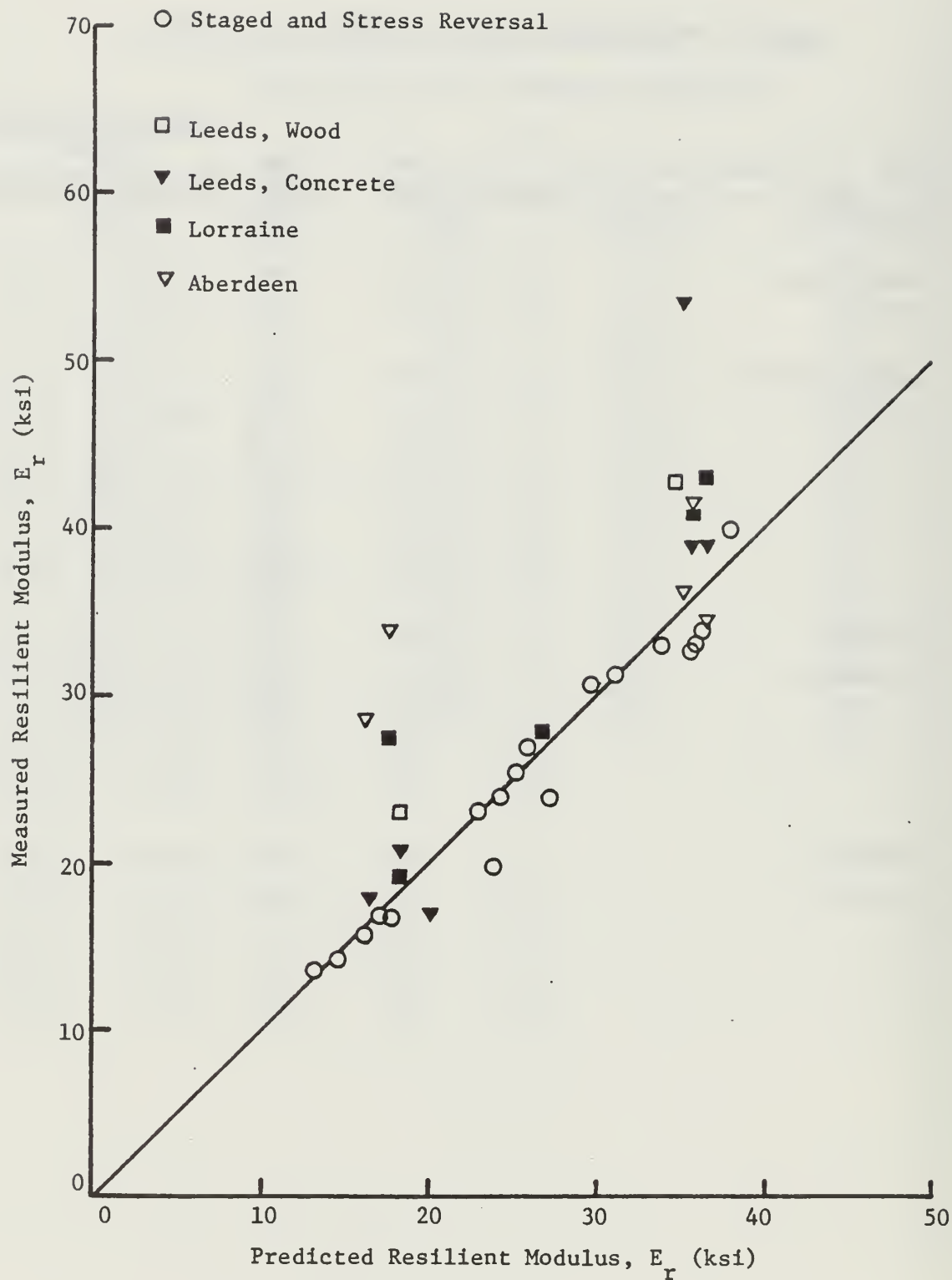
Figure 7.   Measured and Predicted Moduli for All Ballasts

42

test conditions for the shear stress reversal tests on the granite ballast were given in Table 8.

In addition to the triaxial tests, experiments were conducted using a special box test intended to simulate the field loading conditions. The deformation properties of ballast due to a repeated application of vertical loads were measured in this device. Lateral stresses were also measured under both loaded and unloaded conditions, and residual stress build-up in the ballast was determined.

Constant-Amplitude Tests

The permanent strains resulting from the repeated loadings of the revenue field site ballasts have been previously reported by Siller [26]. The permanent strains developed during the first thousand cycles of each of the staged tests are given in Table 14, and will be considered in this section. However, the staged tests were carried out to 14000 cycles, and the loading conditions changed every 1000 cycles. The permanent strains for all but the first stage will be presented later.

Previous research on the permanent strain behavior of ballast under repeated loading conditions has shown that under moderate stress levels, a linear relationship exists between the permanent strain at the Nth cycle and the log of the number of cycles [22,27,28,29]. This relationship has been expressed by

$$\varepsilon_N = \varepsilon_1 (1 + C \log N) \quad , \tag{16}$$

where ε_N is the permanent axial strain at the Nth cycle,

ε_1 is the permanent axial strain developed due to the first cycle of load, $N = 1$, which is also the intercept of the ε_N vs. log N relationship,

C is a soil constant, and

N is the number of applied load cycles.

Past research has indicated that $C \simeq 0.2$ for all ballasts [22,27,28], independent of the applied stress levels or compaction state.

The ballast constant, C, can be calculated in several ways, each of which should give the same result if the relationship given in Eq. 16 holds. Four methods for calculating C are as follows:

1. Method 1 is the Office of Research and Experiments (ORE) method [28], which has been frequently used in the past [22,27]. Details of the ORE method will not be presented, since they have been clearly outlined in past works.

2. Method 2 is a regression of

$$\left(\frac{\varepsilon_N}{\varepsilon_1} - 1\right) \text{ vs. log N to calculate C.}$$

3. Method 3 determines C by calculating

$$\frac{\left(\frac{\varepsilon_N}{\varepsilon_1} - 1\right)}{\log N} \quad \text{for all N.}$$

4. Method 4 uses the slope of the semi-log ε_N vs. log N relationship divided by the strain at the first cycle to calculate C.

43

Table 14. Permanent Strain for First Stress Path Loading from Staged Tests

Test	$\bar{\sigma}_3$ (psi)	q (psi) Min	Max	Permanent Vertical Strain after Cycle, ε_N (%)					
				N=1	N=4	N=100	N=250	N=500	N=1000
S-8	3.0	0.0	1.56	0.011	0.013	0.018	0.020	0.020	0.020
S-9	3.0	0.0	3.13	0.077	0.093	0.125	0.134	0.140	0.146
S-10	3.0	0.0	4.69	0.172	0.194	0.258	0.280	0.296	0.315
S-11	3.0	0.0	6.26	0.259	0.319	0.438	0.465	0.490	0.513
S-3	6.0	0.0	3.00	0.015	0.019	0.024	0.026	0.028	0.030
S-5	6.0	0.0	6.00	0.078	0.090	0.122	0.138	0.152	0.165
S-6	6.0	0.0	9.00	0.342	0.383	0.506	0.542	0.600	0.616
S-7	6.0	0.0	12.00	0.420	0.476	0.635	0.670	0.702	0.743
S-12	12.0	0.0	3.00	0.035	0.041	0.048	0.050	0.051	0.052
S-13	12.0	0.0	6.00	0.055	0.060	0.081	0.091	0.099	0.101
S-14	12.0	0.0	9.00	0.088	0.101	0.136	0.153	0.169	0.184
S-15	12.0	0.0	12.00	0.194	0.225	0.304	0.339	0.369	0.399

The resulting values for the coefficient C for each of the ballasts tested are given in Table 15. The results given in Table 15 show that all of the methods used were in very close agreement for the revenue site ballasts and for the staged tests done on the FAST granite.

Since the four methods for determination of the coefficient C gave consistent results for the revenue site ballasts and the granite ballast tested most recently, the average values given in Table 15 were taken to be representative of those materials. These soil constants and the measured first cycle strains were used to calculate strains from Eq. 16 for comparison with the measured strains after 10,000 cycles for the revenue site ballasts and after 1000 cycles for the FAST granite. As indicated in Fig. 8, the agreement is very good.

Variable-Amplitude Tests

The results for the staged tests at effective confining pressures of $\bar{\sigma}_3 = 3$, 6 and 12 psi are shown in Figs. 9, 10 and 11, respectively. The magnitude and sequence of the applied stresses used in these variable-amplitude tests are given in Tables 4 and 5. Several very clear trends were evident for the staged test results. They were:

1. For a given effective cell pressure, the permanent strain at the first cycle increased as the applied vertical deviator stress increased.

2. For a given applied vertical deviator stress, the permanent strain at the first cycle decreased as the effective confining pressure increased.

3. When the deviator stresses were increased to values greater than any past maximum values, the permanent strains continued to increase.

4. When the deviator stresses were reduced to values less than any past maximum values, negligible changes in permanent strain resulted with additional cycling.

5. Partial unloadings resulted in negligible increases in permanent strains with cycles.

6. For any given effective confining pressure, the sequence of applied stresses did not affect the final values of permanent strain so long as the total number of cycles at each stress level was held constant.

Items 1 through 3 listed above are well known and easily understood. Items 4 through 6 deserve attention. The experimental results showed that the maximum stress history of a sample controls future stress-strain response. These ballast test results imply that the maximum wheel loads for a given maintenance life cycle will control the amount of strain accumulation.

The observation that maximum load controls future cyclic deformations has been reported for other ballast materials [21,27]. However, past research on ballast behavior under repeated load [27] and other granular materials [30] has indicated that the sequence of applied loads does have an effect on the total permanent strain developed, and that a sequence beginning with high loads will result in larger final permanent strains. This was not evident from the staged test results presented here, because the terminal permanent strains were not related to the sequence of applied stresses. Considering the accepted variability of sample preparation techniques and general ballast behavior, the strains measured at the end of all staged test series for similar effective confining stresses were in very close agreement.

The small amount of permanent strain accumulation associated with partial unloadings was also observed by Shenton [27] for ballast material.

Shear Stress Reversal Tests

The linear relationship between permanent vertical strain and log number

45

Table 15. Ballast Constants, C, for use in $\varepsilon_N = \varepsilon_1(1 + C \log N)$

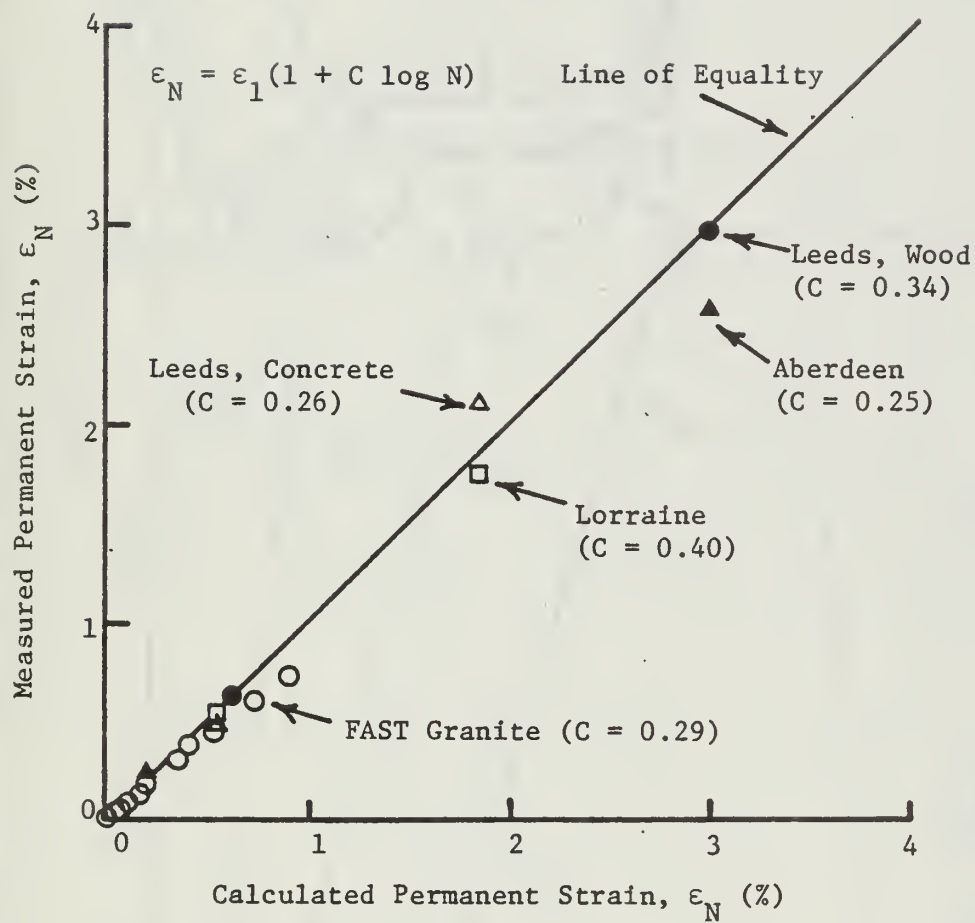| Method	Leeds Wood (Compacted)	Leeds Concrete (Compacted)	Lorraine (Compacted)	Aberdeen (Compacted)	FAST Granite (Compacted)
1 (ORE)	0.36	0.30	0.41	0.20	0.28
2	0.33	0.24	0.39	0.27	0.29
3	0.33	0.24	0.42	0.28	0.29
4	0.34	0.25	0.37	0.26	0.29
Average	0.34	0.26	0.40	0.25	0.29

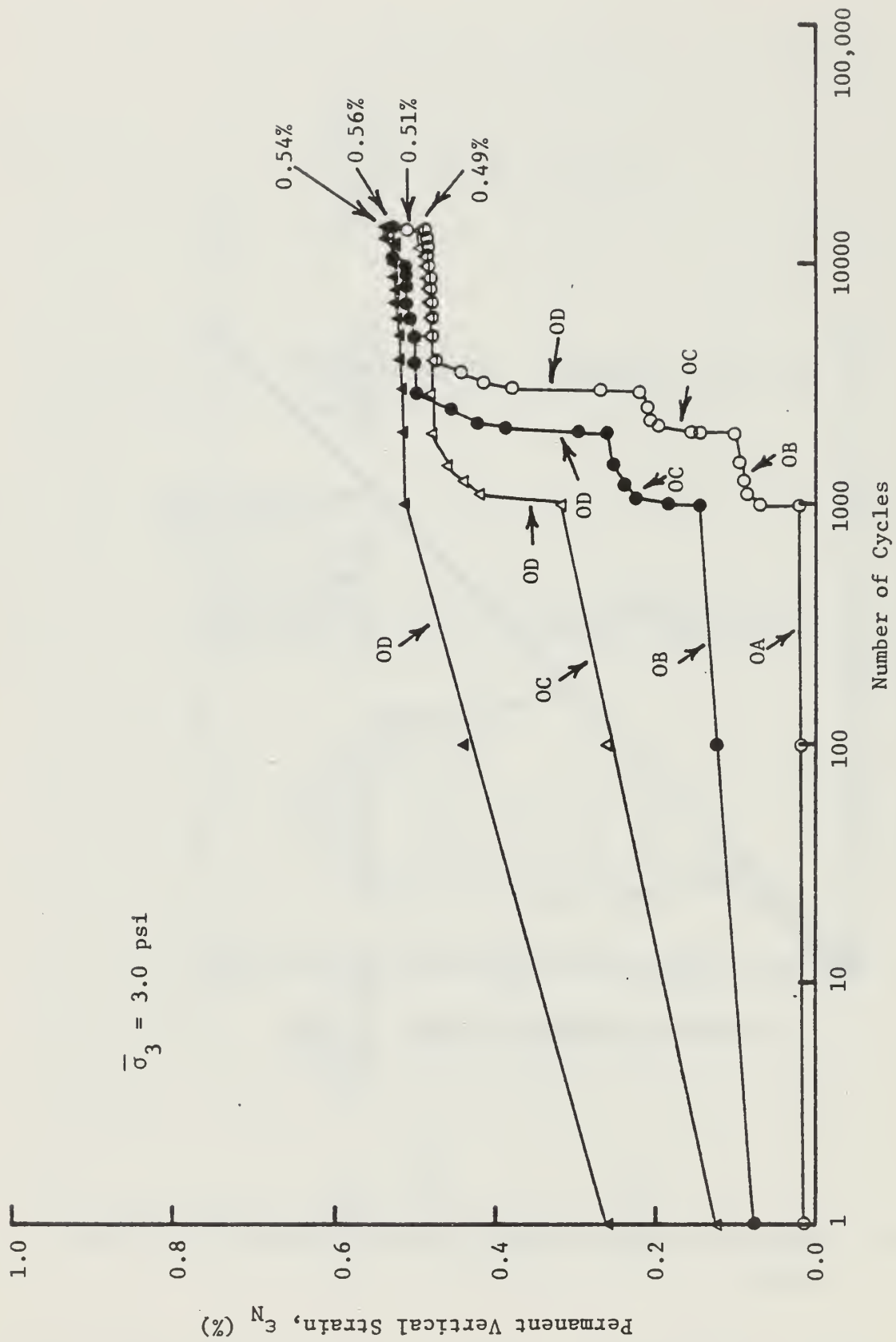Figure 8. Measured versus Calculated Permanent Strains from Triaxial Tests

Figure 9. Permanent Strain versus Number of Cycles for Staged Tests, 3 psi Confining Pressure
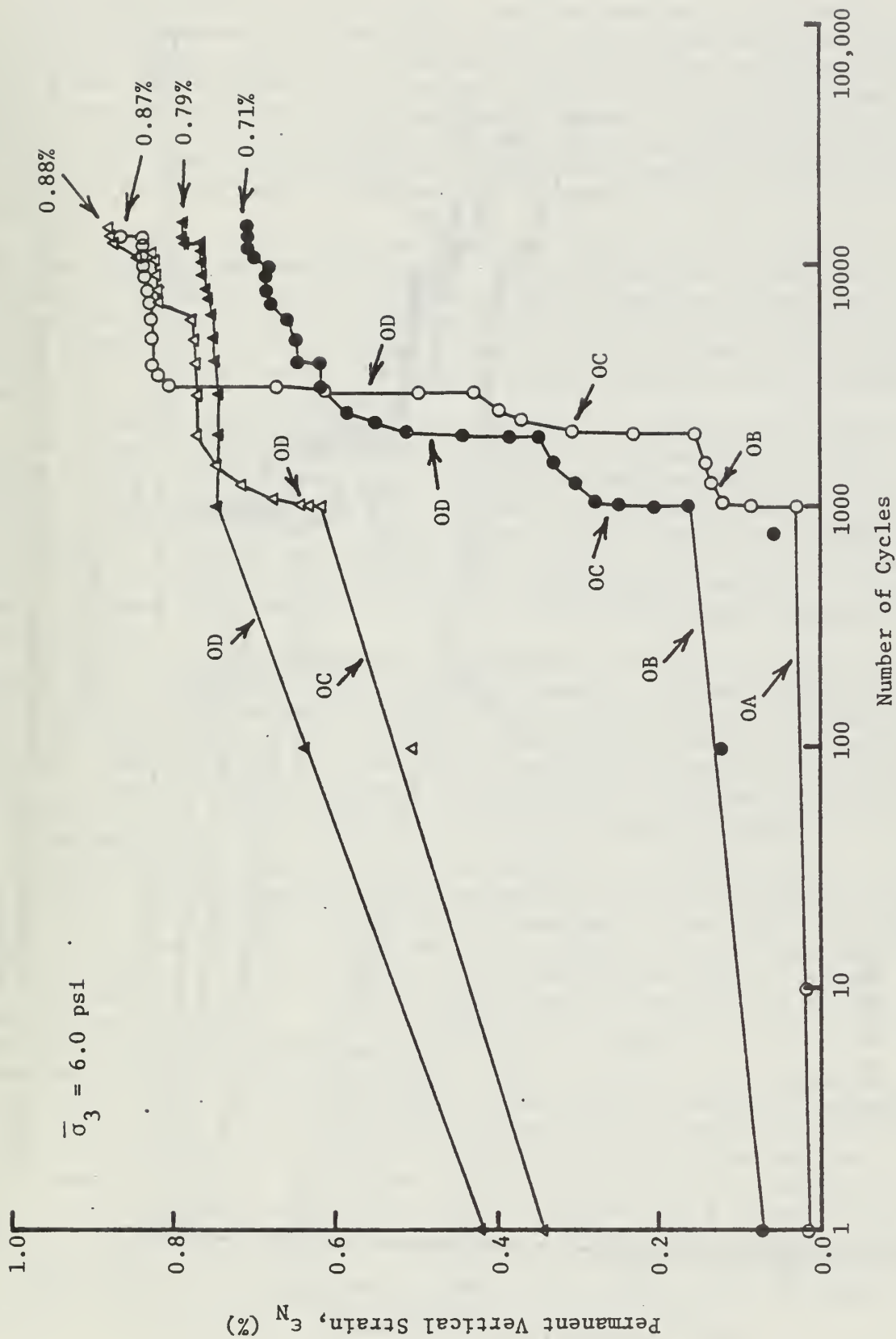
48

Figure 10. Permanent Strain versus Number of Cycles for Staged Tests, 6 psi Confining Pressure
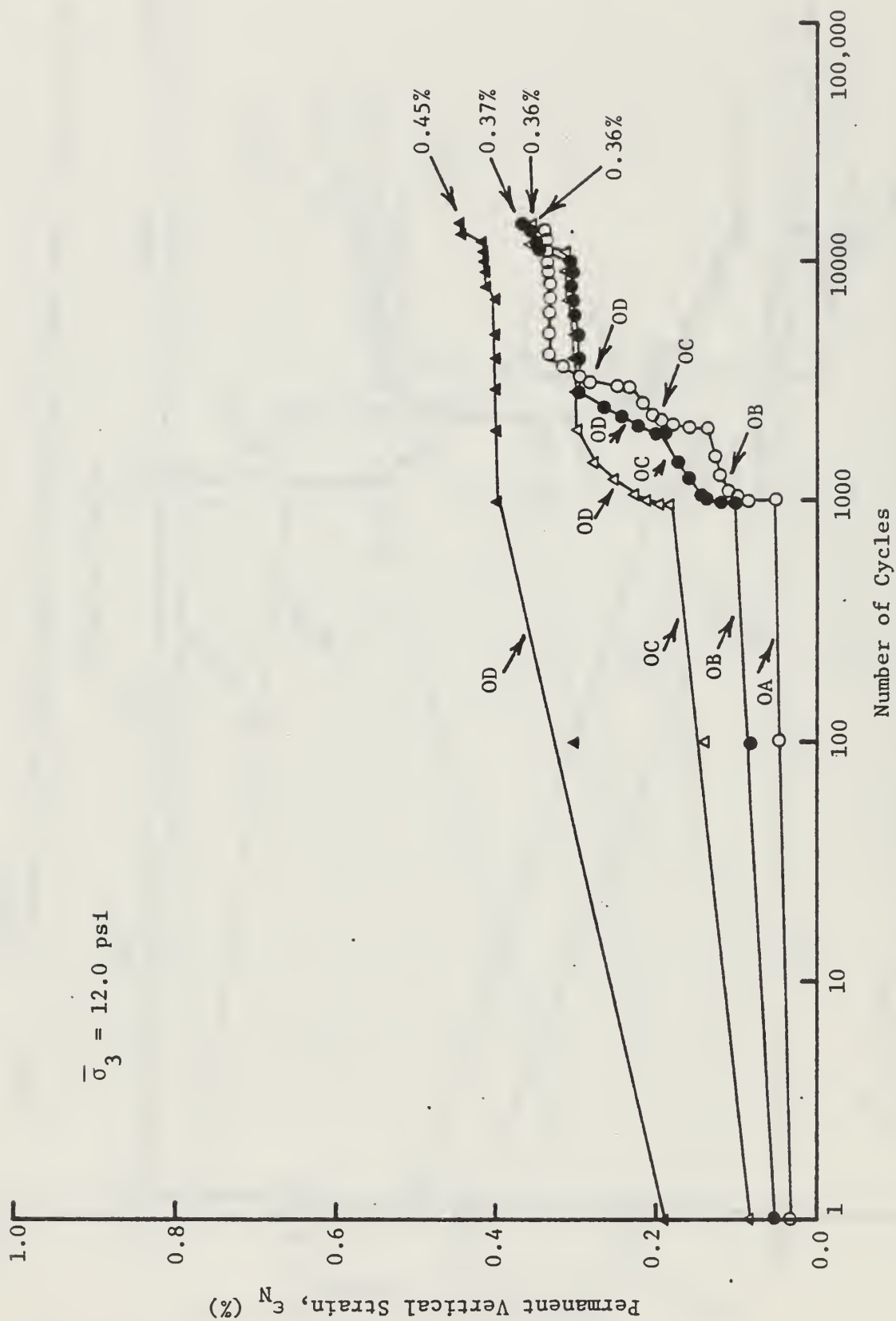
49

Figure 11. Permanent Strain versus Number of Cycles for Staged Tests, 12 psi Confining Pressure

50

of cycles was evident for these tests. The test samples all continued to de-
velop increasing amounts of compressive axial strain after the first cycle.
The general trends noted for the constant repeated stress tests with full un-
loading were also observed for the stress reversal tests. As effective con-
fining pressure increased, the accumulated permanent strains decreased for
constant values of q_{max} and Δq. For constant effective confining pressures
and equivalent levels of negative shear stress, the amount and rate of accu-
mulation of permanent strain increased as the compressive shear stress levels
increased.

The permanent strain developed after the first cycle of loading for tests
involving shear stress reversal was not as clearly defined as for the one-way
loading tests. The strain at N = 1 was in fact extensional (negative) for one
of the stress reversal tests. The sample did, however, still tend to compress
for the subsequent cycles. The explanation for the negative axial permanent
strains that could be developed for these stress reversal tests is clearly
shown in Fig. 12.

The permanent vertical strain developed due to compression loading fol-
lowed by unloading with shear stress reversal is dependent upon not only the
minimum negative shear stress, q_{min}, but also the maximum positive shear
stress. For the same level of q_{min}, the vertical permanent strain at the end
of the first cycle could be negative, zero, or positive, depending on
the magnitude of the applied positive shear stress, such as q_1 or q_2 shown on
Fig. 12. The permanent axial strain at N = 1 for stress reversal tests was
always less than that developed at N = 1 for the staged tests, which had no
stress reversal.

The rate of strain development with number of cycles was very clearly
affected by the existence of shear stress reversals. Figure 13 shows compari-
sons of tests having similar effective confining pressures and maximum posi-
tive shear stress, both with and without shear stress reversal. As previously
explained, the strains at N = 1 were always smaller for the stress reversal
tests. However, the rates of strain accumulation were very much larger for
the stress reversal series, although both types of test had positive rates of
strain accumulation.

It was shown previously that the slopes of the strain versus log N curves
for repeated loading without shear stress reversal were proportional to the
strain at the first cycle, ε_N, through the constant, C, and that C was unchan-
ged for all stress levels. This was not the case for the stress reversal
tests. The slopes of the ε_N versus log N curves for the stress reversal tests
were affected by both the ratio of cyclic shear stress, Δq, to maximum com-
pressive shear stress, q_{max}, and the stress ratio (q_{max}/q_f), where q_f is the
static compressive shear strength for the
prescribed effective confining pressure. The variation of the slopes of the
curves shown in Fig. 13 as a function of these stress parameters are shown in
Fig. 14. Note that $\Delta q/q_{max}$ equal to 1.0 represents the condition of full un-
loading without stress reversal discussed in the previous section. Fig-
ure 14 shows that as the compressive failure stress ratios and amounts of
stress reversal increase, the slopes of the ε_N versus log N curves increase
rapidly. The trends shown in Fig. 14 also support the observation from
the staged tests that the strain accumulation would decrease rapidly for par-
tial unloadings where $\Delta q/q_{max}$ is less than unity. This trend, although not
completely quantified, was also observed by Shenton [27].

Shear Stress,

$q = (\sigma_v - \sigma_h)/2$

(Compression)

$q_2 \longrightarrow$

$q_1 \longrightarrow$

$\varepsilon_{N=1}$

$\varepsilon_{N=1}$

(Extension)

Vertical Strain
(Compression)

q_{min}

$-q$ (Extension)
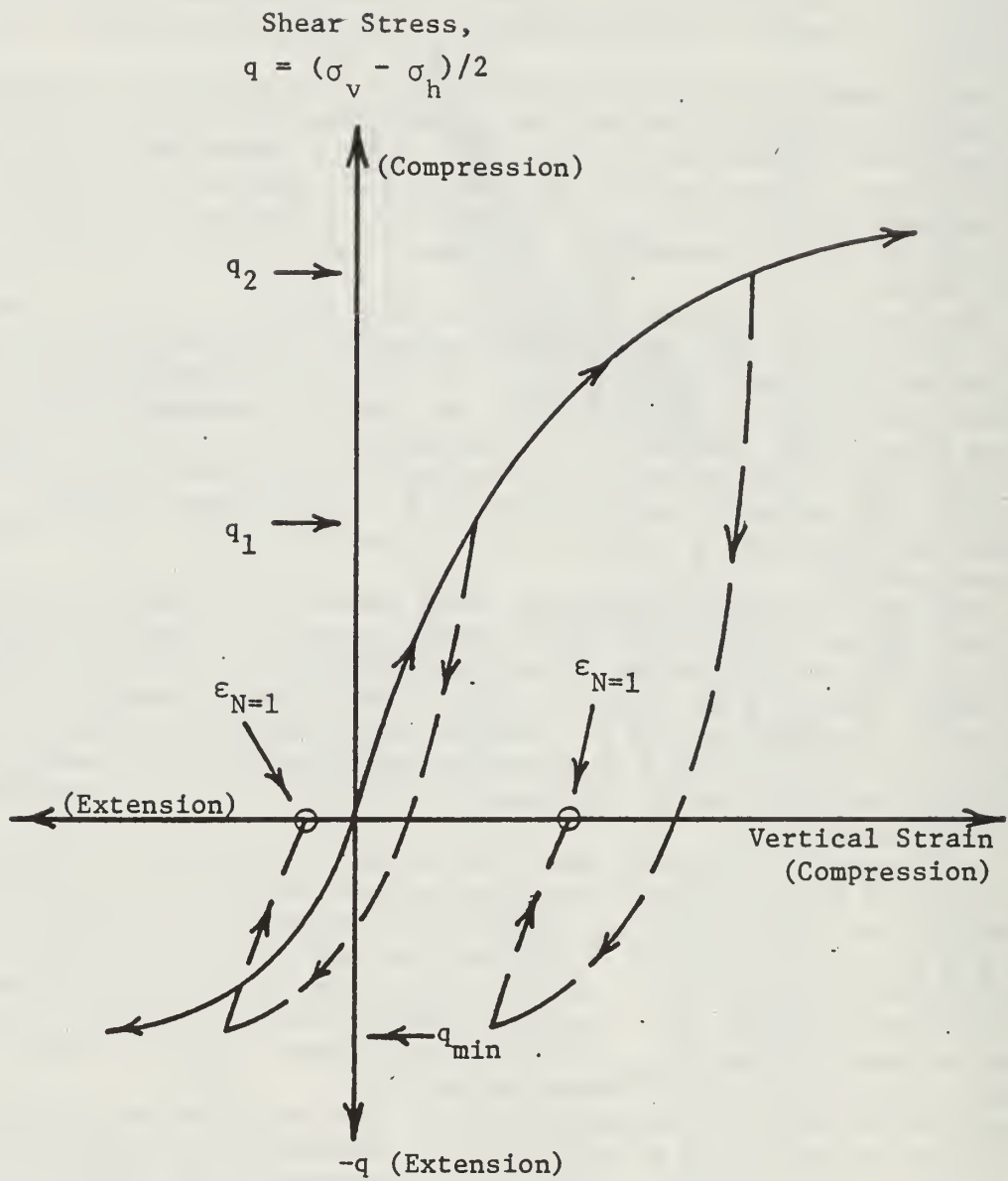
Figure 12. Representation of Stress-Strain Curves for Shear Stress Reversal

52

Figure 13.   Comparison of Strain Development Rates for Tests With and
             Without Stress Reversal

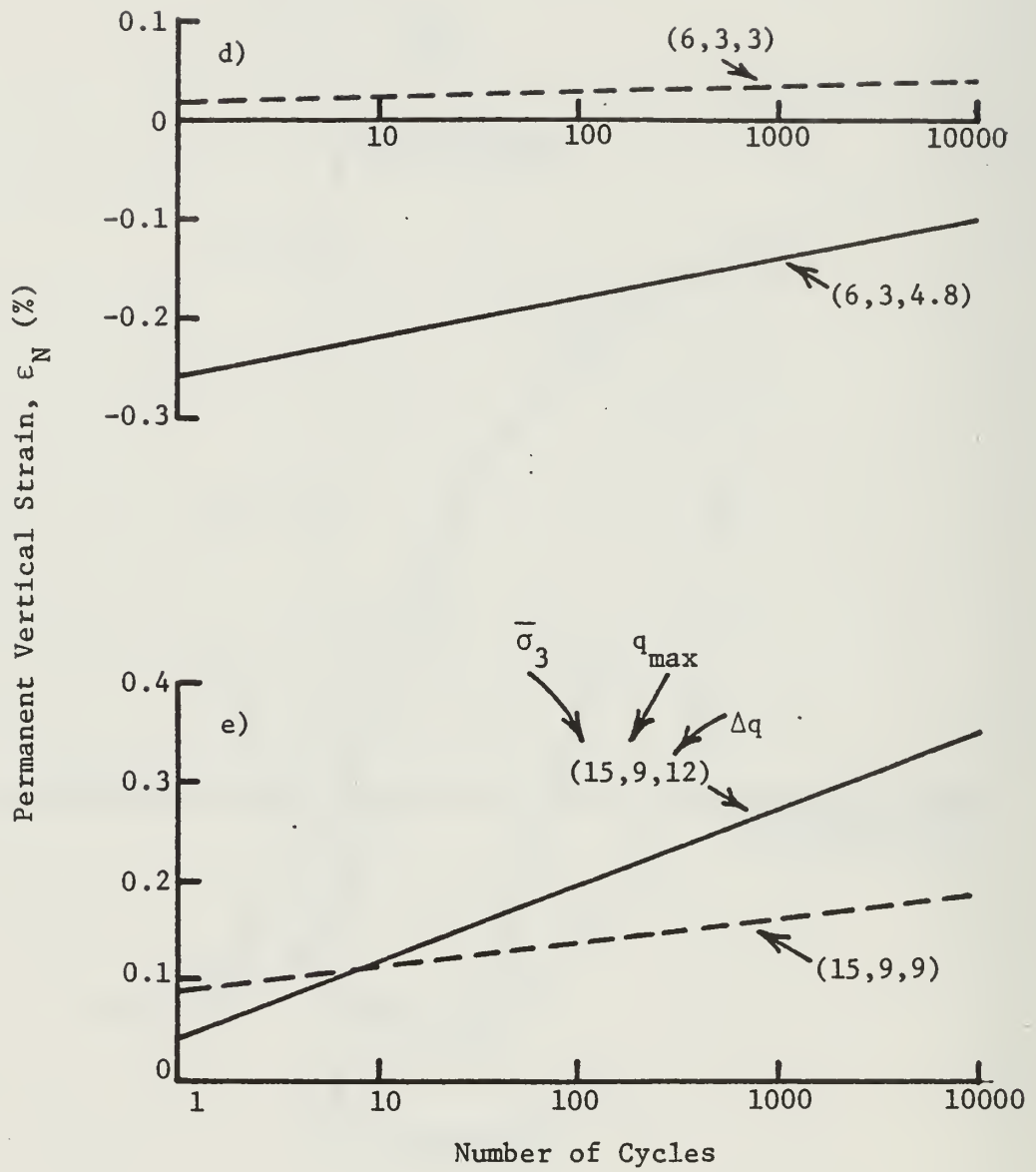Figure 13. (Continued) Comparison of Strain Development Rates for Tests With and Without Stress Reversal

54

$$0.0 < \frac{\Delta q}{q_{max}} < 1.0 \rightarrow \text{partial unloading}$$
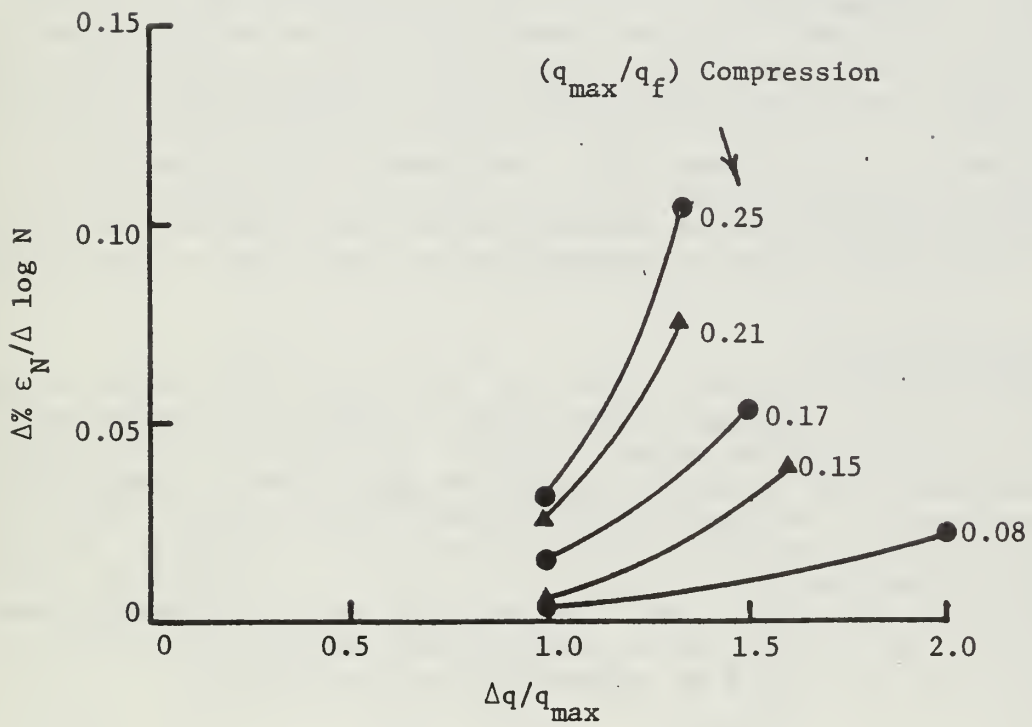
$$1.0 > \frac{\Delta q}{q_{max}} \rightarrow \text{shear stress reversal}$$

Figure 14. Rate of Strain Accumulation as a Function of Stress Parameters

55

3.6   Ballast Box Tests

General Description

In the laboratory box tests, the ballast was loaded vertically using a simulated section of tie. The test setup is illustrated in Fig. 15. The main objectives of these tests were to investigate the settlement characteristics of the ballast under field loading conditions, and to evaluate the horizontal stresses that develop beneath the tie segment. Details regarding the box construction, base support conditions, instrumentation and complete test results can be found in Ref. [31]. Only the results which are pertinent to analysis in this report will be given here.

The ballast box was constructed to represent a section of tie about 11 in. long located directly below a rail. The box was 24 in. long by 12 in. wide. The length was intended to represent one-half of the crib width on either side of the tie segment. The ballast depth was 12 in. below the base of the tie segment. A flexible bottom to simulate subgrade support was incorporated so that the deflection basin below the ballast layer could be represented. The box side and end panels were instrumented so that the lateral stresses in the ballast could be estimated under both loaded and unloaded conditions. The panel numbers and locations are shown on Fig. 15. The physical state of the ballast prior to the cyclic loadings was representative of the conditions found under the tie rail seat after a maintenance tamping operation.

The load applied to the 11.5-in. by 9-in. tie segment was 4000 lb. The stress at the base of the tie segment from this load was equivalent to the stress at the base of the tie beneath the rail seat due to a 33-kip wheel load.

Permanent Settlement

The permanent settlement trends for these tests were similar to those observed in the repeated load triaxial tests in that the settlement was linearly related to the log of the number of cycles. The form of the expression for the settlement of the tie for these ballast box experiments was identical to that developed for the repeated load triaxial tests (Eq. 16), except that d_1 and d_N were substituted for ε_1 and ε_N, where d_1 and d_N were the residual vertical deflections of the tie after the 1st and Nth cycles, respectively. Tests on both compacted and uncompacted samples indicated that the rates of settlement for these two physical states were different, but still both could be expressed by the relationship

$$d_N = d_1 (1 + C_b \log N) \quad , \tag{17}$$

where C_b is the settlement coefficient for the box tests derived the same way as for the triaxial tests. The coefficients determined for the compacted and uncompacted ballast samples were

Compacted	Uncompacted
$C_{bc} = 0.35$	$C_{bu} = 0.63$.

The coefficient C_{bc} for the compacted samples was in general agreement with the results found for the compacted ballast triaxial tests done on the revenue site and FAST granite ballasts. The uncompacted coefficient, C_{bu}, was about double the compacted coefficient.
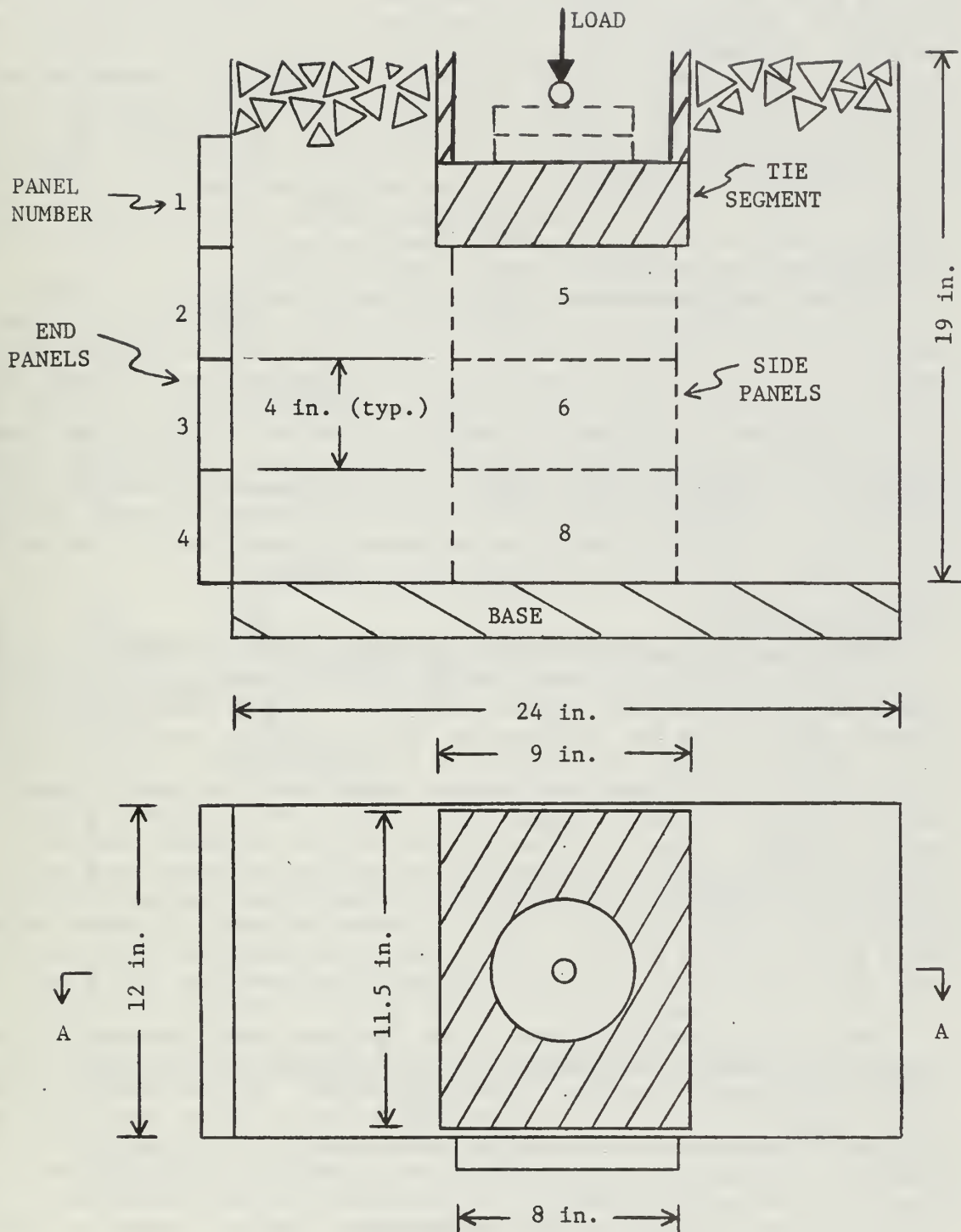
Figure 15. Box Test Apparatus

57

The physical state of the ballast was assessed at the end of these cyclic box tests. Both ballast density and plate load tests showed increases comparable to those measured from the field tests. The ballast densities increased by about 8% in the box tests. The changes between the pre- and post-maintenance ballast densities for the under-tie locations at the field sites were about 9 to 12%. Plate bearing resistances at 0.05-in. deformation were compared for the box tests and the field sites. The field sites showed changes in the range of 400 to 1200% due to traffic effects. The increases in plate load resistance measured in the box tests were on the order of 800% due to the cyclic loading. The changes in ballast density and bearing stiffness measured in the box tests indicated that the field loading conditions were being approximately simulated, and the field repeated-load mechanisms of ballast compaction were being reproduced in these laboratory tests.

Staged loading tests were also done using the ballast box device. Loads of 2000, 4000 and 6000 lb were applied in various sequences. The 4000-lb load resulted in an applied stress at the base of the tie segment that was equivalent to the stress at the base of a tie beneath the rail seat due to a 33-kip wheel load, as determined using the GEOTRACK model. The 2000- and 6000-lb loads were selected as experimental values to demonstrate staged loading effects. The deformation trends for these tests were similar to those observed in the staged triaxial tests. The total amount of vertical deformation was found to be independent of the applied load sequence. Also, as in the triaxial tests, negligible additional permanent deformation resulted due to cycling of loads less than any maximum past load.

Horizontal Stresses

Estimates of stresses, strains and deflections for layered systems such as track and pavement are based upon an idealized continuum approach using either multilayer models, such as GEOTRACK, or finite element methods. In a layered system where the stiffness of the upper layer is greater than that of an underlying layer, all methods of analysis predict that the lower portions of the stiffer layer will develop significant incremental tensile stresses and strains. When the upper layer consists of an unbound granular layer, such as ballast, either a redistribution of these stresses must occur or the initial and therefore final stress state must be different than that predicted. These conclusions are physically rational since the unbound layer cannot sustain tensile stresses. The occurrence of tensile stresses in an unbound granular layer would result in very large inelastic deformations with each load application. Such large inelastic deformations under each load application are not observed in a stable, layered system such as track.

One of the primary purposes of the box tests was to measure the lateral stresses developed in a simplified layered system, with particular interest in the development of residual lateral stresses. It has been recognized that some residual lateral stress can develop in soils such as sands [32] and clays [33] due to compaction and previous load history, but the magnitudes of these residual stresses have not been fully described for such materials as ballast. Thus, the side and end panels of the ballast box were instrumented to provide a direct measure of the lateral stresses that developed under the simulated track loading conditions.

Typical measurements obtained from the side panels of the box are shown in Fig. 16. The results indicated that there was a rapid build-up of horizontal compressive stresses upon initial loading, and that high residual stresses developed after only one cycle of loading. Furthermore, the horizontal
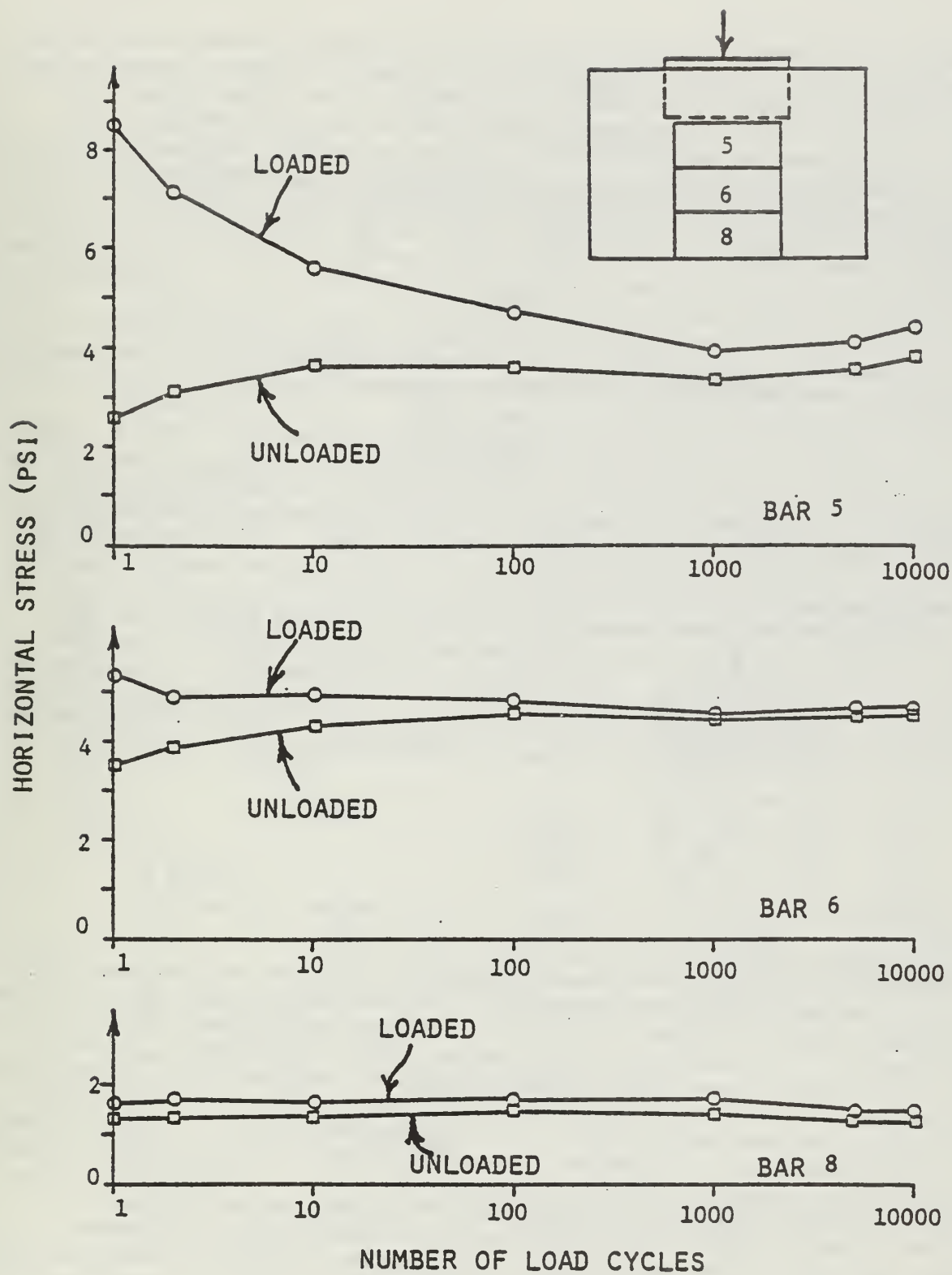
58

Figure 16. Horizontal Stresses on Side Panels [31]

59

stresses in the loaded state decreased and the residual stresses increased up to about 100 cycles. After 100 cycles, the horizontal stresses tended to stabilize and the unloaded value tended to converge to the loaded value. This means that the horizontal stresses tended to become constant during a load cycle. The maximum horizontal stresses acting on the side panels occurred at about the mid-depth of the ballast. The minimum horizontal stress on the side panels occurred near the base of the ballast layer. The box tests showed no evidence of tensile stress development in the ballast under loaded conditions. The stress measurements from the instrumented panels also showed no tendencies for reduction in the horizontal stresses in the ballast due to the applied vertical load on the simulated layered system.

The measured horizontal stresses for the end panels are shown in Fig. 17. Similar trends for rapid buildup of the lateral residual stresses were observed at the end of the ballast box. The maximum lateral stresses again occurred about 6 in. above the base of the ballast layer.

The variations of the horizontal stresses under load and under no applied vertical load as a function of the height above the box base are shown in Fig. 18. In general, the loaded condition produced higher lateral stresses for the first cycle. After about 100 cycles, there were only slight differences between the loaded and unloaded horizontal stress states. After 10,000 cycles, the residual stresses were almost identical to the stresses developed under full vertical load.

The measured residual horizontal stresses from these experiments were used to calculate values of K_o, the ratio of lateral to vertical effective stress at rest in the unloaded state. Theoretically, the maximum residual horizontal stress should be limited by the passive failure condition. The ratio of major principal stress at failure, $\overline{\sigma}_{1f}$, to minor principal stress at failure, $\overline{\sigma}_{3f}$, at the passive failure condition is defined by

$$\frac{\overline{\sigma}_{1f}}{\overline{\sigma}_{3f}} = K_o^{max} = K_p = \frac{1 + \sin\overline{\phi}}{1 - \sin\overline{\phi}} \quad , \tag{18}$$

for a strictly cohesionless material such as ballast.

The calculated K_o values, based on the box test side and end panel measurements, the unit weights of the ballast, and the static surcharge due to the tie segment weight are shown in Fig. 19. The very large values of K_o for the upper portion of the side zone would require a friction angle, $\overline{\phi}$, of about 56.5°, which might appear unreasonable. However, considering the curved failure envelopes, possible particle interlocking due to the ballast angularity, and the very low vertical stresses in the upper ballast zone, a friction angle of this magnitude may be possible. Certainly values of $K_o = 6$ would be possible, since the required friction angle would be only about 45.5°. The results of static triaxial tests have shown that this value would not be outside the possible range of values for low effective confining pressures. These experimental observations of the high residual lateral stresses and correspondingly high K_o values justified the use of such values in the subsequent GEOTRACK analyses for predicting track response.
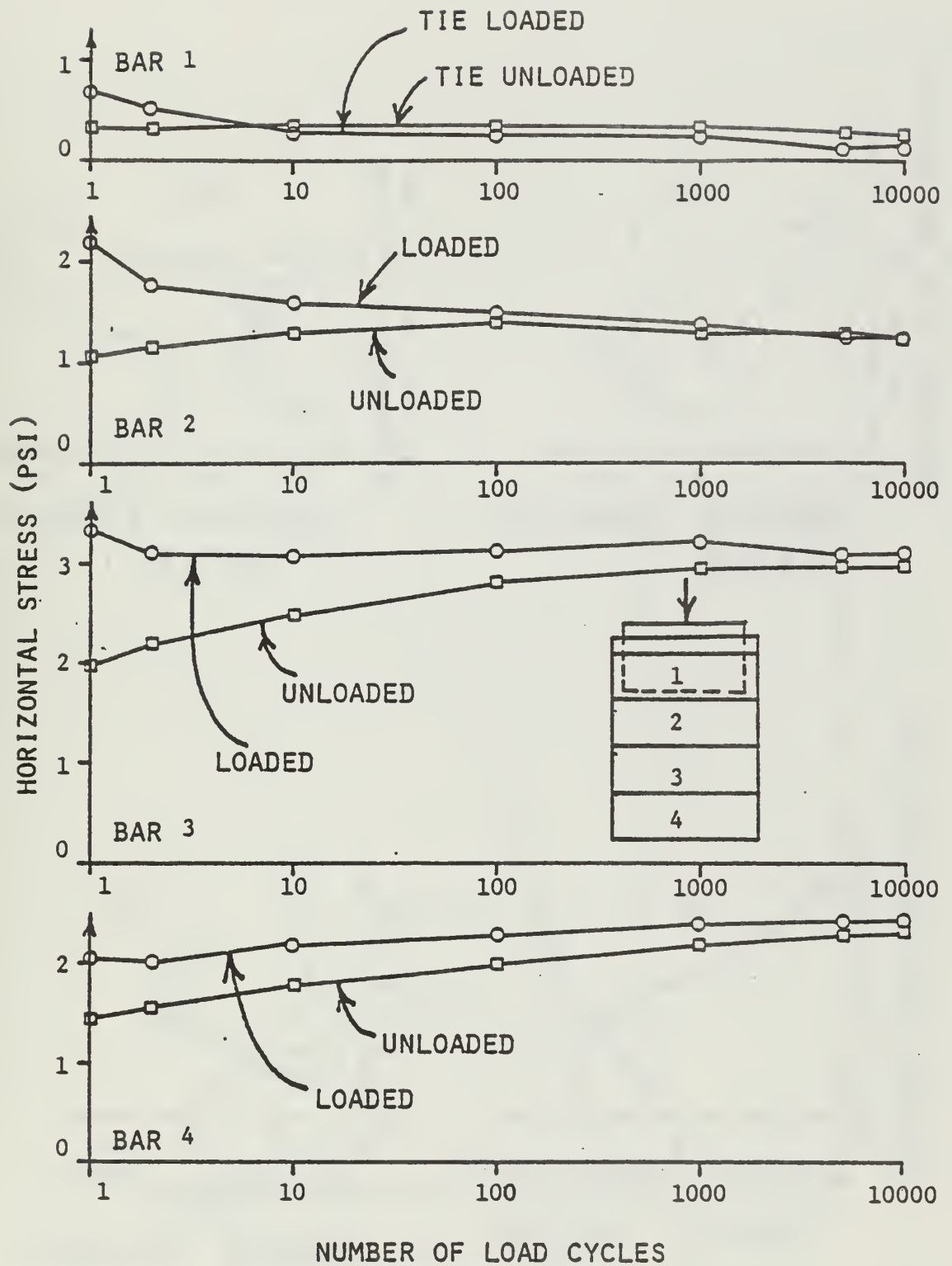
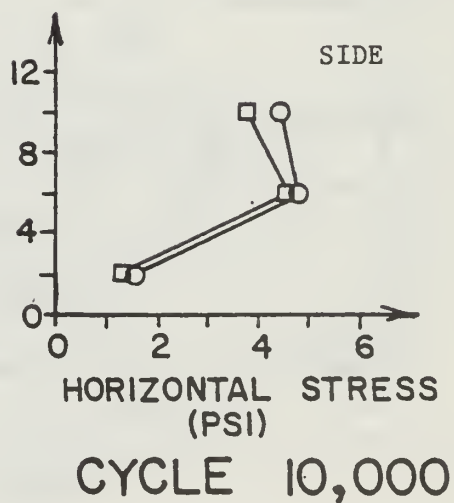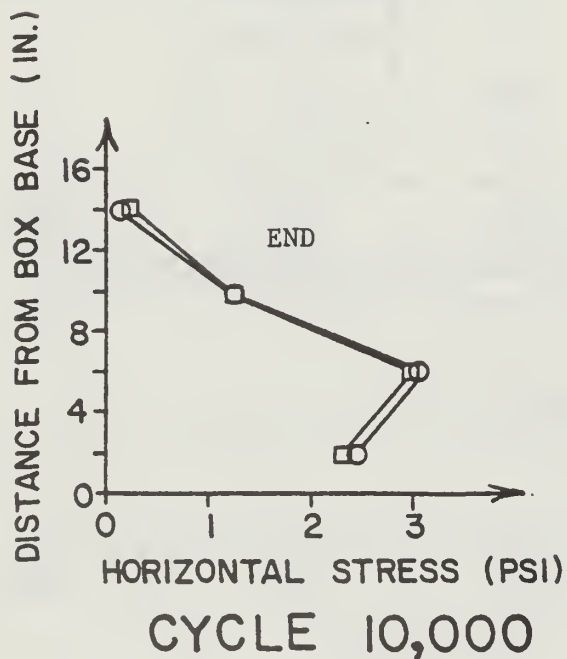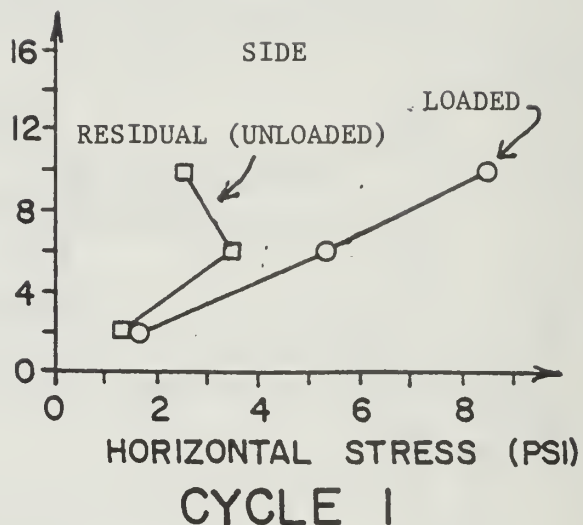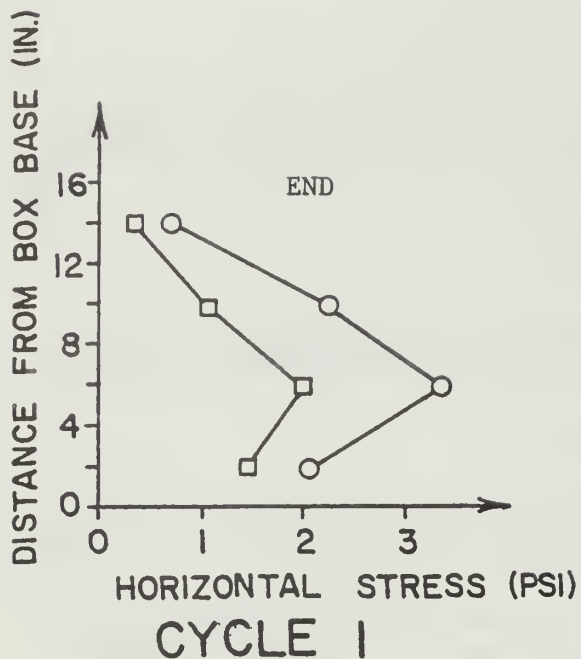Figure 17. Horizontal Stresses on End Panel [31]

61

Figure 18.   Measured Horizontal Stress Distribution from Ballast Box
             Experiments [31]

62
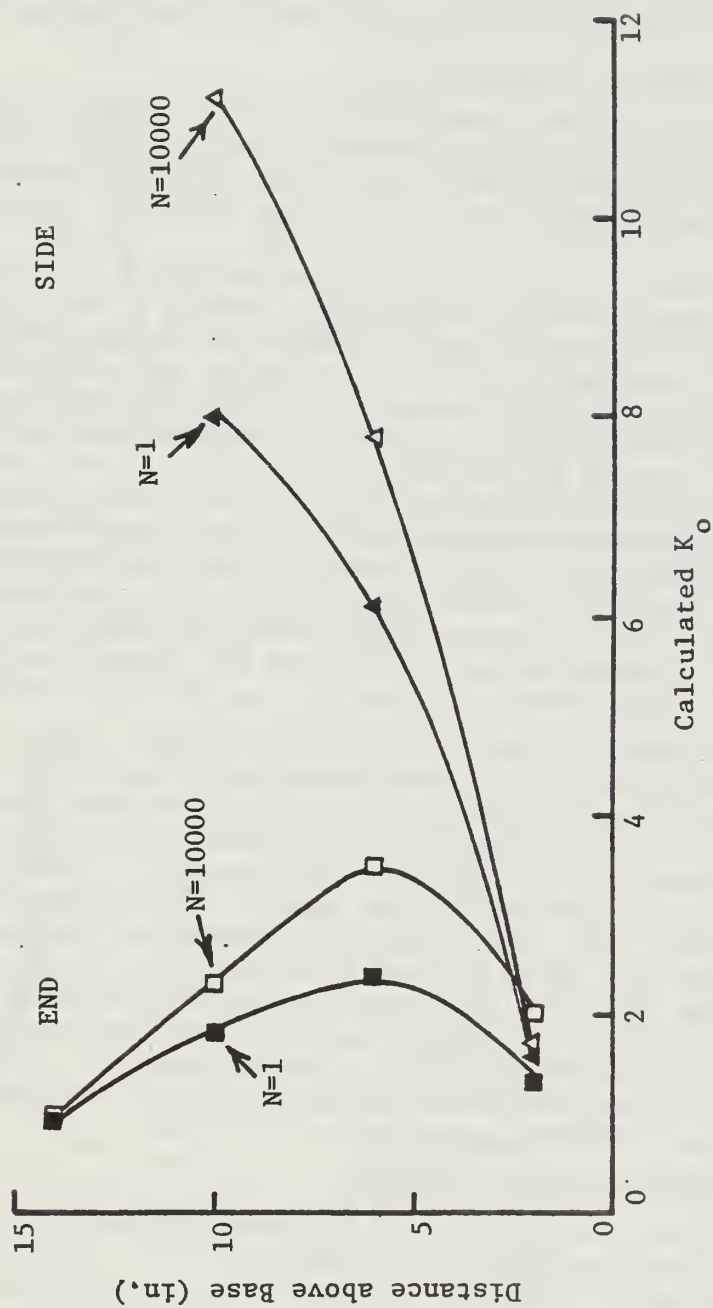
Figure 19. Variation of K_o as a Function of Depth from Box Experiments

3.7 Subgrade Material

Sampling Program

Along with the standard penetration (SPT) and cone penetration (CPT) tests previously described in Volume 1 [1], undisturbed soil samples (UDT) were taken at locations near the SPT locations, generally only a few ties away along the centerline of the track.

In addition to the samples recovered from the field sites, subgrade material was recovered from the FAST track. Undisturbed samples were not taken.

Repeated-Load Testing for Revenue Sites

Unconsolidated-undrained repeated-load triaxial tests, as well as static triaxial tests, were done on these recovered subgrade materials. The details regarding the triaxial testing and test results from the revenue service field sites, as well as index and classification test results, can be found in Ref. [34].

The stress states for the triaxial repeated-load tests on the samples recovered from the revenue service sites were intended to match the total stress states estimated at the sample location depths under representative train loadings. Three basic steps were necessary to define these stress states. The initial total vertical geostatic stresses at required depths were calculated based on the average soil densities as determined from the tube samples. The coefficient of lateral stress, K, defined as the ratio of total horizontal stress to total vertical stress, was assumed to be 0.75 for the revenue site subgrade materials. The incremental stresses due to multiple-axle train loadings were estimated using the GEOTRACK computer model. The three-dimensional stress states at various depths of interest were converted to axisymmetric constant confining pressure triaxial stress states using the method of stress invariants [22]. The individual stress paths used for these triaxial tests, shown in terms of $p = (\sigma_1+\sigma_3)/2$ and $q = (\sigma_1-\sigma_3)/2$, can be found in Refs. [34 and 35].

The resilient moduli values determined from these tests were correlated with the cone penetration and standard penetration test data. These correlations were necessary since it was not possible to perform a series of triaxial tests under a range of stress conditions for each of the identified soil strata and develop stress-dependent modular relationships. This is particularly true since remolding of the undisturbed samples would have significantly changed their properties. The cone soundings represented a continuous measure of the soil properties that could be used to extrapolate the properties measured in the lab to other depths. Based upon the correlations made and the test data presented in Refs. [34 and 35], ranges of resilient moduli values for the subgrade materials were determined. These ranges of resilient moduli are shown in Fig. 20 for the Leeds wood and concrete test sections and in Fig. 21 for the Lorraine and Aberdeen concrete test sections.

Repeated-Load Testing for FAST Subgrade

The FAST subgrade was also tested for resilient modulus parameters as well as for index properties and strength parameters. The subgrade at FAST is generally uniform throughout the test sections. The material was classified as a moderately uniform medium-to-fine silty sand. The Unified Soil Classification System (USCS) designation of the FAST subgrade was SM. The classification based on the American Association of State Highway and Transportation Officials (AASHTO) was A-2-4(0). Since undisturbed samples were not available, remolded specimens of the silty sand were prepared at moisture contents of 9.4 to 10.0
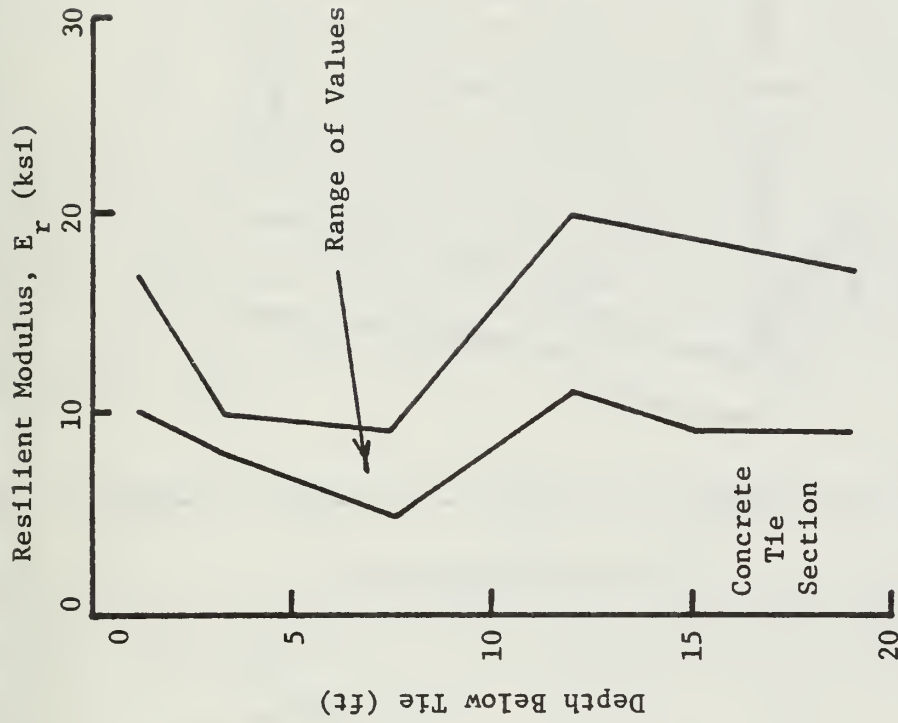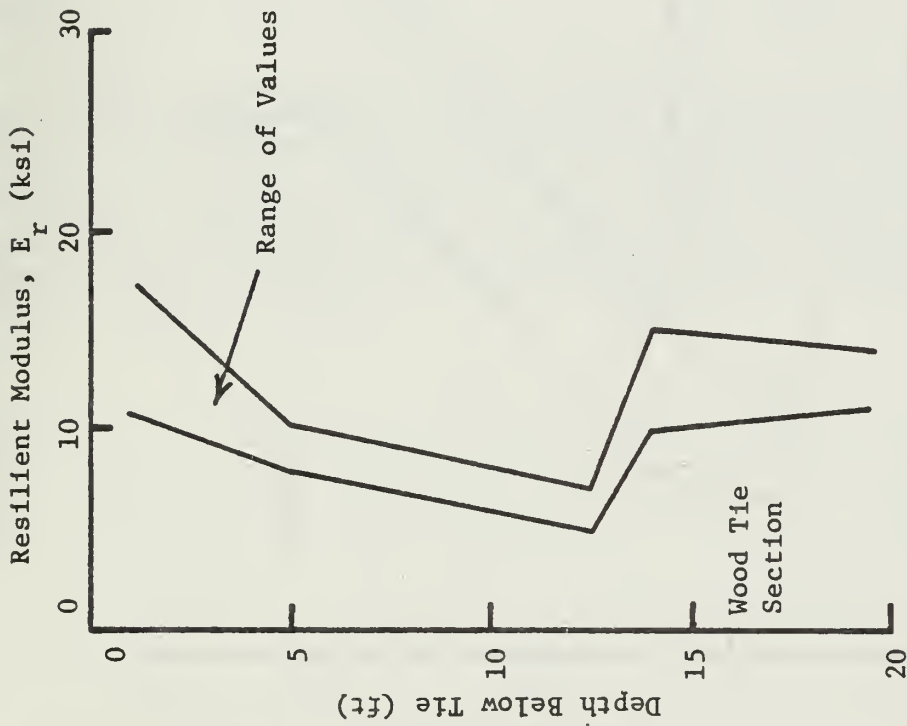
Figure 20. Resilient Modulus versus Depth for Leeds Wood and Concrete Tie Sections
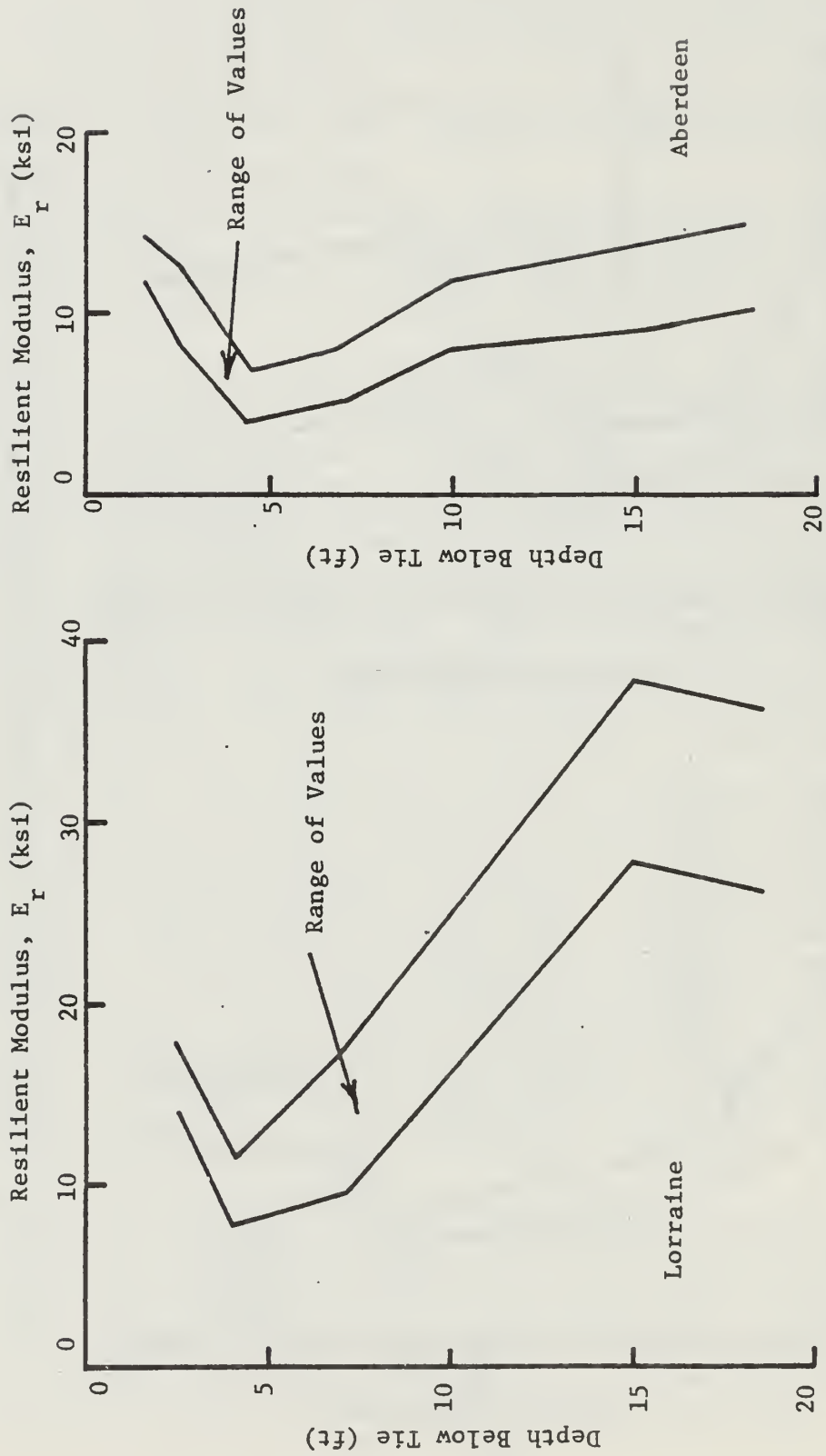
Figure 21. Resilient Modulus versus Depth for Lorraine and Aberdeen

percent.

Two methods were used to prepare FAST subgrade soil samples. The first sample type was made using a Harvard miniature compaction mold. These samples had dry unit weights, γ_d, of approximately 124 pcf (101% AASHTO T-99). The other sample type was made using a specially fabricated sample mold and using a preparation technique similar to that described by Ladd [36] with which the soil density state could be controlled. The resulting dry unit weights, γ_d, using the controlled compaction technique were 112 pcf (91% AASHTO T-99). All soil samples had length-to-diameter ratios of 2.5:1. Specific details regarding testing procedures, index test results, and strength parameters for the FAST subgrade are given in Ref. [37].

The results from the FAST subgrade tests indicate that the type of compaction used to prepare samples can have an effect on the measured resilient moduli values. Samples prepared using the undercompaction method resulted in generally higher moduli than those prepared using the Harvard miniature method. However, the data from both of these methods were combined and used to determine the modulus coefficient, K_1, and modulus exponent, K_2, for the following resilient formulation:

$$E_r = K_1 P_a \left(\frac{\Theta}{P_a}\right)^{K_2} . \tag{19}$$

A vibratory method of compaction was used to prepare the subgrade samples tested in Ref. [17]. Values for K_1 and K_2 were also obtained for the data from this source. The resulting parameters are as follows:

Source	K_1	K_2
Stewart	877	1.10
Thompson [17]	654	1.08

The main difference is in the coefficient of K_1.

A possible explanation for this difference is that the resilient moduli values taken after 40,000 cycles were used from the tests in this study, whereas the values reported in Ref. [17] were based on staged test results taken after 5000-load repetitions following a stress state change. It was previously shown that single stage testing generally results in increasing modulus with increasing number of cycles, but staged testing does not show a continuous increase with number of cycles.

CHAPTER 4. TRACK MODULUS

4.1 Introduction

The use of track modulus for assessing track performance is common in the railroad industry. The theoretical formulation of track modulus is based on the assumption that the rail acts as a beam continuously supported on an elastic foundation. The track modulus is defined as the supporting force per unit length of rail per unit deflection in the track system. The resulting equation for track modulus is

$$
u = \tfrac{1}{4} \sqrt[3]{\left(\frac{P}{\delta}\right)^4 \cdot \frac{1}{EI}} \quad ,
\tag{20}
$$

where u is the track modulus (units = F/L/L),
    P is the applied load (units = F),
    δ is the vertical rail deflection (units = L), and
    EI is the rail bending stiffness (units = FL^2).

An important difference between the actual track support and the idealized formulation of a rail on an elastic support is that the rail load is actually applied to the foundation through discrete supports, which are the ties, rather than through support distributed along the track foundation. Another difference, for concrete tie track systems, is the inclusion of flexible tie pads between the rails and the tie rail seats. Even though these differences exist between the actual track structure and the theoretical formulation, the track modulus has historically been used as a measure of track quality. Further details on the historical development and interpretation of track modulus can be found in Refs. [38 and 39].

This chapter will present the track structure and foundation properties selected for input into the GEOTRACK program in order to predict the track modulus at each of the revenue field sites. These predictions will be compared with field measurements, and the trends will be discussed.

4.2 Selection of Parameters

The GEOTRACK model [40] was used to determine elastic track deflections for predicting values of track modulus for the revenue field sites. The GEO-TRACK computer program is a three-dimensional, multi-layer model for determining the elastic response of the track structure, using stress-dependent properties for the ballast, subballast, and subgrade materials. The output of the program provides rail seat loads, tie-ballast reactions, tie and rail deflections, and tie and rail bending moments. In addition, the output provides vertical displacements and the complete three-dimensional stress state at selected locations in the ballast, subballast and subgrade. The validity of this model for evaluating the resilient response of track was established by comparing measured foundation responses obtained from FAST instrumentation with predictions made using the GEOTRACK model. Details regarding the model validation, measured FAST foundation responses, and the results of parametric studies

68

done using the GEOTRACK model can be found in Refs. [41 and 42].

In order to make determinations of the elastic responses of the revenue sites, the structural and foundation properties were determined for each of the sites. The structural properties are given in Table 2. Figures 22 to 25 show the ballast and subgrade layer divisions and properties.

The shear stress-resilient strain formulation developed in Chapter 3 was used to characterize the stress-dependent resilient moduli for these sites. The other ballast parameter values are shown in Figs. 22 to 25.

The subgrade layer properties used for the GEOTRACK analyses were chosen based on the results shown in Figs. 20 and 21. Layer divisions for the sub-grades were made (Figs. 22 to 25) where there appeared to be significant changes in the measured resilient properties. The average resilient modulus for each subgrade layer was used as the representative value for the layer. The moduli for the subgrade layers were held constant, since stress-state-dependent relationships were not available for the subgrade. The values of total unit weight were determined from the subgrade samples recovered from the un-disturbed tube sampling. The values of Poisson's ratio used for the subgrade were based upon static triaxial tests and were generally very close to 0.5. The ratio of lateral to vertical stress, $K = 0.75$, was estimated from the soil conditions as a reasonable value for the subgrade layers. An exception to these values was that a $K_o = 2$ value was used for the upper granular subgrade at the Leeds sites.

The parameter K_o is defined as the ratio of lateral effective stress to vertical effective stress in the granular layers under the condition of zero lateral strain. The values of $K_o = 4$ to 6 in the upper granular layers may appear to be unusually high. However, these values were based upon experimental observations of ballast behavior in a laboratory ballast box de-vice developed for simulating field conditions.

4.3 Comparison with Field Measurements

Measurements of track vertical load-deflection response were made at each of the revenue field sites by Battelle-Columbus Laboratories (BCL). For the test, a point load of known magnitude was simultaneously applied to both rails, using vertical hydraulic jacks reacting against a loaded freight car. Rail de-flections were measured by sighting a steel scale with a surveyor's theodolite. The scale was attached to the rail. Seven to ten measurements at random tie locations were made to assess the variability in the load-deformation respon-ses within the track sections. These measurements were made both before and after the maintenance operations to see what differences in track support re-sulted from the surfacing operation.

Track load-deflection measurements were made at 7 to 10 tie locations at each site. The measured averages and standard deviations for the pre- and post-maintenance load-deflection curves were given in Volume 1 [1]. A small amount of slack between the bottom of the tie and the top of the ballast layer may have contributed to the nonlinear response in the initial portion of the load-deflection curves. Most of this initial slack was assumed to have been eliminated after about a 6-kip load was applied. To minimize this effect, the track moduli values used for this comparison were calculated for the 6- to 30-kip load range.

The mean track moduli measurements and estimates of the standard devia-tion were made using the mean load-deflection curves and the deflections at ±1 standard deviation, both taken at the 6- and 30-kip load levels. The

Bottom of Tie

0 ── ───

K_o = 6.0 ν = 0.3
γ_d = 116 pcf   9 in. } BALLAST

───

E_r = 11500 psi

ν = 0.40

2 ──
γ_d = 133 pcf

K_o = 2.0   50 in.   SUBGRADE

4 ──

───

E_r = 7000 psi

ν = 0.47

6 ──
γ_T = 120 pcf

K = 0.75   90 in.

12 ──

───

E_r = 10000 psi
ν = 0.49
γ_T = 132 pcf   ∞
14 ── K = 0.75

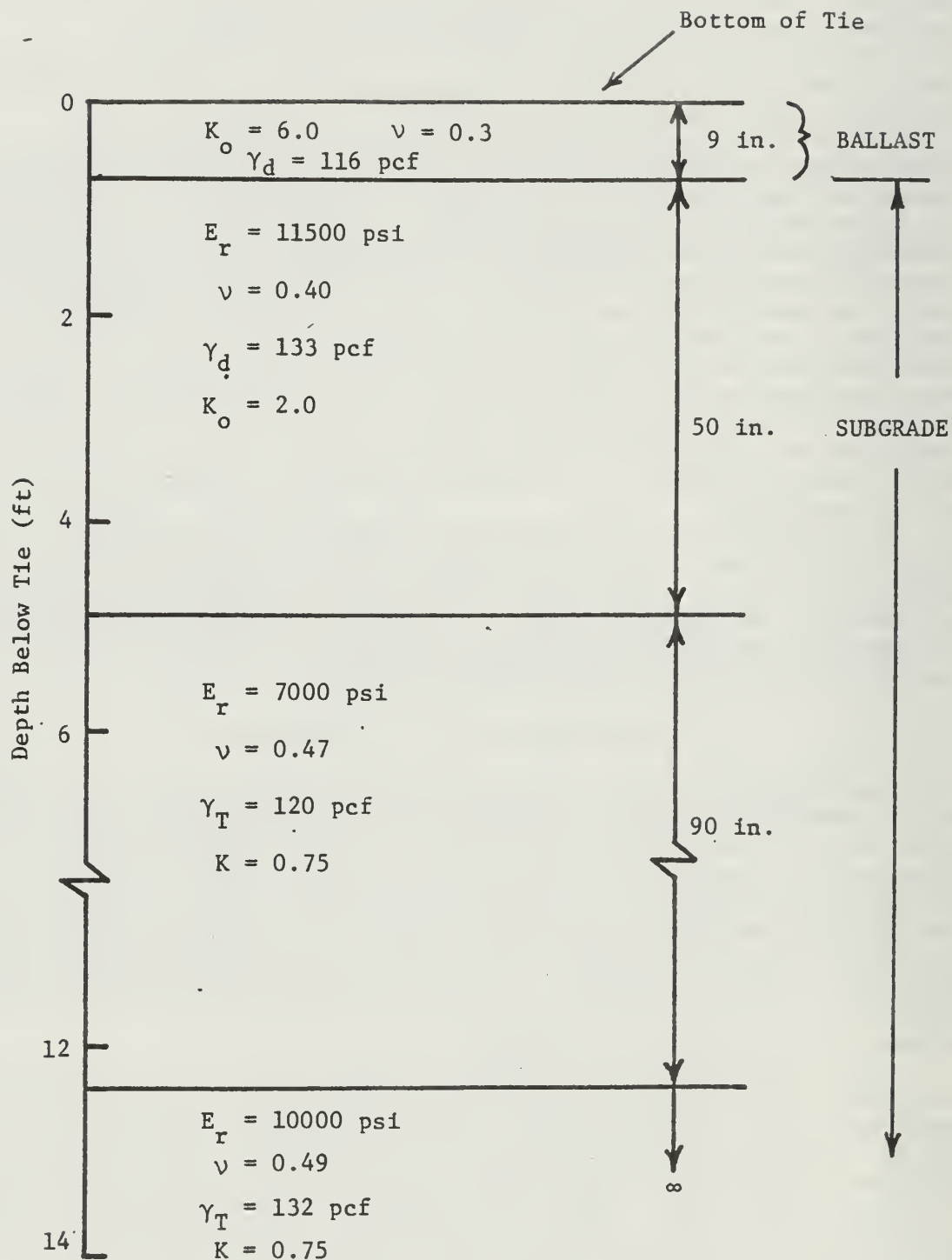Depth Below Tie (ft)

Figure 22.   Layer Description for Leeds Wood Tie Section
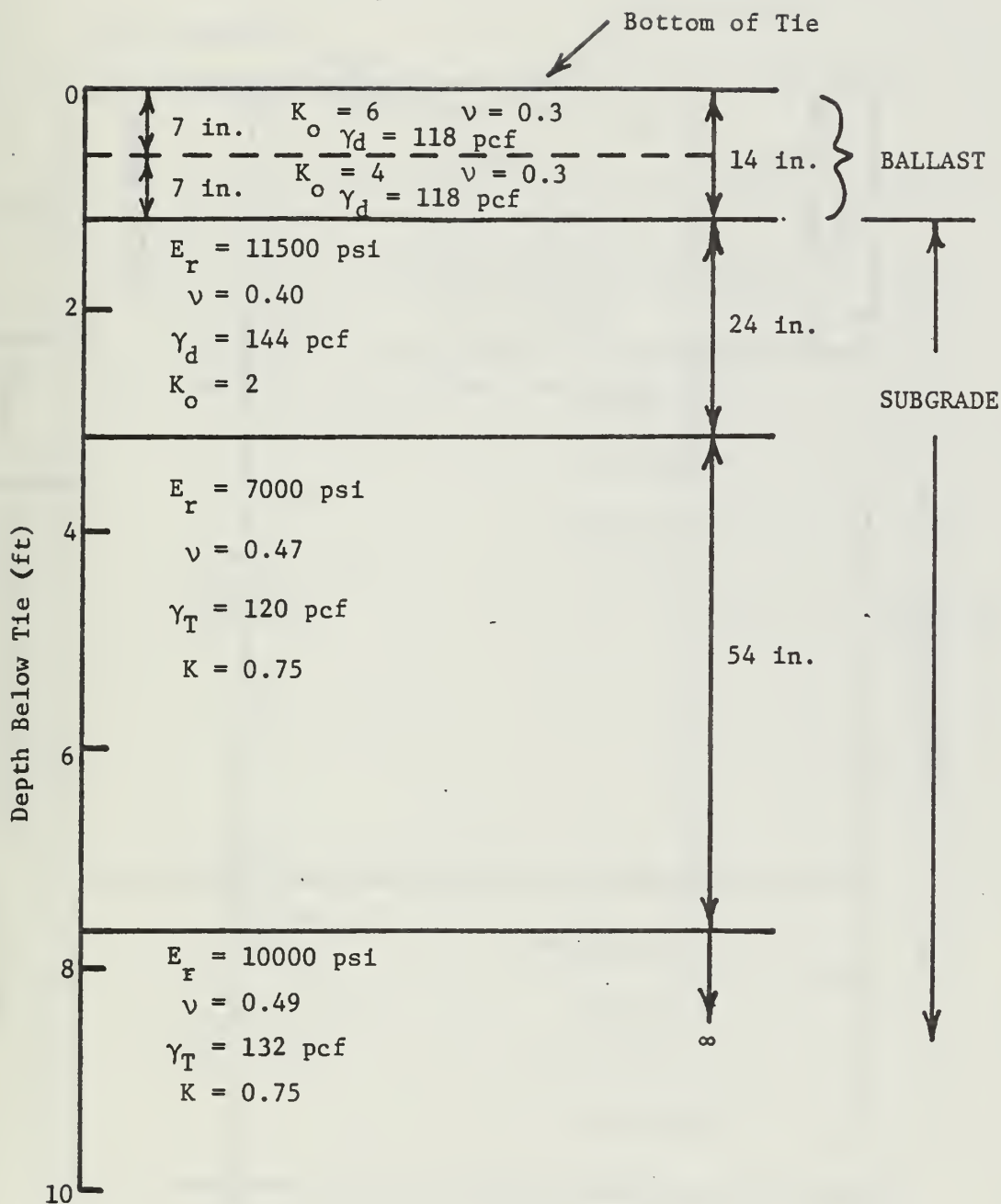
Figure 23.   Layer Description for Leeds Concrete
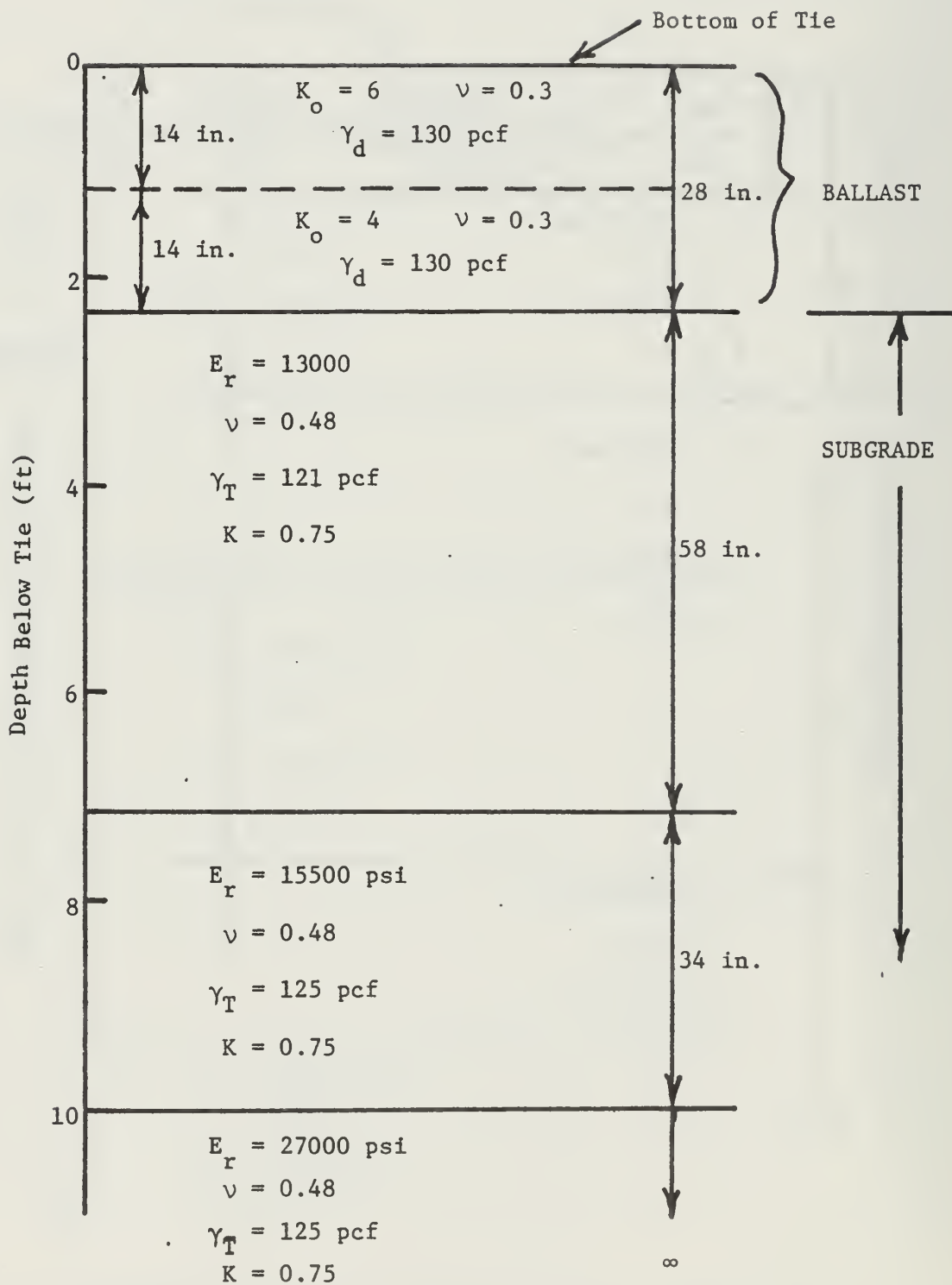   Tie Section
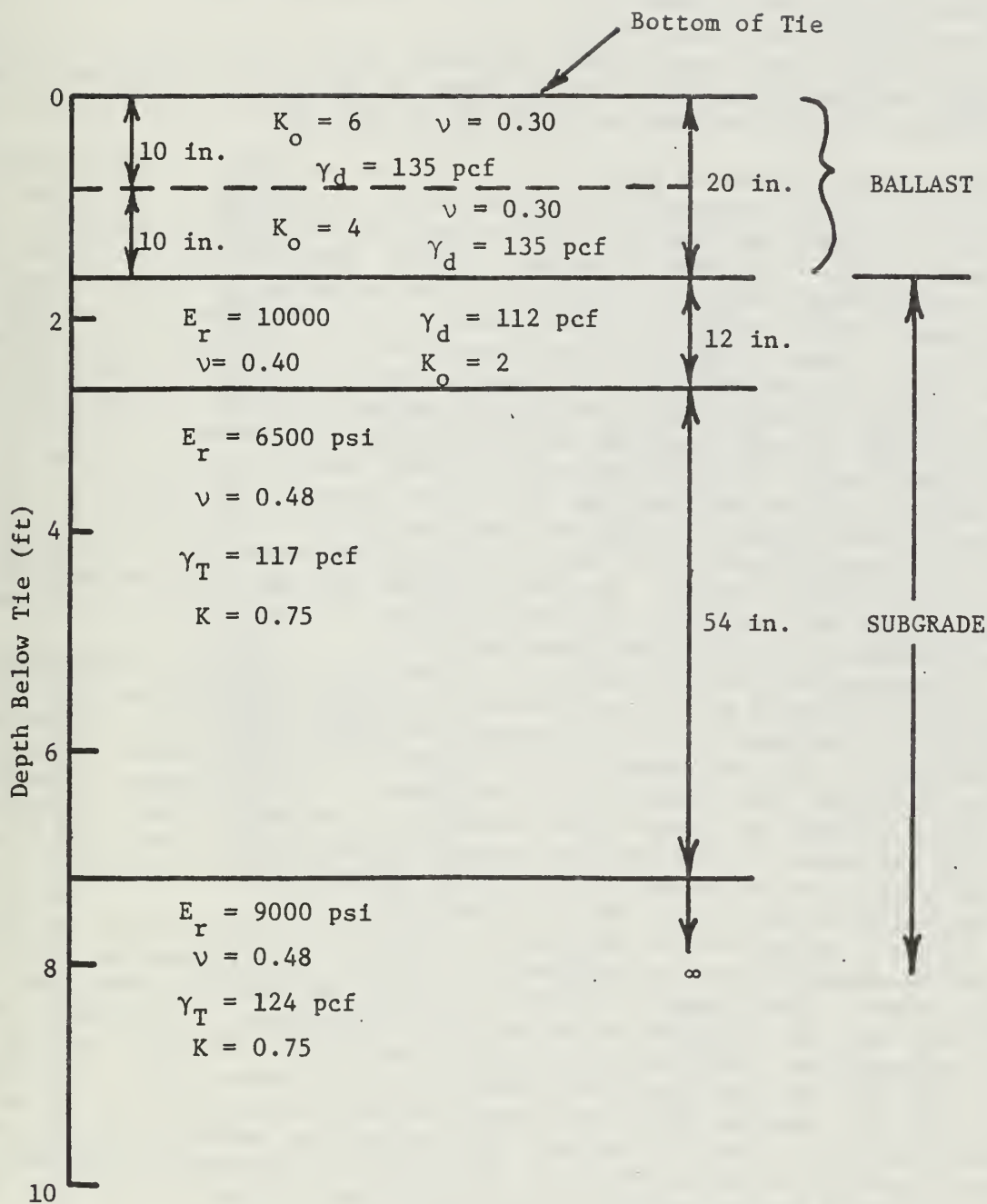
Figure 24. Layer Description for Lorraine

72

Figure 25. Layer Description for Aberdeen

73

standard deviations of track modulus calculated in this way are not symmetrical about the mean value, and slightly underestimate the actual standard deviations. For the purposes addressed in this chapter, the standard deviations of the track moduli values will refer to the limits calculated, based on the standard deviations of the rail deflections.

To determine track modulus with GEOTRACK, deflections were calculated for the single axle solution with loads of 6 and 30 kips. The difference in loads and difference in deflections were substituted into Eq. 20 to get track modulus.

The measured values of track modulus and the estimated standard deviations for all of the revenue field sites are given in Table 16 and shown in Fig. 26, along with the predicted values based on the GEOTRACK analyses. Several items on Fig. 26 deserve attention. First, there was no significant change in the track moduli values as a result of the surfacing operations. However, the pre-maintenance values did seem to be less variable than the post-maintenance values. This variation was also apparent in the average load-deflection curves, where the scatter about the mean was visibly larger for the post-maintenance values. The fact that the average measured values were greater in the Leeds wood and Lorraine sections after maintenance is probably not statistically significant, since the estimated standard deviations all overlap.

Another observation from Fig. 26 is that there did not appear to be a correlation between height of raise and post-maintenance track modulus. Raises of 1.5 to 2 in. were given to the Leeds and Lorraine sections and only about 0.1 in. to the Aberdeen section. In spite of this, the pre- and post-maintenance values for any one test section were approximately equal, and the Aberdeen value was between the Lorraine and Leeds values.

An explanation for the increased variability of the post-maintenance moduli values as compared to the pre-maintenance values could be that the surfacing decreased the uniformity of track support conditions between tie locations. One purpose of track maintenance is to improve the overall track surface, meaning to smooth out the vertical track roughness. A larger amount of raise must be applied beneath the lowest ties to achieve a uniform surface. These variations in the actual raises applied beneath the individual ties could cause local differences in the amount of ballast disturbance, hence variations in the ballast physical state from one tie to another.

Part of the differences in absolute magnitude of the average field track modulus measurements can be explained in terms of the differences in the track substructures. The parametric study [41] using the GEOTRACK model indicated that track modulus increased as ballast depth increased. The ballast profiles and the simplified layer characterizations used in the GEOTRACK analyses (Figs. 22 to 25) show that the Leeds wood section had only about 9 in. of ballast beneath the tie, whereas the Leeds concrete section contained about 14 in. The Aberdeen site had 20 in. of ballast, and the ballast depth at Lorraine was estimated to be 28 in. below the tie. This trend of increasing track modulus with increasing ballast depth for the field sites is clearly confirmed by the field measurements in Fig. 27.

The track modulus is also influenced by the subgrade characteristics. The GEOTRACK model indicates that the compression of the ballast layer accounts for about 10 to 20% of the total vertical rail deflection. Most of the remaining 80 to 90% of the rail deflection is accounted for by the compression of the subgrade materials. Furthermore, 25 to 40% of the subgrade deformation indicated by GEOTRACK occurs below a depth of about 10 ft, even though the stresses below this depth are low [41].

Table 16. Measured and Predicted Vertical Track Modulus

a) Measured Averages and Estimated Standard Deviations for Revenue Field Sites

Field Site	Track Modulus for 6- to 30-kip Load Range					
	Pre-Maintenance			Post-Maintenance		
	$\overline{x}-\sigma$	Average, $\overline{x}$	$\overline{x}+\sigma$	$\overline{x}-\sigma$	Average, $\overline{x}$	$\overline{x}+\sigma$
Leeds, Wood	2.1	2.2	2.5	2.3	2.9	3.7
Leeds, Concrete	3.5	3.9	4.3	2.9	3.3	3.8
Lorraine	6.4	7.0	7.9	6.0	7.6	10.6
Aberdeen				4.9	5.5	6.5

b) Predicted Values for Revenue Field Sites

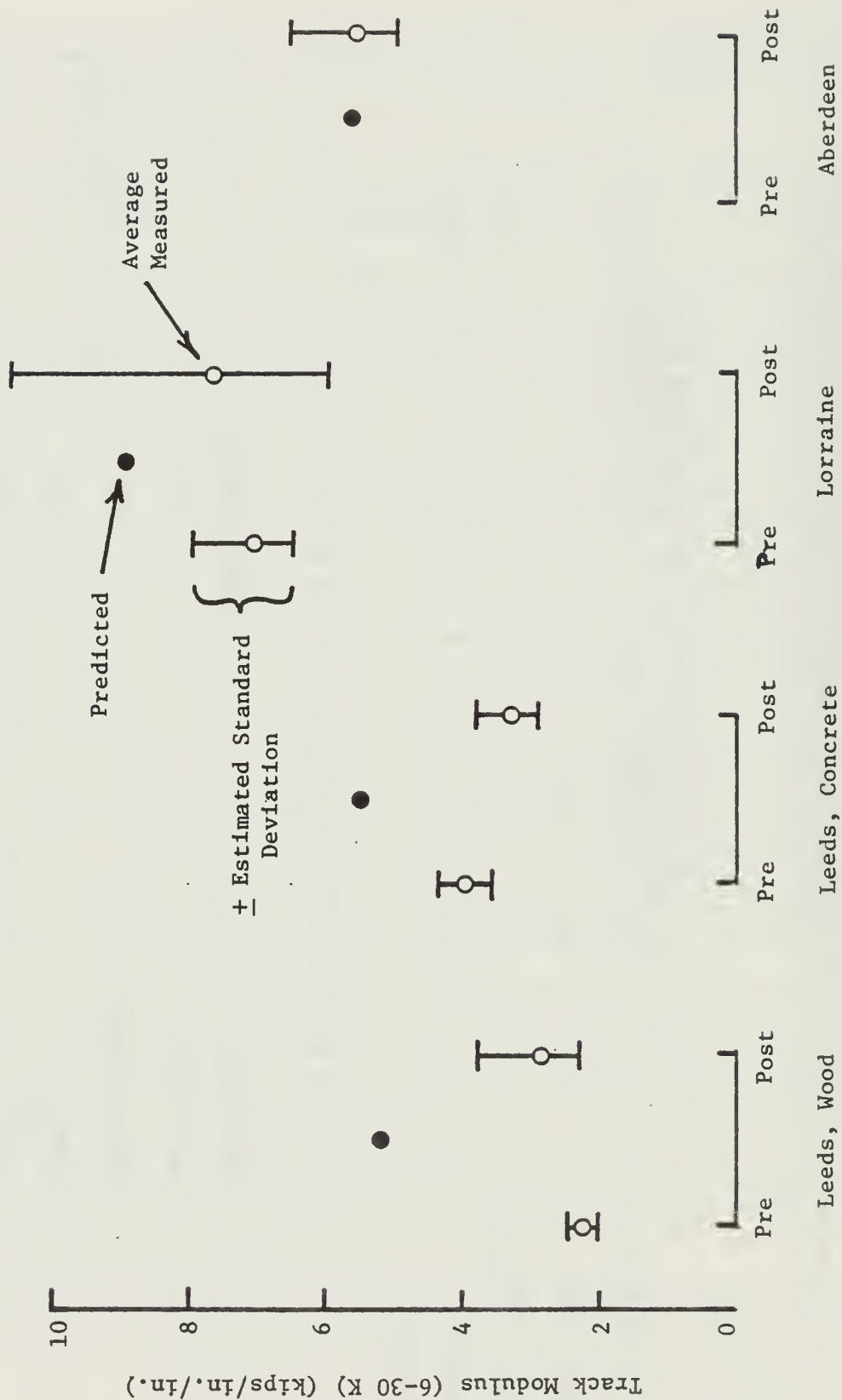| Field Site	Track Modulus, u
Leeds, Wood	5.2
Leeds, Concrete	5.5
Lorraine	8.9
Aberdeen	5.6

Units of u = kips/in./in.

75

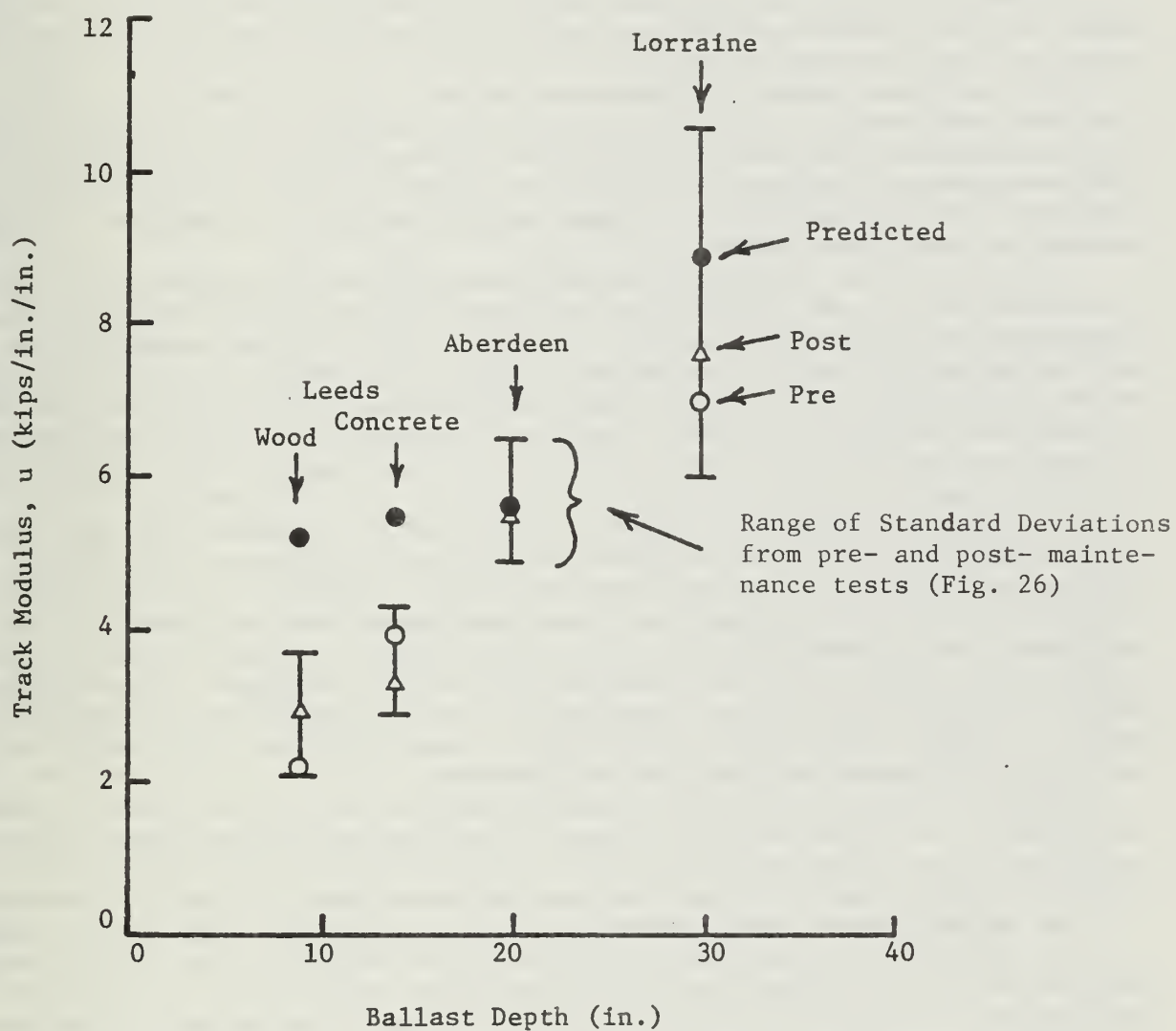Figure 26. Measured and Predicted Track Moduli for Revenue Field Sites, 6- to 30-kip Load Range

76

Figure 27. Ballast Depth versus Track Modulus for Revenue Field Sites

77

The Lorraine test section was found to have the greatest depth of ballast-type material and the stiffest subgrade. Correspondingly, the Lorraine section had the highest values of measured and predicted track modulus of these four revenue sites. As can be seen in Fig. 27, the predicted value of track modulus was higher than the average measured values, but well within the estimated standard deviations.

The Aberdeen post-maintenance value was lower than the Lorraine value due to a combination of reduced ballast thickness and lower overall subgrade stiffness. The predicted track modulus for the Aberdeen site was in very close agreement with the measured values.

For the Leeds sites, the predicted values of track modulus were higher than the field values. However, the field values appear to be unusually low. The lower ballast thickness at the Leeds sites can account for some of the difference between the Leeds sites and the other two field sites, but these differences in ballast layer thickness were not enough to cause the low values measured at both Leeds sites.

Considering the similarity between the subgrade stiffnesses at the Leeds sites and the Aberdeen site, closer agreement between the field measurements from these sites would be expected. It is possible that the embankment in the Leeds wood section resulted in reduced subgrade confinement and hence increased vertical deflections. This would result in lower values of track modulus. However, the concrete section at Leeds, which was built at grade, had comparably low track moduli values as well. Thus, the embankment condition must not have been a major factor.

It would be necessary to reduce the subgrade stiffnesses that were used in the GEOTRACK analyses by at least 50% in order to match the field track modulus measurements at the Leeds test sections. However, no rational justification for making adjustments of these magnitudes could be found. If the soil moduli were overestimated at the Leeds sites, a similar systematic error should have occurred with the Lorraine and Aberdeen subgrades. Since the predicted Lorraine and Aberdeen values were in good agreement with the measurements, a similar adjustment to the subgrade moduli at those sites would shift the predicted values away from the measurements.

The measured and predicted values of track modulus are dependent on several factors, one of which is the support condition of the tie. These support conditions are a function of track settlement and maintenance effects. The support conditions would affect concrete and wood ties in a different fashion.

The GEOTRACK model uses uniform properties throughout each layer, including the support and contact under all ties. The field plate load tests showed that the ballast stiffness was not uniform under the ties, but was greater near the rail seat areas than under the tie centers. Furthermore, after the maintenance the ballast physical state was more uniform than before maintenance. However, even uniform physical state or modulus does not result in uniform support conditions along the tie.

After a maintenance operation in which a high raise was given to the track, the ballast physical properties would be more uniform. However, the tamping and raise during the maintenance is done only near the rail seats, which could cause a gap near the center of the ties. This causes the actual load bearing areas to be near the rail seats due to the lack of contact near the tie centers. This increased load bearing near the rail seats would cause higher rail deflections directly under the applied load than would result from a continuously supported condition. The GEOTRACK model uses continuous contact between the tie directly under the applied vertical load and the ballast surface, leading to a lower rail deflection and higher track modulus than

measured in the field after maintenance.

As traffic accumulates over the track, the ballast beneath the rail seats is recompacted and becomes stiffer, but the tie contact approaches a continuous condition. The more uniform support across the tie leads to a lower rail deflection and hence a higher track modulus. After a small maintenance raise, the initial ballast physical states may be less uniform under the tie than after a large raise. However, in the former case, the contact may be more continuous and the ballast will have greater stiffness. This would result in a higher track modulus after a small raise than after a large raise, or at least not much change in the pre- and post-maintenance values.

Further traffic leads to a centerbound track, in which a greater portion of the rail load would be carried by the central portion of the ties than in non-centerbound track. A gap also tends to develop between the ballast and tie beneath the rail. If the gap is included in the deflection measurement, then the calculated track modulus would appear to decrease as a result of centerbinding. However, if the gap is eliminated by a seating load, then the track modulus would probably increase with centerbinding.

The interactions between the variable ballast physical states, tie support conditions, and structural factors such as tie stiffness and rail size make generalizations about track modulus uncertain. This is particularly true since the degree and type of maintenance disturbance and traffic history of a site can change the ballast physical states in varying amounts. The scatter of the field measurements were such that there were no clear trends distinguishing the pre-maintenance track moduli values from the post-maintenance values. The predictions of track modulus using the GEOTRACK program are somewhat limited by the uniform layer property and full contact representations, and the inability to represent the maintenance factors for the field sites. For these reasons, variations between the measured and predicted track moduli values for the sites can be expected due to the variations in ballast properties and support conditions which were affected by the maintenance operations.

The possible centerbinding and uniformity of support conditions beneath the tie bottom may not, however, be a significant contributing factor to the track modulus values, although the effects are physically rational. Differences between the bending stiffnesses of the wood and concrete ties would also not result in large differences in track moduli. Since only 10 to 20% of the total track deformation occurs due to ballast compression, the subgrade deflections appear to be much more important. It was shown in previous parametric studies [41,42] that variations in tie stiffnesses do not have a major effect on the vertical subgrade stresses beneath the rail seats. The effects of a concrete tie (EI $\simeq$ 1,740,000 to 2,360,000 K-in.[2]) have shown that the vertical stress beneath the rail seat may be only about 1 psi greater than the wood tie (EI $\simeq$ 386,000 K-in.[2]) for similar conditions. Thus, the subgrade contribution to track modulus should be about the same for wood and concrete ties. The FAST dynamic measurements of resilient subgrade deflection also showed no significant difference between the deflections in wood and concrete sections. This would indicate that although the stress distributions and deformations in the ballast layer were affected by tie stiffness and possibly centerbinding, the subgrade responses were controlled mainly by the subgrade properties for the same ballast layer thickness.

A comparison between the measured and predicted values of the revenue site vertical rail deflection is shown in Fig. 28. The differential deflection equals the deflection at 30 kips wheel load minus the deflection at 6 kips. A change in rail deflection causes a larger change in the calculated value of

79
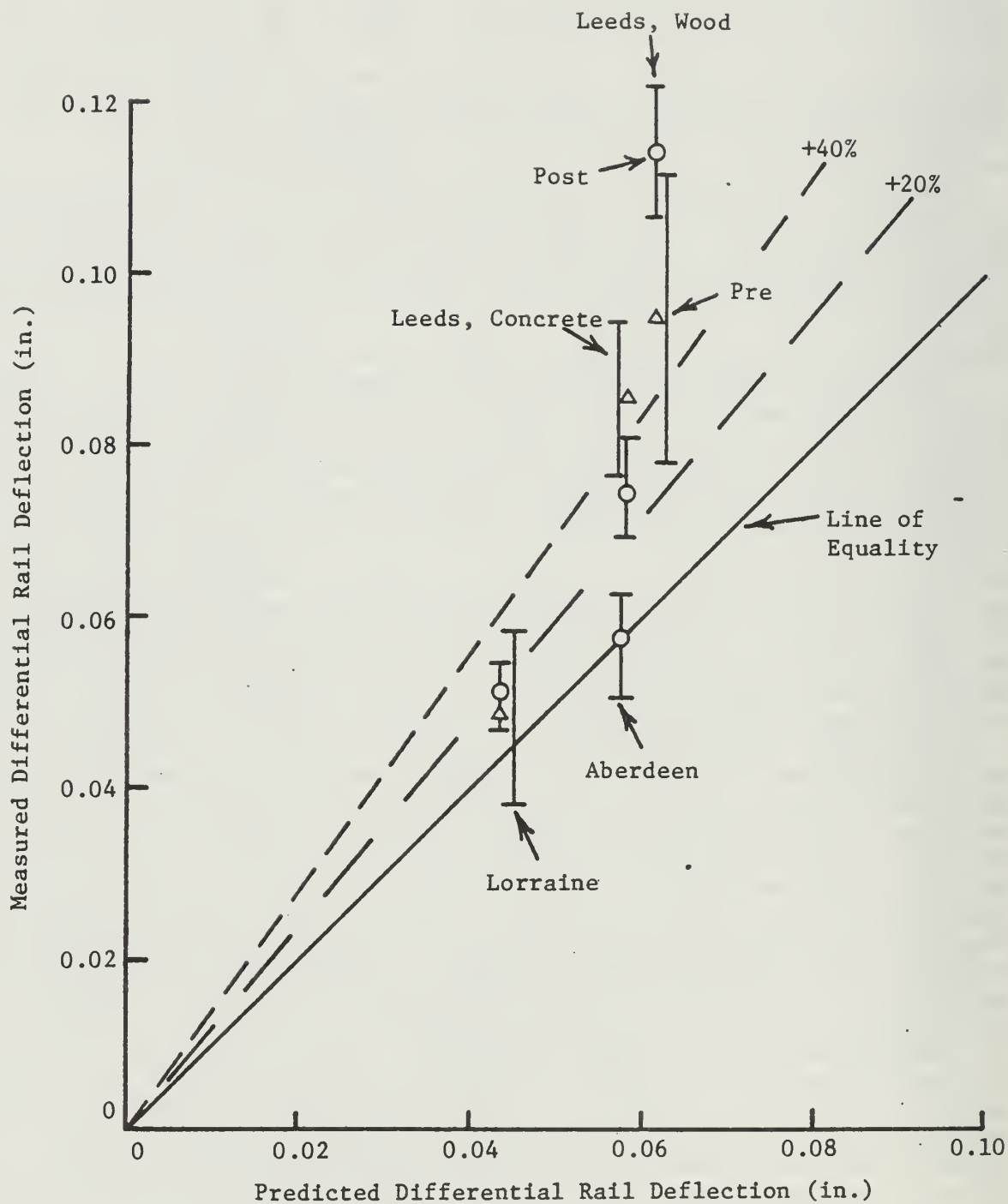
Figure 28. Measured versus Predicted Differential Rail Deflections
for 6- to 30-kip Load Range

track modulus. For example, the predicted values of track modulus at the Leeds wood and concrete sections were in error by about 60 to 100%, but the errors in predicted rail deflections were less. Furthermore, the differences between predicted and measured deflections were small in absolute magnitude. Thus, the predicted values of the rail deflections were in reasonable agreement with the measured values. In fact, considering the complexity of soil behavior, the accuracy of deformation prediction obtained was very good.

CHAPTER 5. TRACK LOADING

5.1 Introduction

Any methodology for predicting the accumulated permanent strains and settlement of track must take into account the actual loading conditions. The actual loading of a given track will consist of a mix of many different wheel loads which are defined by individual car weights and the dynamic response of the moving train.

The approach taken in this study for determination of the mix of wheel loadings at the sites was based on the direct measurement of the actual wheel loads at each site, rather than the use of empirical load factors. The following sections will present these measurements, and describe the method used to characterize the mix of wheel loads present at each of the field sites, including FAST. The static wheel load distributions for each of the sites were obtained from the railroad companies, based on the car weights and tonnage records.

5.2 Measured Wheel Loads

Strain gauge instrumentation was installed on the rails to measure the actual wheel loads. This work was performed by BCL. Descriptions of the strain gauges, the calibration procedures, the instrument locations, and the data recording methods are given in [44] and in Volume 3 [43]. On the basis of past experience in wheel load detection, a sufficient number of loads were recorded at each site so that the load distributions were accurately defined.

The data were reduced to the form of the percent of wheel loads that exceeded a given load level. This is analogous to the cumulative distribution function (CDF) of random variables. The random variables in this case were the static and dynamic wheel loads. The percent exceeded level for the measured wheel loads was converted to the CDF by

$$F_X(x) = \frac{100 - \text{percent exceeded}}{100} = P(X \leq x) \quad , \qquad (21)$$

where $F_X(x)$ is the probability that the given wheel load, X, is assigned a value equal to or less than a specified value, x. This statement is equivalent to the expression $P(X \leq x)$.

The cumulative distributions for the static and dynamic wheel loads were given in Volume 1 [1] for the field sites at Leeds, Lorraine, Aberdeen, and FAST. Several trends were identified in these distributions. There were significant differences between the low frequency of occurrence wheel loads at the sites. These differences appeared as wide separations between the static and dynamic CDF's near the upper tails of the distributions. These separations began at about the 80-90 percent exceeded level (CDF = 0.8 - 0.9) for the revenue sites. The largest variation between the low frequency of occurrence static and dynamic wheel loads was at the Aberdeen site. The very high dynamic loads, a factor of 3 to 5 times greater than the mean dynamic load, are thought to be caused by tread surface irregularities and the high speeds of the passenger trains.

The wheel load distributions for the Lorraine site showed two distinct traffic patterns. The breaks in the wheel load distribution curves for this site were due to the fact that approximately equal numbers of loaded and empty trains pass over this site. Most of this traffic consisted of unit coal trains that traveled full in one direction and returned empty along the single mainline track.

The differences between the measured static and dynamic wheel loads were not as severe at FAST. The relatively close agreement between the static and dynamic wheel loads at FAST was due to the test control and well maintained equipment at that site. For example, tread surface irregularities are regularly repaired at FAST, eliminating a major cause of high dynamic impact loads. In addition, the static wheel loads at FAST were very uniform for the consist used.

On the basis of the data collected by BCL, the mean dynamic and static wheel loads for each of the sites were calculated according to methods described in Ref. [45]. These mean static and dynamic wheel loads are given in Table 17 for the revenue sites and FAST.

5.3   Load Distribution Methodology

Selection of Wheel Loads

Although the complete dynamic load distributions were defined for the sites, it would not be practical to determine the effect that the continuous load spectrum would have on the track structures. To simplify the continuous load distributions and reduce the number of computer analyses necessary, dynamic wheel loads corresponding to the 50, 10, 1 and 0.1 percent exceeded levels were chosen to represent the entire dynamic load distributions. The meaning of the 0.1 percent exceeded level, for example, is that only 1 out of 1000 loads will be greater than the specified value. The CDF corresponding to the 50, 10, 1 and 0.1 percent exceeded levels were 0.5, 0.9, 0.99 and 0.999, respectively. More rigorous methods have been suggested to represent the loadings for highway systems, but the chosen levels of exceedance are sufficient to adequately cover the range of expected dynamic wheel loads.

Once these CDF values were chosen, it was necessary to determine the relative frequencies of occurrence for these dynamic load levels. The method used was such that the midpoint loads between two values of the CDF were those loads corresponding to the 50, 10, 1 and 0.1 load levels. The CDF ranges for each load level were chosen such that the average CDF values corresponded to the selected values of 0.5, 0.9, 0.99 and 0.999. Thus, the difference between any two successive values of the CDF was used to represent the relative frequency of occurrence for the given dynamic load. The procedure used was as follows:

1) Begin at the upper limit of the CDF, where $F_X(\infty) = 1$.

2) Calculate the next value of $F_X(x_1)$ such that

$$\frac{F_X(\infty) - F_X(x_1)}{2} = 0.999 \quad . \tag{22}$$

Note that $F_X(\infty) - F_X(x_1) = P(x_1 \leq X_1 \leq \infty) = f_x(x_1)$,

where $f_x(x_1)$ = relative frequency of occurrence for the 0.1 percent exceeded load, and X_1 = dynamic wheel load at the 0.1 percent exceeded level.

83

Table 17. Mean Static and Dynamic Wheel Loads (kips)

	Leeds	Lorraine	Aberdeen	FAST
Static	15.9	17.6	18.6	30.1
Dynamic	16.4	17.6	20.2	32.0

Table 18. Relative Frequency of Occurrence Assigned to Dynamic Wheel Loads

Percent Exceeded Level	$F_X(x_i)$	$f_x(x_i)$	Avg. $F_X(x_i)$	Dynamic Wheel Load, P (kips)			
				Leeds	Lorraine	Aberdeen	FAST
	1						
0.1		0.002	0.999	43.5	45.0	75.0	48.0
	0.998						
1		0.016	0.990	35.7	39.8	46.2	40.5
	0.982						
10		0.164	0.900	27.3	32.0	34.2	38.3
	0.818						
50		0.636	0.500	15.0	15.0	18.7	32.8
	0.182						
≈99.91		0.182	0.091	6.2	5.5	8.2	8.9
	0						

84

3) Calculate the next value of $F_X(x_2)$ such that

$$\frac{F_X(x_1) - F_X(x_2)}{2} = 0.99 \quad . \tag{23}$$

Note that $F_X(x_1) - F_X(x_2) = P(x_2 \leq X_2 \leq x_1) = f_x(x_2)$,

where $f_x(x_2)$ and X_2 are the relative frequency of occurrence and dynamic wheel load for the 1 percent exceeded level.

4) Continue this process for CDF = 0.9 and 0.5.

5) Since

$$\text{all} \Sigma_{x_i} \, f_X(x_i) = 1 \quad , \tag{24}$$

the remainder of the loads below the 50 percent exceeded level must be accounted for. To do this, calculate $f_X(x_5)$ such that

$$f_X(x_5) = 1 - \sum_{i=1}^{4} f(x_i) \quad , \tag{25}$$

where $f_X(x_5)$ = relative frequency of loads less than the 50 percent exceeded level. The dynamic load, X_5, is the load where the CDF has a value given by

$$F_X(x_5) = \frac{F_X(x_4) - F_X(-\infty)}{2} = 0.091 \quad , \tag{26}$$

where $F_X(-\infty) = 0$.

This method is somewhat arbitrary, but the approach is rational and should approximately represent the mix of wheel loads. The dynamic loads for the 0.1, 1, 10 and 50 percent exceeded levels for the field sites and FAST, along with the relative frequencies calculated using the above outlined procedure, are given in Table 18.

Number of Load Applications

In order to relate laboratory repeated load tests to the traffic levels at the sites, it was necessary to convert MGT values to an equivalent number of cycles of load application. The dynamic records obtained from instrumented sections of the FAST track were studied [46], and it was concluded that each axle pair in a truck acts nearly as a single load cycle for the ballast layer of the track support system. At greater depths, the stress distributions from the adjacent axles overlap sufficiently so that the four axles from adjacent wheel trucks represent a single load cycle. Therefore, two axles will be used to represent a load cycle for the ballast layers and four axles to represent a single load cycle for the subgrade layers.

Now 1 MGT equals 2×10^6 kips, and the number of kips per axle equals twice the wheel load in kips. Thus the number of axles per MGT is

$$N_a = \frac{10^6}{E(X)} \quad , \tag{27}$$

where N_a = number of axles per MGT, and

E(X) = expected or mean value of the static wheel load distribution, in kips.

The mean static wheel load (Table 17) was used rather than the mean dynamic load, since railroad tonnage records are based upon the actual weights of the cars.

The train's axle load in tons is numerically equal to the wheel load in kips, assuming equal distribution of load on both wheels. Since the axle load acts on both rails, the number of wheels passing a particular location per MGT is the same as that calculated using Eq. 27.

Based upon the previous conclusions regarding the number of axles per cycle for the ballast and subgrade layers, the conversion from MGT to number of load applications for the ballast is

$$N_b = \frac{N_a}{2} \quad , \tag{28}$$

and for the subgrade is

$$N_s = \frac{N_a}{4} \quad , \tag{29}$$

where N_b and N_s are the number of load applications per MGT for the ballast and subgrade layers. Using the mean static wheel load for the sites as given in Table 17, the equivalent numbers of load applications per MGT for the individual field sites were calculated. These results are summarized in Table 19.

The distributions of the dynamic loads as previously calculated were used to define the mix of wheel loads at each of the sites. To determine the number of axle loads of the prescribed magnitudes, the relative frequency for that load level, $f_X(x_i)$, is multiplied by the equivalent number of cycles per MGT, as given by

$$N_{bi} = f_X(x_i)N_b \quad , \tag{30}$$

for the ballast, and by

$$N_{si} = f_X(x_i)N_s \quad , \tag{31}$$

for the subgrade. The equivalent number of load cycles per MGT, at the prescribed dynamic wheel loads, is given in Table 20 for both the ballast and subgrade layers. Again, note that the single wheel load in kips is equal to the axle load in tons.

Multiple-Axle Loadings

The GEOTRACK computer model, to be used later in analyzing the track performance, was modified during this program to handle multiple-axle loads. A four-axle loading condition, representing two adjacent wheel trucks, was used to represent the dynamic loadings at the field sites. Since it was unlikely that actual train loadings would consist of several wheel loads of the same magnitude occurring sequentially, the complete representation of dynamic track loadings was defined by combining three axles of the mean dynamic load with one axle from the individual values of representative dynamic loads.

86

Table 19. Number of Cycles per MGT for Ballast and Subgrade

	Leeds	Lorraine	Aberdeen	FAST
Ballast, N_b	31000	28000	27000	17000
Subgrade, N_s	16000	14000	13000	8000

Table 20. Number of Cycles per MGT at Prescribed Dynamic Wheel Loads for Ballast and Subgrade

Leeds	P (kips)	6.2	15.0	27.3	35.7	43.5
	N_b	5700	20000	5200	500	63
	N_s	2800	10000	2600	250	31
Lorraine	P (kips)	5.5	15.0	32.0	39.8	45.0
	N_b	5200	18000	4700	460	57
	N_s	2600	9000	2300	230	28
Aberdeen	P (kips)	8.2	18.7	34.2	46.2	75.0
	N_b	4900	17000	4400	430	54
	N_s	2400	8500	2200	220	27
FAST	P (kips)	8.9	32.8	38.3	40.5	48.0
	N_b	3000	11000	2700	270	33
	N_s	1500	5300	1400	130	17

The equivalent track loadings for track sections having wood ties are shown in Fig. 29a. The mean dynamic wheel loads were used on three of the axles. The fourth axle load was based upon the wheel loads determined for the 50, 10, 1 and 0.1 percent exceeded levels. The variable wheel loadings were placed second in the sequence. The load positions shown in Fig. 29a were used for the Leeds wood and FAST 22 wood tie sections, but the magnitudes of the mean and variable dynamic loads differed as indicated in Table 18.

The equivalent track loadings for the sites having concrete ties are shown in Fig. 29b. Again, the load sequence used was the same for all concrete tie sections, although the magnitudes of the applied dynamic loads used did vary among the sites, according to Table 18.
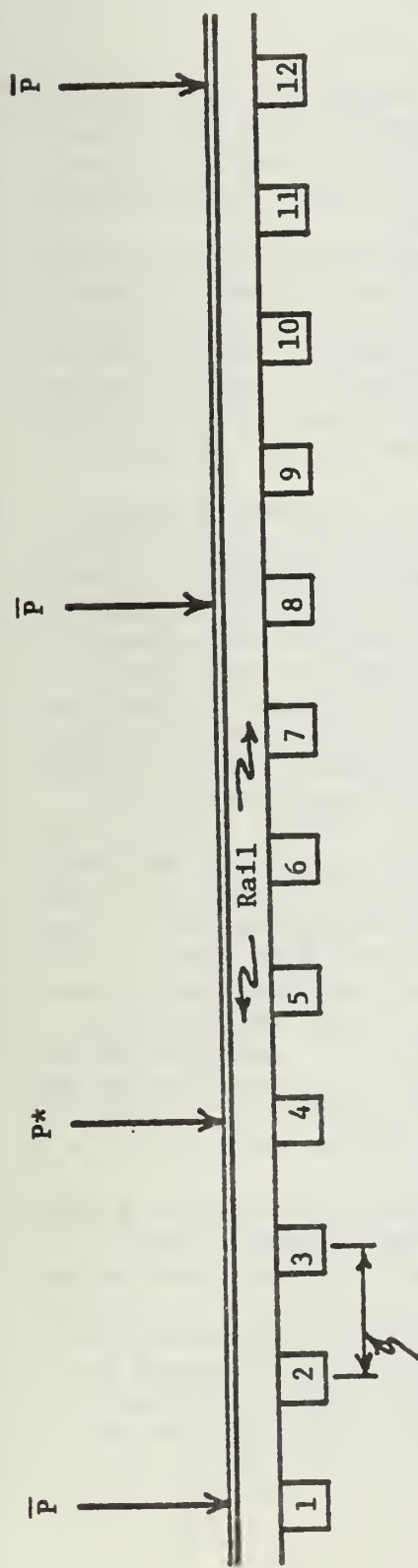
a) Tie Spacing = 19.5 in. for Wood Tie Sections
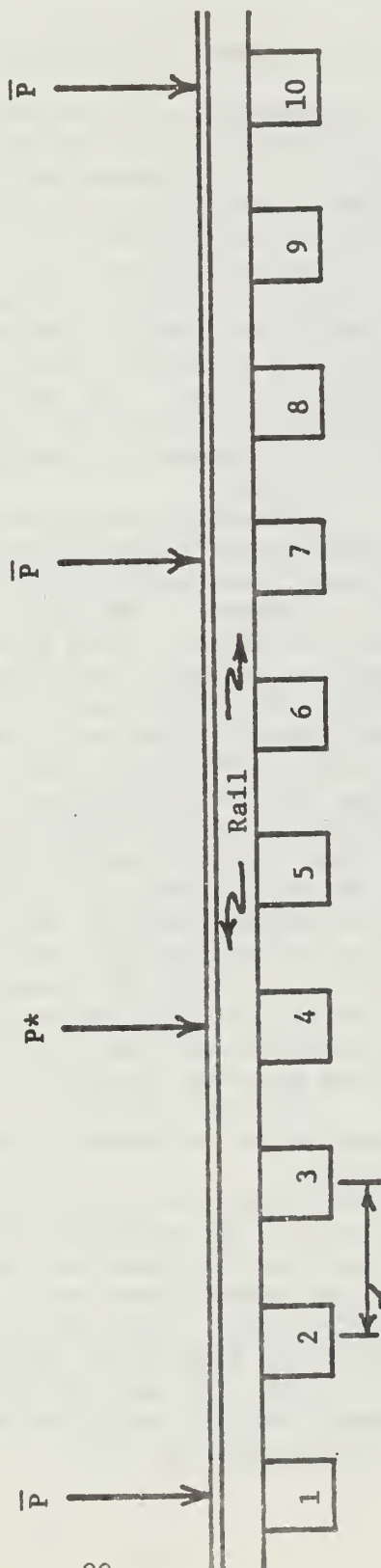
b) Tie Spacing = 24 in. (25 in. for Lorraine) for Concrete Tie Sections

$\overline{P}$ = mean dynamic wheel load

P* = dynamic wheel load at 50, 10, 1, 0.1 percent exceeded level

Figure 29. Equivalent Track Loading for Wood and Concrete Tie Sections

89

CHAPTER 6. METHODOLOGY FOR DEFORMATION PREDICTIONS

6.1 Stress Path Determination

The approach to the prediction of the permanent deformation that accumulates in track due to repeated traffic loadings is based upon the conceptual ideas developed primarily in the pavement area. A logical extension of the pavement approach has been investigated for track [22,42] and will serve as the basis for the methodology presented in this volume.

The methodology for the prediction of track permanent deformations starts by determination of the stress states at various locations within the track foundation. These stress states derive from two sources: the initial stresses due to the unloaded track condition, and the incremental stresses resulting from the imposed train loadings. The initial vertical geostatic stresses are determined by the weights of the track superstructure and the soil. The initial horizontal geostatic stresses are related to the initial vertical stresses through the K_o parameter.

The incremental   stresses are determined using the GEOTRACK program. The GEOTRACK program computes the complete incremental stress tensor for various locations in the track formation. These incremental stresses are added to the initial geostatic stresses to determine the final three-dimensional stress states at various locations. These final three-dimensional stresses are converted into equivalent triaxial stress states using the concept of stress invariants [22,47]. The resulting triaxial stress states are then used to determine the representative stress paths for points within the roadbed.

A typical stress path for a point in the ballast directly below a moving load, as calculated using the invariant formulation, is shown in Fig. 30. Point A represents the initial stress state. Since the K_o value for the ballast layers is greater than one, the initial shear stress, q_{min}, is negative. Point B represents the equivalent stresses at a point   directly below a wheel load. The cyclic stress path for the point in the roadbed due to the moving load thus is given by the line AB. Two alternatives were considered for representing path AB as an equivalent constant confining pressure triaxial stress path. First is stress path CB, which matches only the maximum shear stress, q_{max}, and the minimum or initial shear stress, q_{min}. Second is stress path DE, which matches the mean stress, $\bar{p}_m$, as well as the maximum and minimum shear stresses. Since the actual   traffic consists of a mix of wheel loads, these stress paths, as shown in Fig. 30, will be required for a variety of loading conditions.

The depths within the track foundation at which the representative stress paths should be calculated are not uniquely defined. The approach taken in the pavement area [48] has been to calculate the triaxial stress states at the center of the various layer subdivisions to determine the deformation contributions from each of these layers. This may be appropriate when predictions are to be made for newly built facilities, but when dealing with systems such as maintained or rebuilt track, the contributions of the undisturbed lower layers are often negligible and can therefore be ignored. This will be explained more fully in a subsequent section.
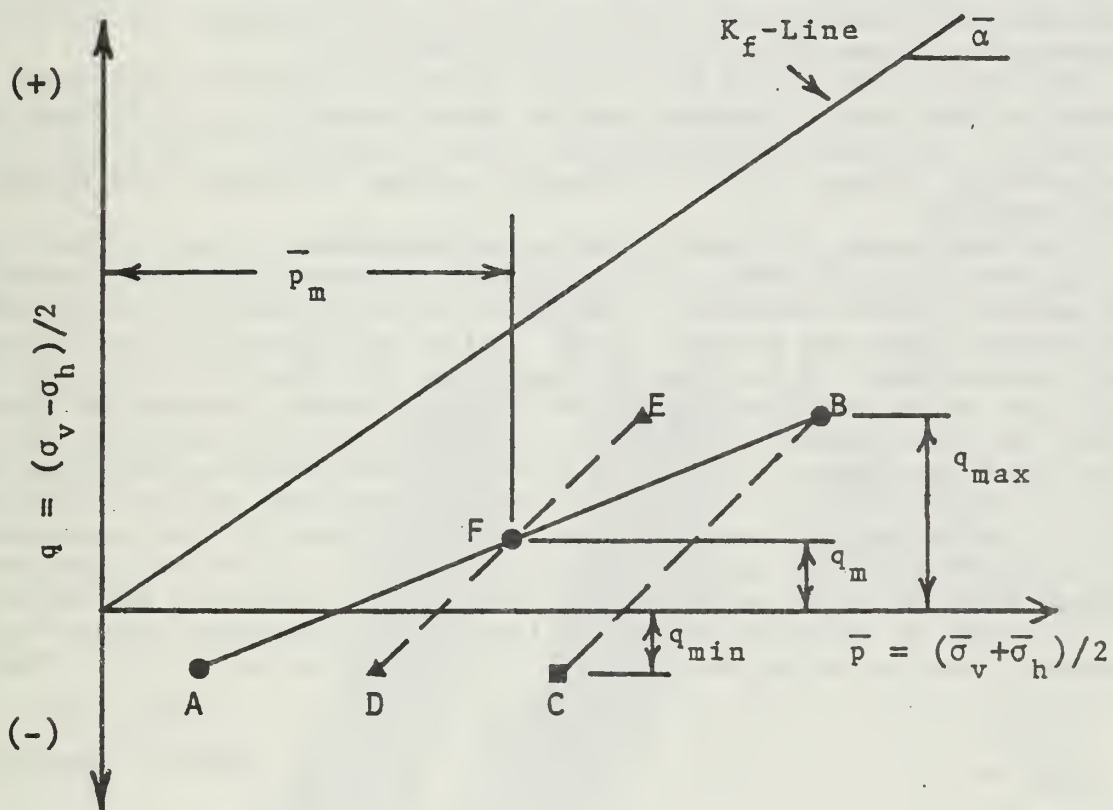
Figure 30. Equivalent Stress Paths for Roadbed Points

6.2 Strain Determination

First Cycle Strains

Once the stress paths have been established for the various combinations of dynamic wheel loadings, the next operation is to determine the strains that would be expected to develop due to repeated applications of the prescribed stresses. This is done using the laboratory results from the various test series described in Chapter 3.

The deformations that accumulate in ballast due to repeated application of vertical stresses were shown to be related, in general, to the permanent strain or deformation that occurred in the first cycle of load. Thus, the first step in predicting the track deformations is to determine the strains that are expected to develop from the first load cycle. Since the stress paths for the ballast layers involve shear stress reversals, the accurate determination of these first cycle strains is difficult.

The first cycle strain for one-way repeated loading has been shown to be related to the ratio of maximum applied shear stress, q_{max}, to failure shear stress, q_f. For tests involving shear stress reversal, the stress ratio used is $\Delta q/q_f$, where Δq is the difference between the maximum and minimum shear stresses.

The relationships between first cycle strains and stress ratios for the ballast materials are shown in Fig. 31, both for tests involving one-way loading and shear stress reversals. The shear stress reversal data were obtained from the box tests and triaxial tests. All of the data with a cyclic stress ratio greater than 1.0 are from the box tests. The results for all of the field site ballasts tested, as well as the FAST Wyoming granite, were used to define the trends shown in the figure. In each case, the permanent strain after the first cycle, ε_1, has been divided by the effective confining pressure, $\bar{\sigma}_3$, in an attempt to normalize the existing data so they could be extrapolated to pressures other than those used for the experiments. The effective confining pressures and stress ratios for the box tests were calculated based on the measured residual horizontal stresses in the box tests.

For each of the field site predictions, the first cycle strains will be estimated from the curves shown in Fig. 31 for four stress ratios. These are:

Ratio	Stress Path	Strain Curve
q_{max}/q_f	CB	One-Way Uncompacted
q_{max}/q_f	DE	One-Way Uncompacted
$\Delta q/q_f$	CB	Uncompacted Stress Reversal
$\Delta q/q_f$	DE	Uncompacted Stress Reversal

Strain Accumulation Rates

The rate of strain accumulation with repeated load cycles for the ballast materials was previously discussed in Chapter 3. The ballast constants, C, used for the predictions will be both the individual results given in Table 15 for one-way loading and the uncompacted constant, C_{bu}, derived from the box test results. These soil constants, together with the permanent strain after the first cycle, will be used in predictive Equation 16 to determine the

92
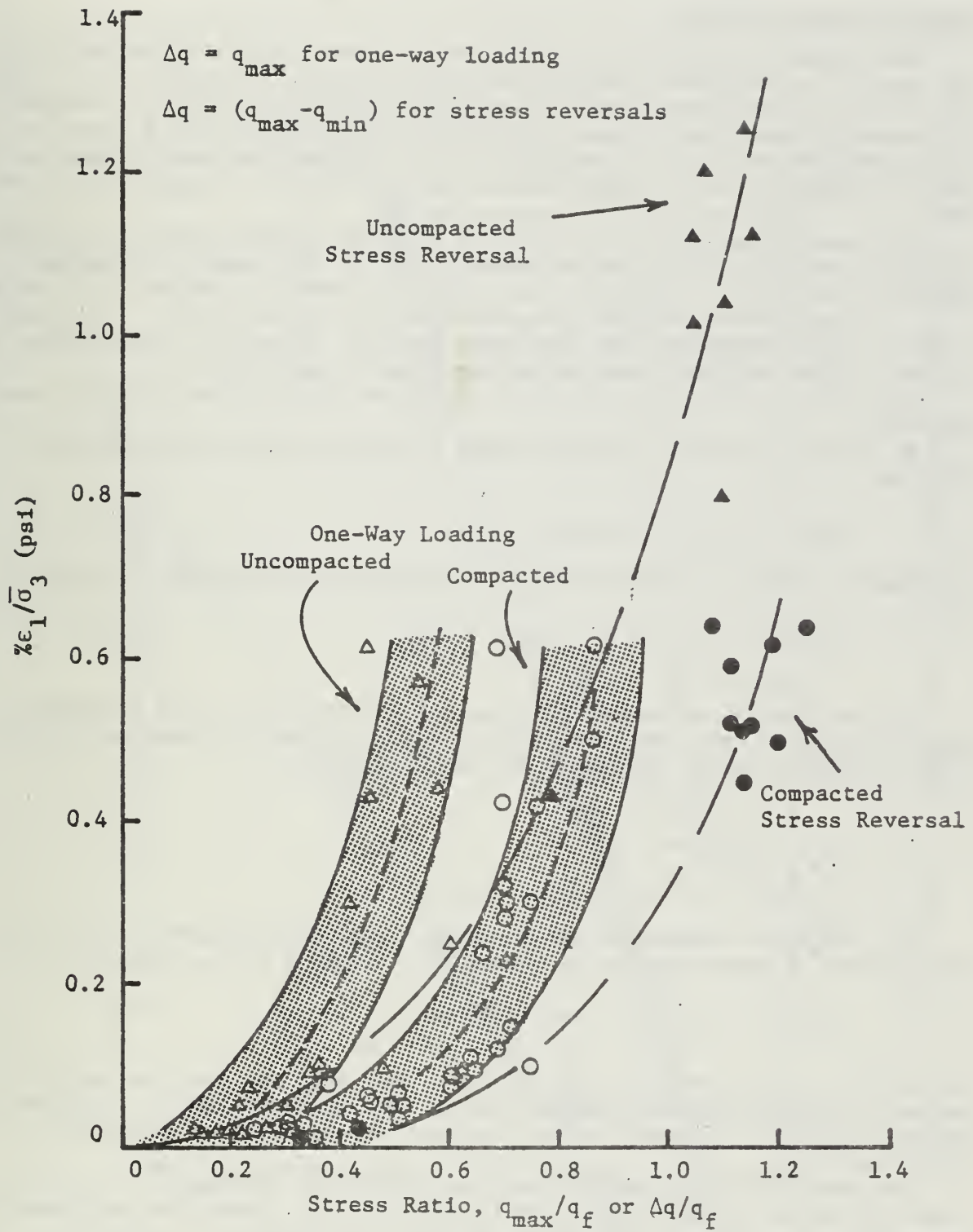
Figure 31. Normalized First Cycle Strains as a Function of Stress Ratios

93

strain after additional cycles for each of the field site stress paths.

Superposition of Strains

The cumulative strains due to the mix of wheel loads will be handled on the basis of a cumulative damage relationship similar to Miner's rule. This type of cumulative damage rule has been frequently used in fatigue studies for asphalt pavement and pavement deformation methodologies by a number of researchers [49,50,51]. The validity of this approach was established for the ballast on the basis of experimental results from the staged testing program.

The basic procedure for application of Miner's rule starts with the observation that after N_i cycles at stress level i, the amount of permanent strain, $\varepsilon_N(i)$, will develop. An equivalent number of cycles, N_j*, can be calculated such that the permanent strain after N_j* cycles is equal to the strain already developed after N_i cycles at stress level i. For the ballast strains, this can be expressed as follows:

1. Let ε_{1i} and ε_{1j} be the strain developed at $N_i = 1$ and $N_j = 1$, respectively.

2. After N_i cycles at stress level i, the permanent strain will be given by

$$\varepsilon_N(i) = \varepsilon_{1i}(1 + C \log N_i) \quad , \tag{32}$$

and after N_j cycles at stress level j, the permanent strain will be given by

$$\varepsilon_N(j) = \varepsilon_{1j}(1 + C \log N_j) \quad . \tag{33}$$

3. The equivalent number of cycles at stress level j that would have been necessary to cause strains equal to $\varepsilon_N(i)$ is found by equating $\varepsilon_N(i)$ to $\varepsilon_N(j)$, in which case N_j becomes N_j*. The result is

$$N_j* = 10^{\frac{1}{C}\left[\frac{\varepsilon_N(i)}{\varepsilon_{1j}} - 1\right]} \quad . \tag{34}$$

4. The total cumulative strain after N_i cycles of stress level i plus an additional N_j applications of stress level j is then given by

$$\varepsilon_N(i+j) = \varepsilon_{1j}[1 + C \log (N_j* + N_j)] \quad . \tag{35}$$

The method is illustrated in Fig. 32 for a case with two load levels, the second of which is greater than the first. The procedure may be repeated for all other successive stress levels, and can even be used for returning to stress level i.

For the field site predictions, the first cycle strains for the 50, 10, 1 and 0.1 percent exceeded load levels will be used, along with the prescribed number of cycles at each load level, as given in Chapter 5. However, for comparison with the field measurements, the calculated strains are plotted as a function of the actual number of cycles (or MGT), not the equivalent number of cycles used for the superpositions.
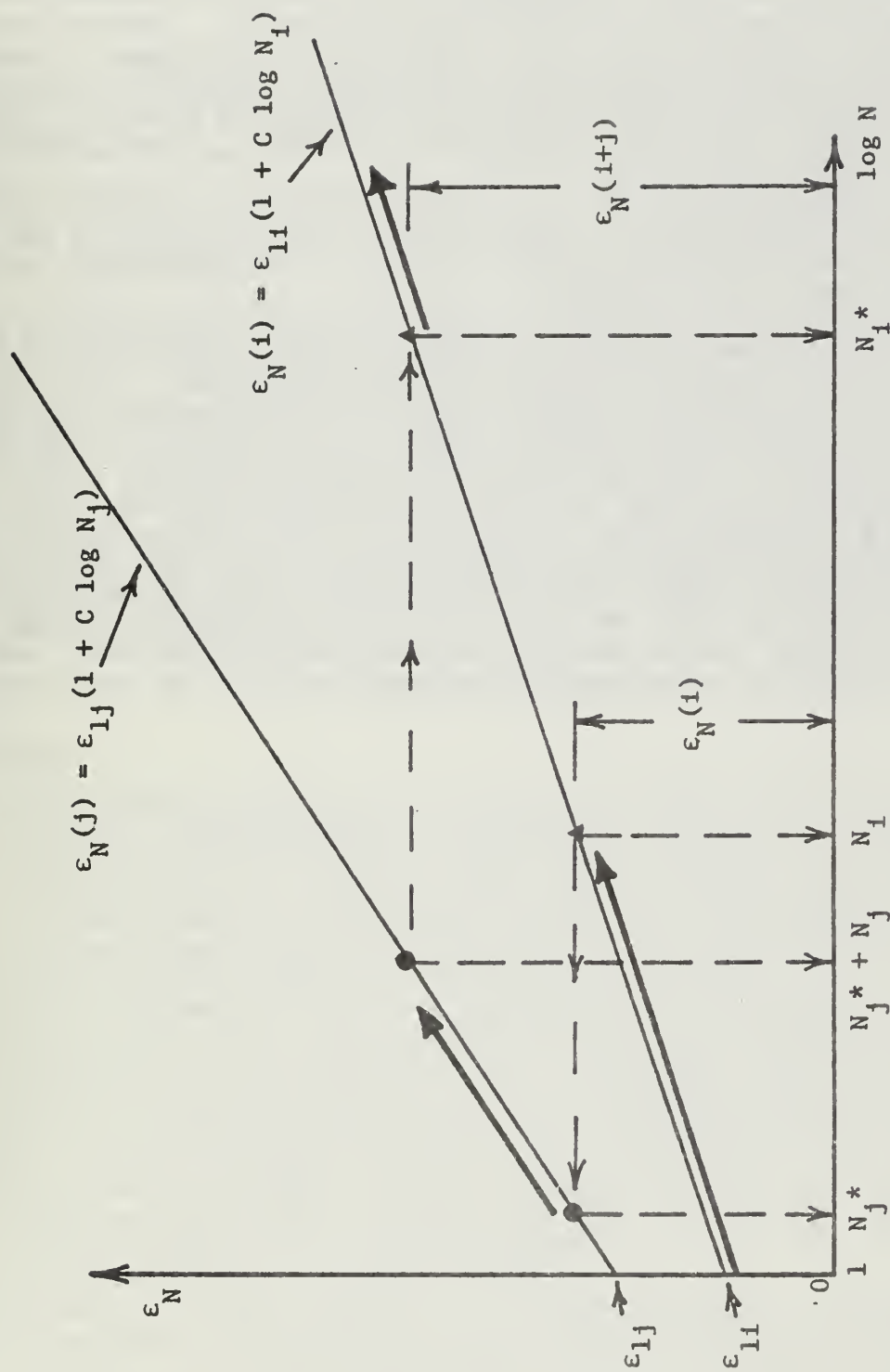
Figure 32. Method Used for Ballast Strain Calculations for Mixed Loading

95

6.3 Deformation Determination

The calculated strains in each layer must be multiplied by the layer thickness to get the layer compression. All of the layer compressions are then summed to determine the track vertical deformation. However, the track maintenance operation disturbs only a shallow depth of ballast, at most 6 to 8 inches below the base of the ties. The layers and materials below this depth which have been subjected to years of traffic and hundreds of MGT should contribute little to the total track settlement, unless pumping or embankment instability exists.

The stresses used for all of the revenue field site predictions therefore will be those estimated at depths of 3 to 4 inches below the tie, representing a layer thickness of 6 to 8 inches. The contribution to settlement from lower layers will be ignored.

The FAST track was rebuilt and the ballast layer was completely replaced in 1979. Then a major maintenance operation was done after about 93 MGT traffic. Thus, two sets of predictions are needed for FAST. The first will be for the first 93 MGT traffic after rebuild, considering deformations that develop in the entire 15-in. ballast layer. The second set of FAST predictions will be for the traffic after the maintenance at 93 MGT. Since the maintenance affected at most the top half of the total ballast layer, this prediction will consider only the 7.5-in. depth of ballast assumed to be affected by the disturbance. The subgrade materials at FAST had been subjected to over 400 MGT traffic prior to the rebuild. Thus the subgrade contribution to settlement after the rebuild will be neglected. The errors resulting from neglecting further subgrade deformations should be small, and certainly less than the uncertainty in the method used for the predictions.

96

CHAPTER 7. PERMANENT DEFORMATION EVALUATION

7.1 Introduction

The track settlements at the revenue sites were measured by BCL using optical surveys. For these vertical survey-to-benchmark readings, measurements were taken at the top of the railhead, at 10-ft longitudinal intervals, at adjacent locations on each rail. At the Aberdeen site, inductance strain coils were also installed in the ballast to determine the contribution of the ballast layer to the total vertical settlement. These coils were placed in pairs beneath the rail seats under three ties. One coil in each pair was placed at a depth of approximately 13 in. below the bottom of the tie, in the ballast layer. The other coil was at the bottom of the tie. This configuration measured the change in upper ballast thickness relative to the initial thickness (about 13 in.) prior to maintenance when the coils were installed. The principle of operation for this instrumentation can be found in Ref. [52], along with the calibration procedures. Measurements of the deformations in the track at FAST also have been recorded using vertical survey and foundation instrumentation. Only the measurements since the 1979 rebuild will be considered for correlation with the revenue service track results. Measurements from the earlier FAST experiments prior to the rebuild have been previously reported [22,46,53].

This chapter will present the track settlement results obtained from the field sites and compare the measured responses with the predictions made using the methodology outlined in Chapter 6.

7.2 Field Measurements

Revenue Sites

The correlation plan called for survey measurements to be taken immediately after the track surfacing, prior to any traffic, followed by readings taken at about 6-month intervals. However, in some cases as much as 7 to 10 days elapsed, representing up to 0.5 MGT traffic, before the zero reference survey was made. This presented a significant uncertainty in the magnitude of the initial settlement, when relatively large displacements are likely to occur.

The actual railhead elevations obtained by the survey at each site were detrended by BCL to correct for the slight grades that were present in the track vertical alignments. These detrended profiles were referred to as the baseline profiles for the reference surveys. For example, if there was a constant gradient in track elevation over the test section, linearly proportioned corrections to the railhead elevations were made throughout the test section. The initial corrected baselines were used as a reference for the follow-up surveys to determine the profile change. The mean detrended rail elevations from the follow-up surveys were subtracted from the mean initial rail elevation (baseline) to obtain the track settlements.

The average settlement at each of the field sites as a function of MGT after maintenance is given in Table 21. The zero settlement at each site, as previously explained, represents the average detrended reference elevation of the test sections. The standard deviations of the detrended rail profiles for the reference survey and the follow-up surveys are also given in Table 21. This standard deviation can be interpreted as a measure of track roughness. These track roughness values did not appear to be correlated to the magnitudes of track settlements.

97

Table 21. Uncorrected Vertical Track Settlement Measurements from BCL Survey

Site	MGT Since Surfacing	Settlement (in.)	Roughness or Standard Deviation of Detrended Rail Profiles (in.)	Change in Roughness or Standard Deviation of Settlements Relative to Reference Values (in.)
Leeds, Wood	0.5*	0.00	0.29	—
	12.5	0.44	0.28	0.02
	22.5	0.46	0.33	0.04
Leeds, Concrete	0.6*	0.00	0.27	—
	11.1	0.09	0.30	0.03
	24.0	0.44	0.30	0.03
	36.6	0.47	0.30	0.03
Lorraine	0.0*	0.00	0.19	—
	34.5	0.80	0.23	0.06
	56.5	1.18	0.27	0.08
	64.0	1.29	0.26	0.07
Aberdeen	0.4*	0.00	0.25	—
	10.9	0.17	0.27	0.02
	24.4	0.50	0.27	0.02

*Initial or reference value.

98 -

The standard deviation of the track settlement as referenced to the initial baseline profiles is also given in Table 21. The standard deviation values were computed from the variations between the initial baseline and the subsequent profiles, as supplied by BCL. These values were small, indicating little change in track roughness with settlement.

Since the zero reference surveys at the Leeds sites and at Aberdeen were taken after some amount of traffic following maintenance, a correction had to be estimated to account for the missing initial settlements for these sites. Fortunately, the strain coils installed in the ballast at the Aberdeen site were monitored frequently during the first field site visit. These strain coils allowed a direct measurement of the amount of raise at the site and subsequent deformations. However, the strain coil measurements would probably give an overestimate of the ballast deformations throughout the entire track section. The reason is that a 13-in. depth of ballast was excavated and replaced when the coils were installed. Although the ballast in the areas under the ties and in the cribs was compacted with a portable mechanical tamper, the replaced material may not have been as compact and stiff as the undisturbed ballast at locations without strain coils. The effects of this ballast disturbance at the strain coil locations could have resulted in greater track settlement at these locations than at the remaining tie locations.

The initial deformations that developed in the upper 13 in. of ballast at the Aberdeen site are shown in Fig. 33. The coils indicated a surface raise of about 0.1 in., followed by a rapid initial settlement. The reference zero survey was made 10 days after the surfacing. The ballast strain coils indicated that there had been about 0.20 in. of vertical deformation in the ballast since the surfacing due to the first 0.4 MGT traffic. Therefore, the BCL surveys had to be adjusted by this amount to correct for the missed initial deformations.

The similarity between the trends of the corrected survey measurements and the ballast strain measurements supported the conclusion that the subgrade and deeper ballast settlements could be neglected.

The two Leeds sites did not have strain coils embedded in the ballast, so the corrections to the survey measurements at these sites were uncertain. The amount of initial settlement at these sites, where the raise was about 1-½ in., could only be estimated. Data from FAST indicated that about .25 in. of settlement occurred after 0.3 MGT of traffic had passed over section 22 following a comparable raise. Based on this information, the correction to the Leeds survey measurements was estimated at 0.2 in. The actual survey data will be used for the Leeds sites, and the estimated corrections shown as an increase. Thus the survey measurements represent a lower bound to the actual track settlements. For the Leeds sites, the probable corrections for initial settlements were on the same order as the subsequent settlements over the remaining 18 months.

The survey was done directly after maintenance at the Lorraine site. However, an interval of over 30 MGT elapsed from the zero reference point to the first follow-up survey. Thus, the shape of the settlement curve could not be defined, even though the end points were known for this traffic interval.

FAST Measurements

Measurements of vertical track settlement at FAST section 22 were obtained from both embedded foundation instrumentation and track surveys. Details of the FAST 22 instrumentation used after the 1979 rebuild can be found in Ref. [54].
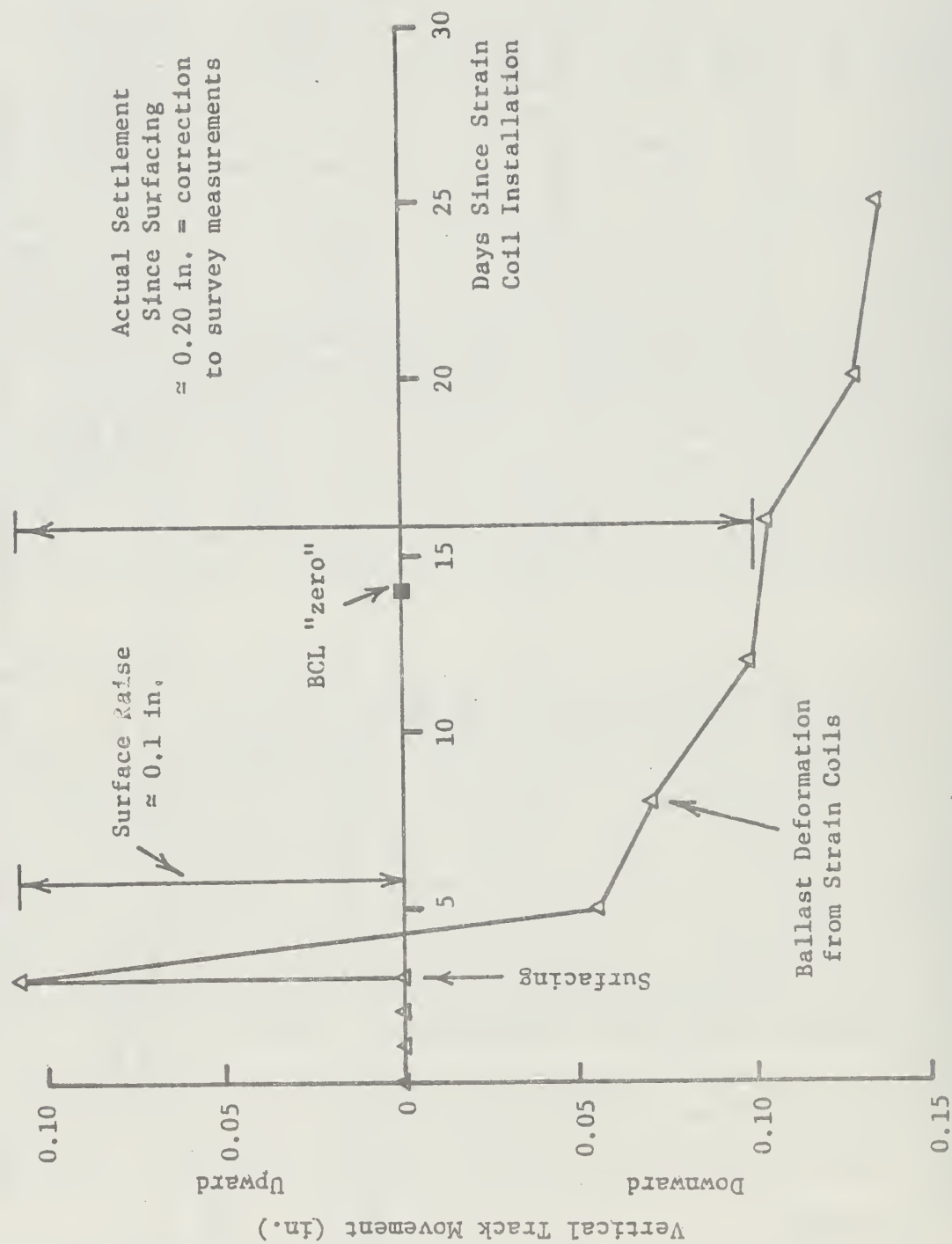
Figure 33. Initial Track Deformations for Aberdeen

100

The measured ballast and subgrade deformations after the rebuild, as ob-
tained from the instrumentation, are shown in Fig. 34a for the wood tie sec-
tion. The results from the instrumentation measurements for the concrete tie
section of FAST section 22 are shown in Fig. 34b. The vertical lines on these
figures represent ± one standard deviation of the measured results. Analyses
of the ballast and subgrade data shown in Fig. 34 indicated that there were no
statistically significant differences in the measured ballast deformations and
in the measured subgrade deformations between the wood and concrete sections
of FAST section 22 after the 1979 rebuild.

A similar conclusion regarding the ballast deformations was found from
the previous FAST static data from sections 17, 18, and 20. The average bal-
last deformations measured at FAST sections 17, 18, and 20 prior to the rebuild,
along with the average ballast deformations in section 22 measured after the
1979 rebuild, are compared in Fig. 35. Both sets of measurements show an ini-
tially high rate of deformation accumulation. Considering the variability
associated with each set of observations, it was concluded that the deforma-
tions that developed in the earlier FAST experiments were similar to those ob-
served immediately after the 1979 rebuild.

There is some uncertainty about the ballast strain data taken after the
rebuild. The track rebuild construction specifications indicated that the
ballast was to be placed in 2- to 4-in. lifts, followed by tamping and ten
passes of a locomotive with at least 10 loaded 100-ton hopper cars. This pro-
cedure was to be repeated until the final grade was attained. Subsequent in-
formation regarding the rebuild [6] reported 6-in. lifts followed by tamping
and regulating, with no mention of the track loadings. Since this incremental
construction and subsequent loading resulted in some ballast compaction, as
was intended by the rebuild planners, even the FAST ballast strain coil data
from the 0 to 93 MGT interval contain some degree of uncertainty in interpre-
tation. The measured ballast strains shown in Fig. 34 represent lower bounds
to the expected strains developed in a newly constructed track.

Figure 36 shows the cumulative subgrade deformations measured in wood and
concrete tie sections of FAST, since the beginning of the FAST track operation
and after the 1979 rebuild. The wood tie section subgrade deformations after
the rebuild were significantly larger than those measured in the concrete tie
section. Prior to the 1979 rebuild, the cumulative subgrade deformations in
concrete tie section 17 of FAST were larger than in the wood tie sections 18
and 20.

It is unclear why the subgrade deformations after the 1979 rebuild should
show the significant changes indicated in Fig. 36. Only the top few inches of
the subgrade apparently were disturbed during the rebuild and the remainder had
been subjected to over 400 MGT traffic. Extrapolation of the trends from both
wood and concrete sections prior to the rebuild suggests that the subgrade de-
formations due to an additional 100 MGT after the rebuild should have been
small. Thus the rebuild subgrade extensometer data appear to be misleading.

There are other factors that could have resulted in the presumably high
measured subgrade deformations after the rebuild. The actual construction
operations may have disturbed the subgrade to a depth greater than the top few
inches. This could have resulted from deeper undercutting than planned, or
from the vibratory compaction used during the final subgrade preparation. Sig-
nificant vibrations in the sandy subgrade may have relieved the previous stress
history effects, making the material more susceptible to additional cyclic-in-
duced densification. The effects of vibration on the alteration of any pre-
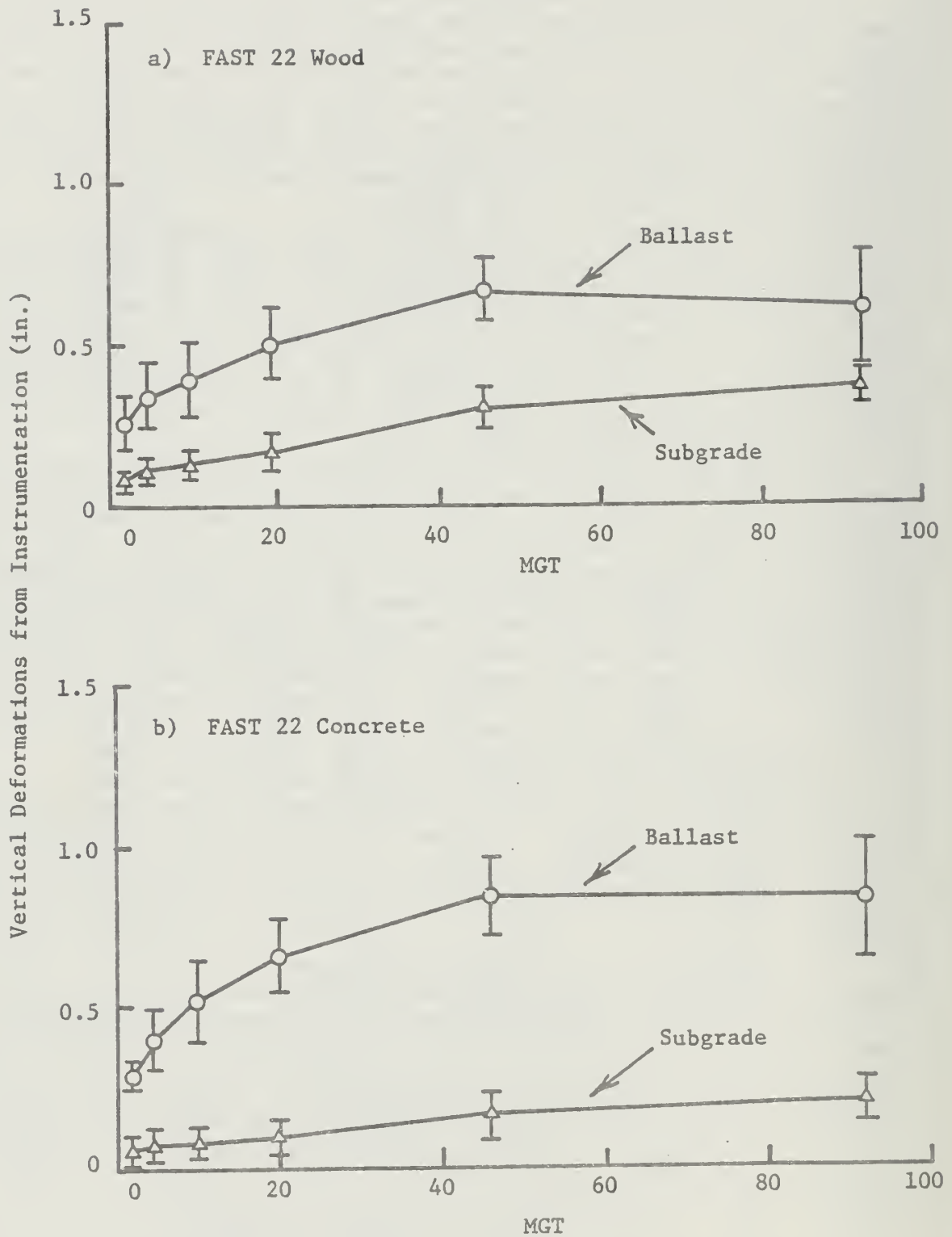vious subgrade structure would be very difficult to quantitatively interpret.

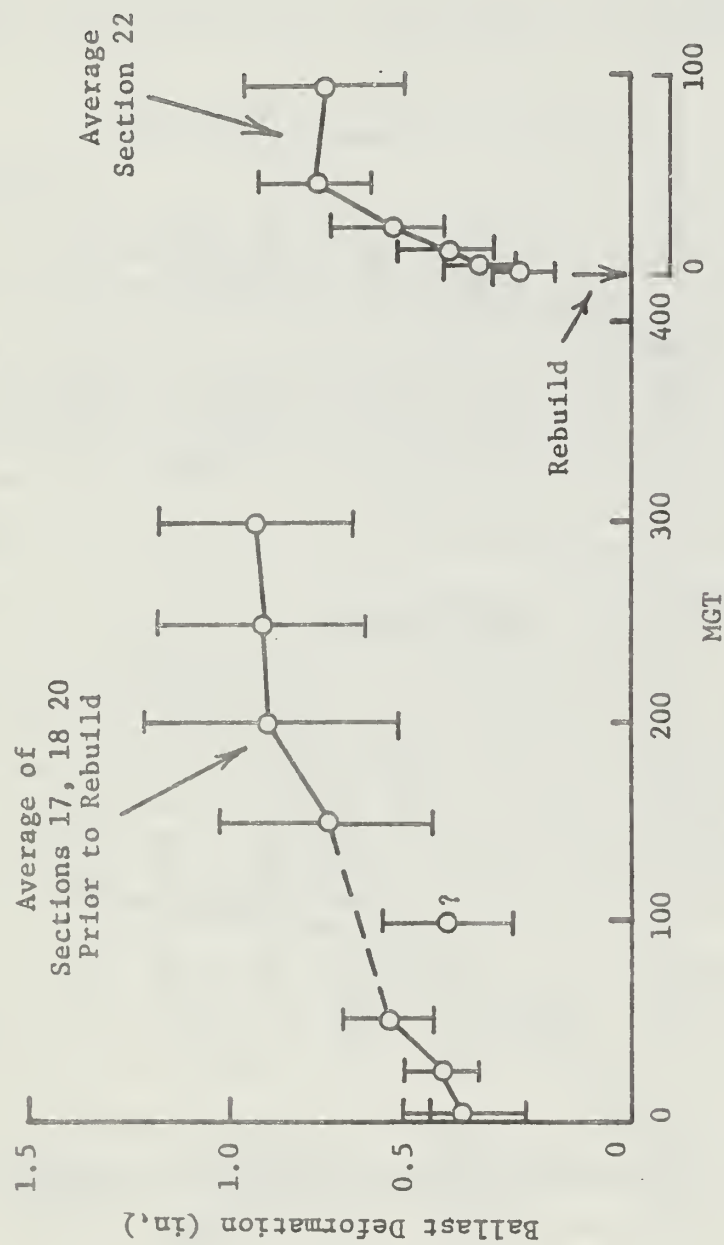Figure 34. Ballast and Subgrade Deformations from Instrumentation at FAST Section 22 after 1979 Rebuild

102

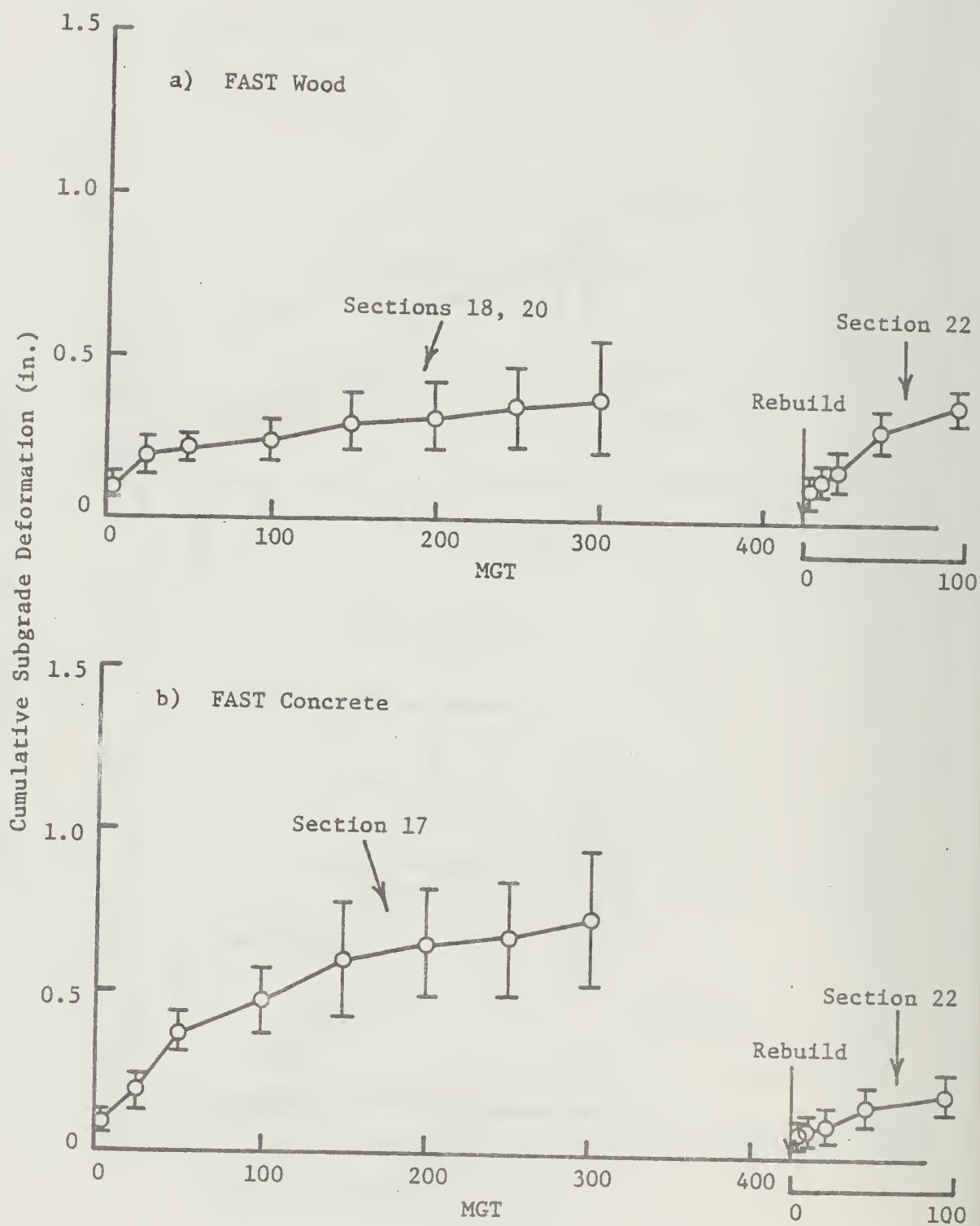Figure 35. Measured Ballast Deformations from FAST Instrumented Sections

103

Figure 36.   Measured Subgrade Deformations from FAST Instrumented Sections

Instrument reading errors, data reduction problems, or calibration errors are also distinct possibilities. All aspects of geotechnical instrumentation require engineering judgment in the final interpretation. Several years of experience directly related to the FAST instrumentation program have lead to the conclusion that these rebuild subgrade deformation measurements should be disregarded, or at a minimum, given little emphasis. The contributions of the subgrade deformation will be disregarded for the prediction comparisons for FAST.

Settlement survey measurements were also made at FAST section 22 after the 1979 rebuild. These measurements (to be shown later) will be used for the comparison with predicted track deformations for FAST.

7.3 Predictions of Track Settlement

General Considerations

The predictions of the vertical track settlements at the revenue field sites and FAST section 22 were based on the methodology outlined in Chapter 6. The depths influenced by the revenue site maintenance operations were from 6 to 8 inches below the ties. The representative points for these ballast depths were thus taken as the midpoint depths for these disturbed ballast zones.

Since the survey data from FAST indicated only slight differences between the wood and concrete track settlements, only predictions for the concrete tie section of FAST section 22 were made. However, these were subdivided into two sets. The first set was for the 0 to 93 MGT period and considered the entire 15-in. ballast depth. The second was for FAST section 22 after the maintenance operations at 93 MGT. For this set, a 7.5-in.-deep disturbed ballast layer was assumed.

The stress states were estimated using GEOTRACK. The track structural properties used for the GEOTRACK analyses are given in Table 2. The layer profiles and divisions and subgrade moduli for the revenue sites were the same as used for the track modulus predictions, and are shown in Figs. 22 through 25. The layer divisions used for FAST consisted of two 7.5-in. ballast layers underlain by the silty sand subgrade material. The subgrade moduli expressions were given in Chapter 3 for the FAST section. The resilient strain-shear stress ballast formulation, as described in Chapter 3, was used to characterize the ballast at all of the sites. The multiple-axle loading configurations used are shown in Fig. 29, and the appropriate mean and dynamic wheel loads are given in Tables 17 and 18.

The calculated stress ratios and strains at the first cycle for the field sites are given in Table 22 for the predictions based on stress path CB (Fig. 30). The calculated stress ratios and the first cycle strains for stress path DE are given in Table 23. The first cycle strain is obtained from the uncompacted data in Fig. 31.

The conversions from MGT to number of cycles at each of the load levels were explained in Chapter 5. The method of superposition of strains due to the mixed loading conditions was explained in Chapter 6. The ballast constants, C, used for each of the predictions are given in Tables 22 and 23.

Predictions based on paths CB and DE using the results from one-way repeated loading will be referred to as predictions CB (1-way) and DE (1-way), respectively. Those predictions based on stress paths CB and DE that used the results from the shear stress reversal and box tests will be referred to as predictions CB (SSR) and DE (SSR), respectively.

105

Table 22. Parameters for Stress Path CB Predictions

Site	z (in.)	h (in.)	Load (kips)	q_{max} (psi)	q_{min} (psi)	$\bar{\sigma}_3$ (psi)	One-Way Loading			Shear Stress Reversal		
							$\frac{q_{max}}{q_f}$	ε_1 (%)	C	$\frac{\Delta q}{q_f}$	ε_1 (%)	C
Leeds, Wood	3.0	6.0	15.0	2.1	-1.6	8.4	0.16	0.25	0.34	0.28	0.42	0.63
			27.3	4.9	-1.6	13.5	0.23	0.81	0.34	0.30	0.81	0.63
			35.7	6.8	-1.6	17.0	0.25	1.02	0.34	0.31	1.02	0.63
			43.5	8.6	-1.6	20.3	0.27	1.62	0.34	0.32	1.22	0.63
Leeds, Concrete	3.5	7.0	15.0	1.3	-2.7	10.4	0.07	0.21	0.26	0.23	0.42	0.63
			27.3	3.4	-2.7	14.8	0.14	0.44	0.26	0.25	0.59	0.63
			35.7	4.9	-2.7	17.9	0.17	0.54	0.26	0.26	0.72	0.63
			43.5	6.2	-2.7	20.7	0.19	0.83	0.26	0.27	1.04	0.63
Lorraine	4.0	8.0	15.0	1.9	-2.9	10.1	0.15	0.30	0.40	0.39	1.01	0.63
			32.0	7.1	-2.9	15.5	0.39	3.10	0.40	0.56	2.79	0.63
			39.8	9.5	-2.9	18.0	0.46	5.40	0.40	0.60	4.32	0.63
			45.0	11.1	-2.9	19.6	0.50	7.84	0.40	0.63	5.10	0.63
Aberdeen	4.0	8.0	18.7	1.7	-3.1	12.4	0.10	0.25	0.25	0.29	0.62	0.63
			34.2	4.0	-3.1	19.0	0.17	0.57	0.25	0.30	1.14	0.63
			46.2	5.7	-3.1	24.1	0.20	0.96	0.25	0.30	1.45	0.63
			75.0	9.9	-3.1	36.4	0.23	2.18	0.25	0.30	2.18	0.63
FAST 22, Concrete	3.8	7.5	32.8	5.7	-2.9	10.3	0.33	1.24	0.30	0.50	1.65	0.63
			38.3	7.2	-2.9	10.6	0.41	2.33	0.30	0.57	2.12	0.63
			40.5	7.8	-2.9	10.7	0.44	2.78	0.30	0.60	2.57	0.63
			48.0	9.9	-2.9	11.0	0.54	5.50	0.30	0.70	3.74	0.63
	11.2	7.5	32.8	3.5	-2.4	6.3	0.33	0.76	0.30	0.56	1.13	0.63
			38.3	4.6	-2.4	8.1	0.34	1.05	0.30	0.52	1.30	0.63
			40.5	5.1	-2.4	8.8	0.35	1.23	0.30	0.51	1.41	0.63
			48.0	6.6	-2.4	11.3	0.35	1.58	0.30	0.48	1.58	0.63

z = Depth for Stress Computation; h = Ballast Layer Thickness; Load = Wheel Load.

Table 23. Parameters for Stress Path DE Predictions

Site	z (in.)	h (in.)	Load (kips)	$\bar{\sigma}_3$ (psi)	One-Way Loading $\frac{q_{max}}{q_f}$	ε_1 (%)	C	Shear Stress Reversal $\frac{\Delta q}{q_f}$	ε_1 (%)	C
Leeds, Wood	3.0	6.0	15.0	6.1	0.22	0.24	0.34	0.38	0.61	0.63
			27.3	8.7	0.36	1.22	0.34	0.47	0.87	0.63
			35.7	10.4	0.41	2.18	0.34	0.51	1.66	0.63
			43.5	12.1	0.45	3.39	0.34	0.53	2.18	0.63
Leeds, Concrete	3.5	7.0	15.0	8.4	0.09	0.17	0.26	0.27	0.42	0.63
			27.3	10.7	0.19	0.43	0.26	0.34	0.75	0.63
			35.7	12.2	0.24	0.73	0.26	0.37	1.10	0.63
			43.5	13.6	0.28	1.09	0.26	0.40	1.36	0.63
Lorraine	4.0	8.0	15.0	8.5	0.18	0.34	0.40	0.45	1.11	0.63
			32.0	11.2	0.53	5.15	0.40	0.74	4.26	0.63
			39.8	12.4	0.64	9.42	0.40	0.84	6.70	0.63
			45.0	13.3	0.71	10.60	0.40	0.89	7.98	0.63
Aberdeen	4.0	8.0	18.7	10.0	0.12	0.20	0.25	0.35	0.80	0.63
			34.2	13.3	0.23	0.80	0.25	0.41	1.33	0.63
			46.2	15.8	0.28	1.26	0.25	0.44	1.90	0.63
			75.0	22.0	0.37	3.52	0.25	0.48	3.08	0.63
FAST 22, Concrete	3.8	7.5	32.8	8.6	0.40	1.72	0.30	0.60	2.06	0.63
			38.3	8.8	0.49	3.17	0.30	0.69	2.82	0.63
			40.5	8.8	0.53	4.05	0.30	0.73	3.34	0.63
			48.0	9.0	0.66	7.56	0.30	0.85	4.86	0.63
	11.2	7.5	32.8	6.4	0.33	0.77	0.30	0.55	1.28	0.63
			38.3	7.3	0.38	1.31	0.30	0.57	1.46	0.63
			40.5	7.6	0.40	1.52	0.30	0.59	1.82	0.63
			48.0	8.9	0.45	2.67	0.30	0.61	2.14	0.63

See footnotes Table 22

Revenue Site Predictions

The predicted track settlements for the Leeds wood tie section are shown
in Fig. 37. The predictions made using stress path DE gave the largest defor-
mation and were close to the uncorrected survey measurements. The settlement
rate appeared to level off for the second field measurement interval, and was
about parallel to the predictions. However, the predictions all underestima-
ted the track vertical settlement, particularly when any adjustments were made
to correct   the initial settlement.

The measurements and predictions for the Leeds concrete tie track section
are shown in Fig. 38. The field survey measurements showed a very large change
in track settlement from the 10 to 24 MGT measurements, which was much larger
than the initial change from the 0 to 10 MGT readings. This occurred over the
winter months and may have been associated with frozen ballast or frost heave.
The two final survey measurements appear to indicate that the track settlement
rate was leveling off, as was expected and predicted, but additional data are
required to substantiate this conclusion. The predicted values are all much
lower than the measured values after 20 MGT and show a slower rate of increase
with MGT.

Figure 39 shows the measured survey track settlements and the predicted
track settlements for the Lorraine site. The field measurements indicated a
continuous settlement of the track, with no indication that the deformations
were leveling off with increased MGT. The predictions always showed a lower
settlement rate after about 10 MGT traffic. All predictions for the Lorraine
site overestimated both the initial settlements and the cumulative settlements.
The first cycle deformations for the Lorraine site predictions can be deter-
mined from Tables 22 and 23, and are not shown on the figure. The first cycle
deformations are much smaller than the first data points shown, since the
first points plotted in the prediction figure represent about 0.1 MGT.

The results from the strain coil measurements and corrected survey meas-
urements, along with the predictions of track settlement for the Aberdeen site,
are shown in Fig. 40. As previously indicated, the track settlement at Aber-
deen apparently was due primarily to the upper ballast deformations. Follow-
ing a high initial deformation rate in the first 3 MGT, the ballast deforma-
tions continued to increase at a lower constant rate, showing no tendency to
level off with increased traffic accumulation. Again, further survey data or
strain coil measurements would have been useful to help interpret longer term
trends past the 30 MGT level. Although the measured values lie within the
range of predicted values, the shapes of the predicted curves after about 5 MGT
were quite different from the observed settlements.

FAST Predictions

Two sets of predictions were made for FAST section 22. Both sets were
done for the concrete tie section track parameters. The first set of predic-
tions considered the 0 to 93 MGT period directly after the 1979 rebuild. For
these predictions, the full 15-in. depth of newly placed ballast was consider-
ed. The second set of predictions assumed that only the top half of the bal-
last was disturbed due to the maintenance operation that took place after 93
MGT of traffic.

The measured and predicted vertical track settlements at FAST are shown
in Fig. 41. The 0 to 93 MGT track settlements and ballast deformations both
showed an irregular increase from about the 30 to 50 MGT interval, followed by
a reduced settlement rate up to the time of the surfacing operations. The
shapes of both measured and predicted ballast deformations were similar.

Figure 37. Measurements and Predictions of Track Settlement for Leeds Wood Tie Section
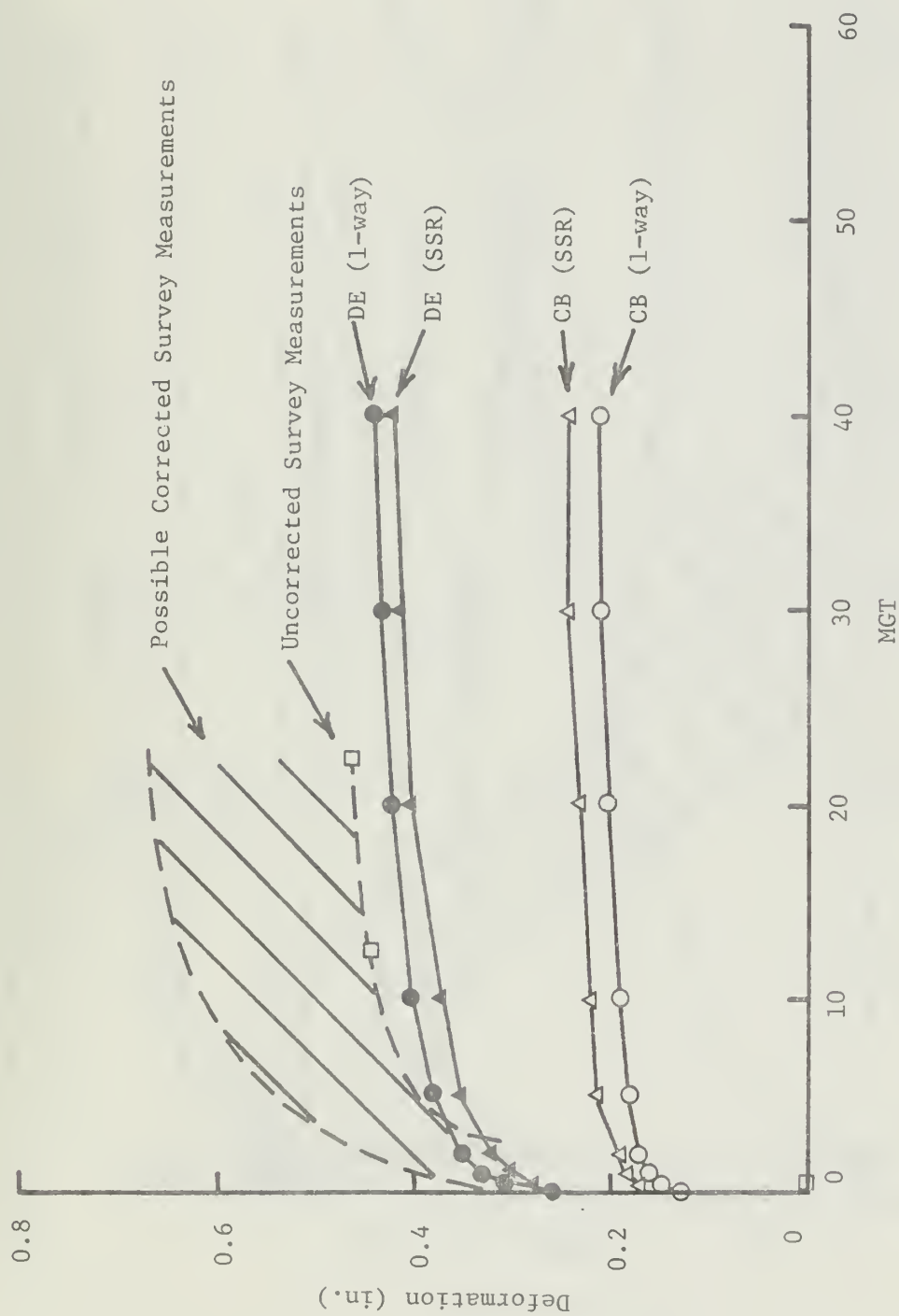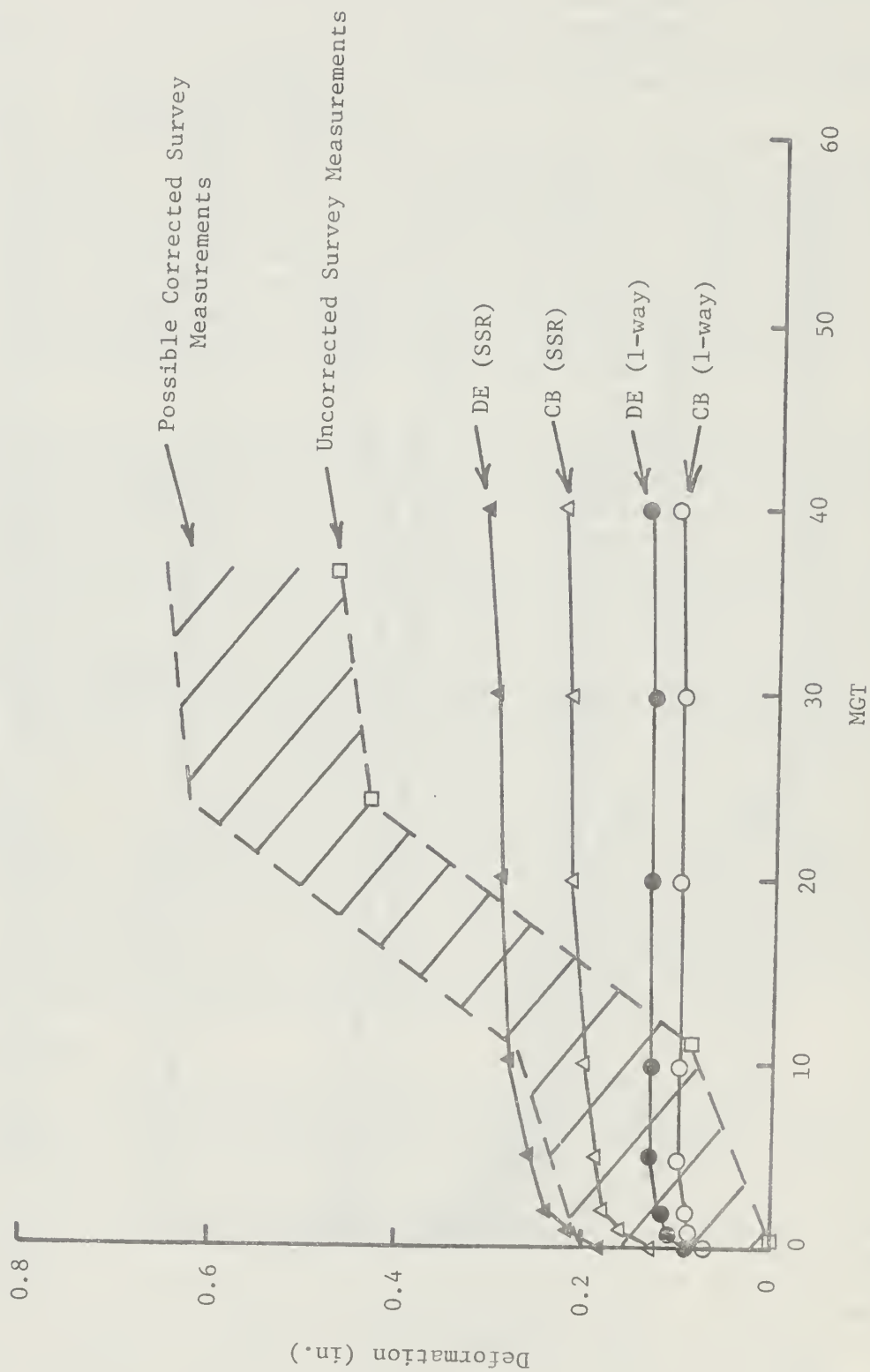
Figure 38. Measurements and Predictions of Track Settlement for Leeds Concrete Tie Section
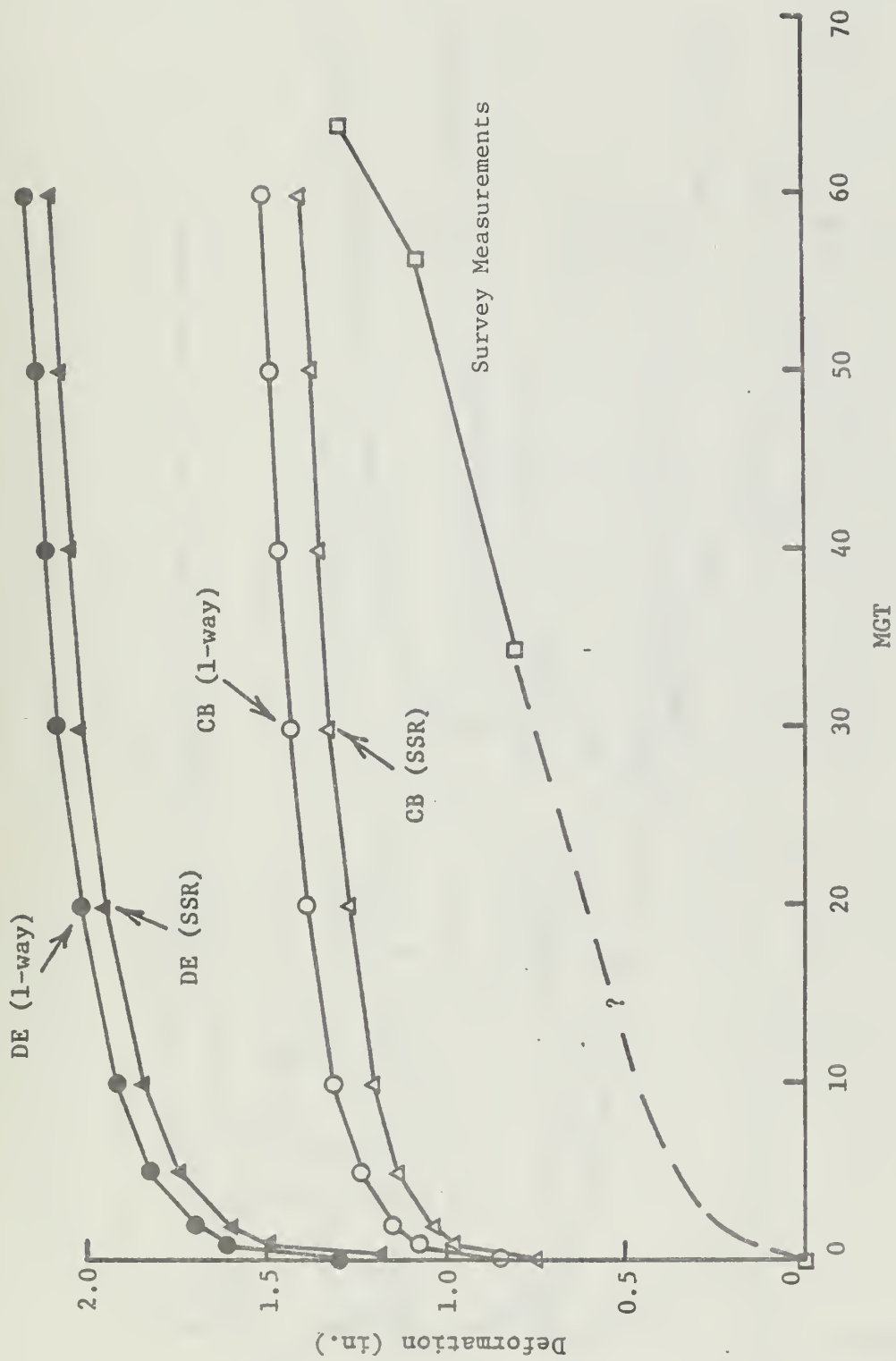
110

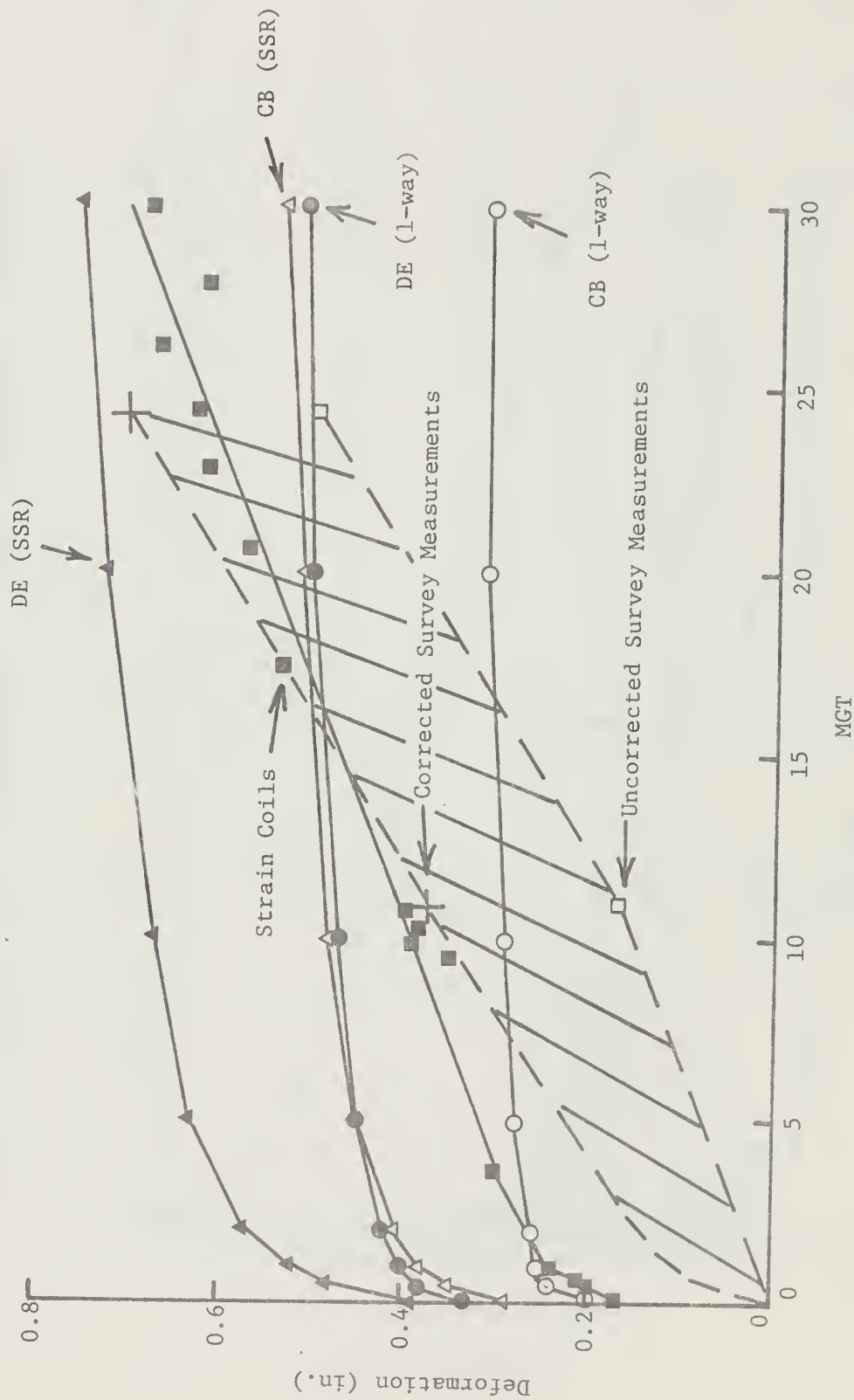Figure 39. Measurements and Predictions of Track Settlement for Lorraine

111

Figure 40. Measurements and Predictions of Track Settlement for Aberdeen
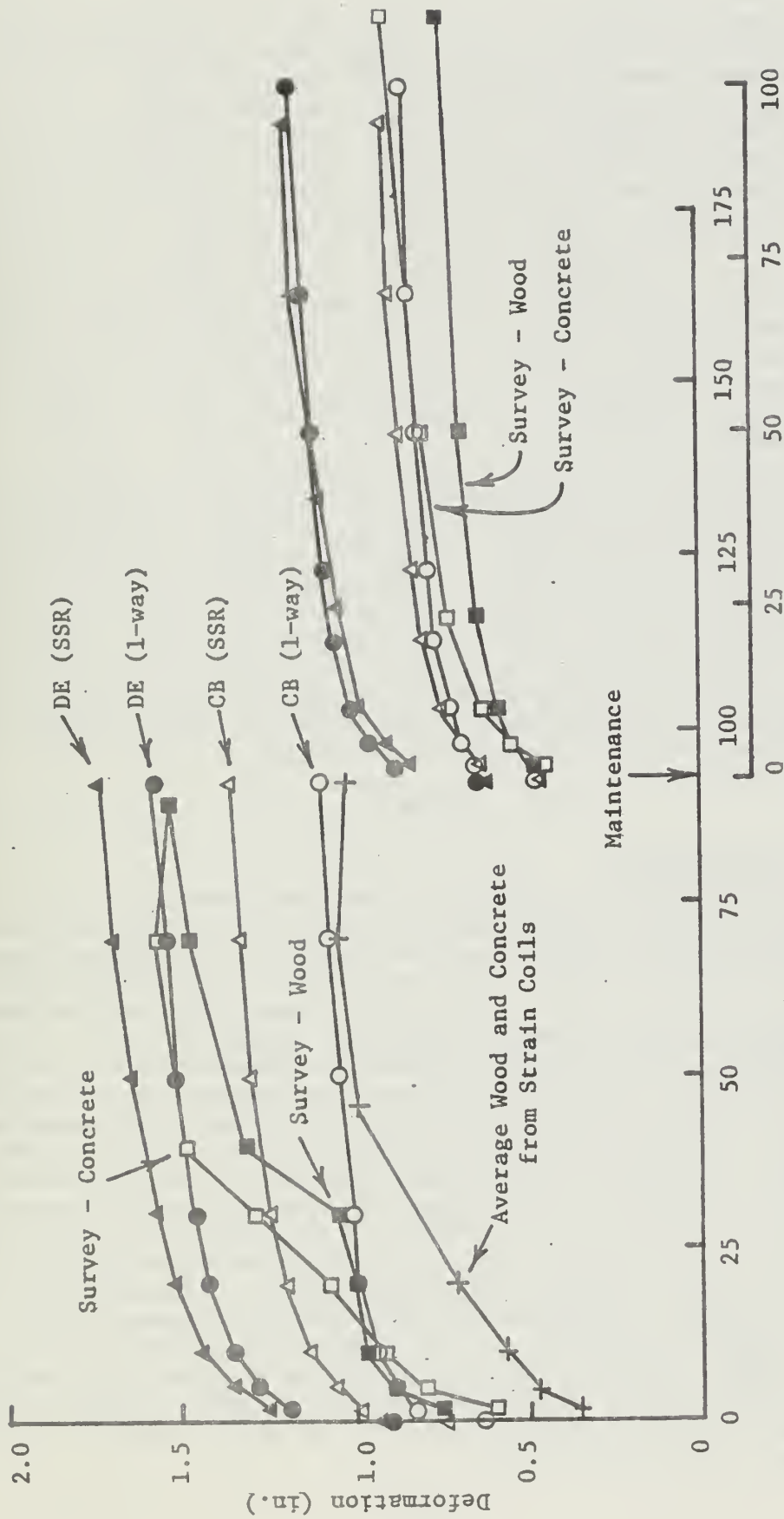
112

Figure 41. Measurements and Predictions of Track Settlement for FAST Section 22 After Rebuild

113

However, the predictions for 0 to 93 MGT were all greater than the measured ballast deformations obtained from the strain coils. This could be due to the compaction sequences used during the rebuild operation, which would have resulted in lower ballast strain under subsequent traffic loading.

The difference between the 0 to 93 MGT survey measurements and the ballast deformations from the strain coil readings appeared consistent with the measured subgrade deformations, even though the subgrade deformation data are questioned. This could have resulted from compensating errors. It is known that there were some problems at FAST with the 0 to 93 MGT portion of the survey data, with respect to reference elevations and data reduction procedures.

Instrumentation measurements of the ballast and subgrade cumulative deformations were not available after the 93 MGT maintenance at FAST. However, the survey measurements and predictions after the surfacing are shown in Fig. 41. Both the shapes of the initial and longer-term predicted settlements were similar to the survey measurements. The magnitudes were also in general agreement for the CB stress paths.

The measured track settlements from 0 to 93 MGT after rebuild for the strain coils and from the surveys after the maintenance showed a similar amount of initial track settlement. However, these data, as well as the predictions, showed larger deformations from traffic after rebuild than were observed after subsequent maintenance. This was primarily due to the differences in the initial ballast physical state in the lower portion of the ballast layers, even though there was some initial compaction of the ballast during the rebuild. This appears to confirm the previous assumptions that only the upper 6 to 8 in. of the ballast layer should be considered as disturbed by maintenance. Considering the variability of the FAST data, the agreements between measured and predicted track settlements were good.

7.4 Discussion

Stress Path Considerations

The predictions made for the field sites were based on the invariant transformations of the three-dimensional stress tensors into axisymmetric, constant-confining-pressure triaxial test conditions. The roadbed stresses were approximated by the assumed equivalent stress paths labeled CB and DE in Fig. 30, since paths similar to the one defined by the moving load, path AB, could not be reproduced using the present laboratory equipment.

The predictions showed varying amounts of agreement with the measurements that were not clearly attributable to any of the particular stress paths. The main difference between the results obtained using the two stress paths, CB or DE, was in the first cycle strains associated with these stress paths. The choice of ballast constant, C, from either the one-way repeated loading tests or from the box test results was of minor consequence compared to the value of first cycle strain used for the predictions. Considering the complex nature of the problem and the material behavior involved, and considering the large field variability, the magnitude of the predicted settlements for the revenue sites was in reasonable agreement with that of the field measurements. Certainly the agreement was within the range normally experienced in geotechnical predictions. The predictions made for the FAST site after the 93 MGT maintenance were in particularly good agreement with the measured values, perhaps due to the more controlled conditions present at FAST, especially in the absence of wheel tread irregularities.

114

It would have been possible to obtain closer agreement between the pre-
dictions and the revenue site measurements by selecting other depth points as
representative for the disturbed ballast zones. This was not attempted for
several reasons. First, reasonably good agreement was obtained between meas-
ured and predicted deformations at FAST using the midpoints of the two 7.5-in.
ballast layers for the 0 to 93 MGT predictions, followed by using only the mid-
point of the upper layer as representing the disturbed ballast following main-
tenance. Secondly, the methodology used to predict track settlements needed
to be applied consistently to all the sites in order to assess the results.
The use of different representative depths in the disturbed ballast layers for
each site could not be justified by available information.

Another possible reason why the predicted deformations disagreed with the
measurements is that the actual stress paths for the representative points
were not similar to either stress paths AB, CB or DE. The box tests indicated
that the loaded and unloaded states resulted in essentially the same magnitude
of lateral stress. In contrast, the GEOTRACK model predicts substantial in-
cremental compressive horizontal stresses at depths of 4 in. below the tie.

As an example of the differences that the incremental horizontal stresses
have on the stress paths, consider the calculated stress paths at $\cong$ 4 in. using
the 50th percentile load from the FAST section 22 analyses, and a K_o value of
6. The initial vertical geostatic stress at this depth was about 1 psi. The
incremental stresses from the GEOTRACK calculations were $\Delta\overline{\sigma}_x$ = 12 psi, $\Delta\overline{\sigma}_y$ =
6.8 psi, and $\Delta\overline{\sigma}_z$ = 26 psi. The x and y coordinate directions were
parallel to the tie and rail, respectively. The z direction was vertical.
The calculations for the equivalent axisymmetric stresses based on these incre-
mental stresses are given in Table 24. The stress path equivalencies assuming
no change in the horizontal stresses but the same increment of vertical stress
as the box tests showed are also given in Table 24. The incremental shear
stresses on the vertical and horizontal planes were neglected for these exam-
ple calculations since, in this case, they were small.

The resulting stress paths are shown in Fig. 42. The box stress path
shows a peak point at the static failure envelope, a condition obviously not
possible. If the box test results were indicative of the actual stress states,
it should be clear from Fig. 42 that deformation predictions would be uncer-
tain and very sensitive to the exact values of stress, since the stresses cycle
between two failure states. This is indicated, in part, by the permanent
strain triaxial results in Chapter 3.

The actual stress paths for the roadbed elements may lie somewhere be-
tween the box test stress paths and those predicted with the GEOTRACK model.
Static failure in the conventional sense did not occur in the box tests, due
to the confinement provided by the rigid side and end boundary conditions.
These boundary conditions were appropriate for measuring the K_o values under
zero lateral strain, but may not have represented the ballast layer boundary
conditions present in the field. The box tests did, however, reproduce the
compaction effects of traffic, as was reflected by the changes in ballast den-
sity and plate bearing resistances.

The predictions were not obtained for either of the stress paths in Fig.
42, but for the constant-confining-pressure "equivalent" paths, as in Fig. 30.
Stress paths DE and CB can be expected to give different results from those in
Fig. 42. Thus, if the stress states actually lie somewhere between the GEO-
TRACK and box states in Fig. 42, the predictions using DE or CB should contain
some error.

Table 24. Comparison of GEOTRACK and Box Test Stress Paths

Given: $\bar{\sigma}_{vo} = 1$ psi and $K_o = 6$

Then: $\bar{\sigma}_{ho} = 6$, $\bar{p}_o = 3.5$ psi, and $q_o = -2.5$ psi

<div align="center">

GEOTRACK

$\Delta\bar{\sigma}_x = 12$

$\Delta\bar{\sigma}_y = 6.8$

$\Delta\bar{\sigma}_z = 26$

BOX

$\Delta\bar{\sigma}_x = \Delta\bar{\sigma}_y = 0$

$\Delta\bar{\sigma}_z = 26$

</div>

<div align="center">

FINAL STRESS STATES

</div>

$\bar{\sigma}_x = 18 \simeq \bar{\sigma}_2$ $\bar{\sigma}_x = 6 = \bar{\sigma}_2$

$\bar{\sigma}_y = 12.8 \simeq \bar{\sigma}_3$ $\bar{\sigma}_y = 6 = \bar{\sigma}_3$

$\bar{\sigma}_z = 27 \simeq \bar{\sigma}_1$ $\bar{\sigma}_z = 27 = \bar{\sigma}_1$

<div align="center">

INVARIANT TRANSFORMATION

</div>

$$I_1 = 1/3(\bar{\sigma}_x + \bar{\sigma}_y + \bar{\sigma}_z) = \bar{\sigma}_{oct}$$

$$J_2 = 1/6[(\bar{\sigma}_x - \bar{\sigma}_y)^2 + (\bar{\sigma}_x - \bar{\sigma}_z)^2 + (\bar{\sigma}_y - \bar{\sigma}_z)^2]$$

$$\tau_{oct} = \left(\frac{2J_2}{3}\right)^{\frac{1}{2}}$$

$$\bar{\sigma}_1 = \bar{\sigma}_{oct} + \sqrt{2}\ \tau_{oct} \qquad\qquad \bar{\sigma}_3 = \bar{\sigma}_{oct} - \frac{\tau_{oct}}{\sqrt{2}}$$

<div align="center">

EQUIVALENT AXISSYMMETRIC STRESS STATES

</div>

$\bar{\sigma}_1 = 27.6$ $\bar{\sigma}_1 = 27.0$

$\bar{\sigma}_3 = 15.1$ $\bar{\sigma}_3 = 6.0$

$\bar{p} = 21.4$ $\bar{p} = 16.5$
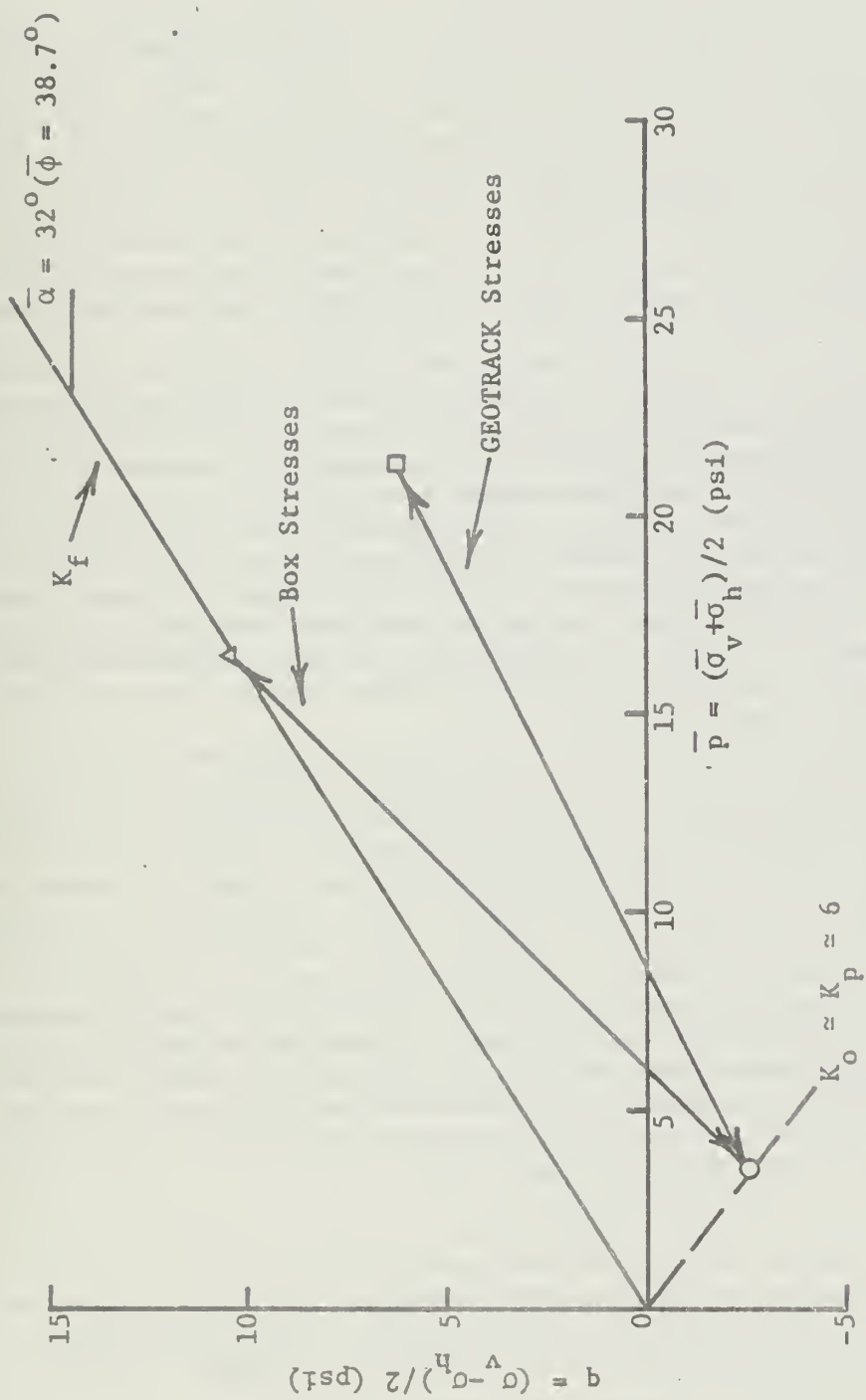
$q = 6.3$ $q = 10.5$

Figure 42. Comparison of Box Test and GEOTRACK Stress Paths

Track Vibrations

Another possible explanation why the predicted magnitudes of track settlement were generally less than the measured values is that the predictions and laboratory testing methods did not consider any possible effects of track vibrations. Field measurements made by BCL at the revenue sites have indicated that the concrete ties vibrate considerably at three principal bending modes: 120, 350 and 650 Hertz, particularly in the presence of wheel impacts. The actual vibrations transmitted to the ballast were not measured, but the coupling between the tie and the top ballast particles is assumed to be poor at these frequencies. Field measurements of the vibration frequencies in railroad track foundations [55] have shown transient values on the order of 30 to 40 Hz in the supporting soil layers. The conclusion was drawn by Morgan [56] that traffic-induced vibrations in the ballast could lead to more rapid accumulation of permanent deformation than would result from repeated loadings alone.

The magnitudes of the ballast deformations that could have been attributed to track vibrations is difficult to quantify. It is likely that vibrations coupled with high loads from wheel irregularities would be most damaging. Because the vibrations occur simultaneously with, and as a result of, the repeated loadings, separation of the settlements due only to vibration from those due primarily to the mixed repeated loadings would be very complicated.

The Aberdeen site could have been subjected to vibrations sufficient to cause the difference between predicted and measured trends of settlement with MGT. Here there were high-speed passenger cars that were shown to cause the high dynamic loads as a result of wheel tread irregularities. Vibrations transmitted to the ballast could easily cause deformations in excess of those resulting from cyclic loading alone.

Although the predicted Lorraine deformations were larger than the measured values, the shapes of the predicted and measured curves were also different. The vibration effects at the Lorraine site were not expected to be as severe as Aberdeen. Without actual field measurements, however, differences in the effects of vibration at these sites is uncertain. The ballast at the Lorraine site was heavily fouled, but still initially loose due to the high raise applied to the track during the surfacing. Clean ballast would be more susceptible to vibratory densification, but laboratory experiments that were conducted indicated that fouled, compacted ballast also can be densified by vibration frequencies and accelerations on the order of those anticipated in track.

The relatively good agreement between measured and predicted settlements for FAST are probably a result of the absence of significant vibrations at FAST. The consists, speeds, and wheel conditions at FAST were very well controlled, compared to the revenue sites.

Other Factors

In addition to the ballast deformations that resulted from cyclic loadings and/or vibration, there are numerous factors that have not been accounted for in the prediction methodology. These include ballast recompaction, ballast degradation, and subgrade effects, as well as possible seasonal effects.

Ballast Recompaction. Laboratory triaxial tests did not show significant amounts of volume change under repeated loadings. Thus, these tests did not reproduce the ballast densification or compaction measured in the field. However, the box tests did reproduce the compaction changes in the ballast.

The measured changes in ballast density due to the maintenance operations

118

could be interpreted in a form analogous to the comparable strains or volume-
tric reductions resulting from one-dimensional compressions. It can be shown
that the relative increase in density of the ballast under zero lateral strain
conditions is given by

$$\frac{\gamma_d - \gamma_{do}}{\gamma_{do}} = \frac{\Delta\gamma_d}{\gamma_{do}} = \frac{\varepsilon_v}{1 - \varepsilon_v} \quad , \tag{36}$$

where γ_d is the dry density at any time,

γ_{do} is the initial dry density after maintenance, and

ε_v is the vertical strain, assuming that densification occurs with no
horizontal strain.

From pre- and post-maintenance ballast densities, particularly under the ties,
the expected track settlements due to recompaction of the ballast could be es-
timated using Eq. 36. The rate and time history of the expected settlements
could not be determined, since the ballast densities at only the two points
were known. Using the results from the pre- and post-maintenance BDT results
[1,42], the vertical settlements from ballast recompaction were estimated.
The Leeds concrete site pre-maintenance densities were not available, as pre-
viously explained. The Aberdeen under-tie BDT showed negligible changes in
ballast density due to the maintenance operations. Thus, the Leeds wood sec-
tion and Lorraine results for under-tie tests will be used to conceptually
illustrate the settlements expected due to recompaction.

The measured density change, the disturbed zone thickness and the result-
ing layer compression for the two sites are as follows:

Site	$\dfrac{\Delta\gamma_d}{\gamma_{do}}$	ε_v	h (in.)	$\varepsilon_v \cdot h$ (in.)
Leeds, Wood	0.094	0.086	6	0.52
Lorraine	0.115	0.103	8	0.83

The assumed influence depths, h, of the recompacted zones were the same as the
disturbed ballast depths used for the strain predictions.

As can be seen from the measured track settlements shown in Figs. 37 and
39, the above values of settlement due to recompaction of the ballasts are of
the same order of magnitude as the field settlement measurements.

The mechanisms of ballast recompaction are the same as those affecting all
aspects of track settlement. All of these mechanisms occur simultaneously,
i.e., cyclic loading, vibration, and possible horizontal shearing at the tie-
ballast interface. Individual contributing factors cannot be separated easily,
then analyzed, and finally recombined in an additive manner.

Ballast Degradation. Breakdown of the ballast particles will cause settle-
ment because of a decrease in volume of the assembly of particles, similar to
the effect of compaction. The causes of long-term ballast degradation can de-
rive from several sources. Particle breakage from the high intergranular con-
tact stresses is one source. The susceptibility of different ballasts to such
breakdown is currently not well defined, nor are the effects that such degra-
dation would have on track performance. Research is currently underway at

UMass to investigate the breakdown potential for various ballasts, including some of the materials used at both the revenue sites and FAST, so that better performance evaluations of ballast can be made.

Ballast degradation also can be affected by factors not associated with traffic loadings, such as chemical attack and weathering. These factors affect different ballasts in different ways.

Freeze-thaw cycles, in areas prone to such seasonal variations, could also contribute to particle breakdown. Ice intrusion into the small fissures in individual ballast particles could lead to increased cracking and reduced particle strength. A completely frozen ballast condition, where the individual particles were "cemented," could lead to higher stresses in the formation and hence increased particle breakage.

Subgrade Effects. The contribution of subgrade to the total track settlement was neglected in the predictions. The relationship between the strain coil measurements at Aberdeen and the agreement between the FAST track survey and predictions partially justified this simplification.

Another reason why the subgrade contributions were not included was that the measured permanent strains from the laboratory tests done on the revenue site subgrade samples were inconsistent with either the measured or expected settlements. In some cases, the strains developed in subgrade samples under assumed representative triaxial stress conditions became very large after a relatively small number of load cycles. This may have been the result of incorrect representative stress paths, sample disturbance, the fact that the cyclic loading conditions were undrained, or a combination of all these factors.

The undrained loading condition is reasonable for representing the train loading effects, but continued cycling without allowing the dissipation of any excess pore pressure that might develop is not representative of the field conditions. The trains do not pass continuously over the sites, but are spaced at relatively long intervals. This allows pore pressure dissipation to occur between loadings, and hence decreases the resulting permanent deformations. The radial strain developments in the triaxial tests with constant lateral stress would also lead to larger axial deformations than anticipated in the field, where the subgrade soils are greatly confined by the surrounding ground.

The extrapolation of the triaxial test permanent strain data would have provided excessively large predicted values of subgrade deformation. This was particularly true for the Aberdeen site, where it was found that there were negligible subgrade contributions to the track settlement. The effects of partial or intermittent drainage, plane strain versus triaxial testing, and stress path effects on the subgrade deformation characteristics are areas that require further study.

Other subgrade conditions can, however, have a large influence on overall track performance. Factors such as subgrade consolidation under static embankment loads and subgrade movements from frost and moisture changes would be important in regions having subsurface conditions susceptible to these mechanisms. Even after many hundreds of MGT, soil embankments may continue to settle by lateral creep induced by the repeated traffic loads, even though confined subgrades are stable. The Lorraine site, in particular, may be susceptible to this condition.

For newly built track, subgrade compaction from the cyclic traffic loads can be significant. The increases in penetration resistance in the FAST subgrade resulting from the first 400 MGT clearly showed densification.

Subgrade penetration into the ballast when inadequate soil filters or no filters are used to prevent particle migration is clearly another source of settlement. However, the field sites involved in this study did not appear to involve this problem.

CHAPTER 8. SUMMARY AND CONCLUSIONS

The objective of this portion of the concrete crosstie correlation study was the prediction of vertical track settlement at four field sites. Since the track systems selected for analysis were in different geographical locations and subjected to different loading and environmental conditions, it was necessary to perform a complete ballast physical state assessment and subgrade investigation of the track foundations present at each site.

The ballast physical states were identified using the plate load test, ballast density test, and lateral tie push test. A maintenance cycle, consisting of raising and tamping the ballast layer, was performed at each of the sites and the resulting changes in ballast conditions were measured. One of the primary effects of the track maintenance was a loosening and disturbance to the previously compacted and stable ballast layer. The ballast structure was disturbed both in the cribs and under the ties. The amount of disturbance was related to the amount of the raise. It was found that for trackbeds subjected to a significant raise, say 1.5 to 2 in., the physical states of the ballast immediately after the raise were approximately independent of ballast type and initial condition.

Samples of the ballast materials were recovered from the sites and subjected to repeated load triaxial testing. Additionally, a granite ballast from FAST was tested in triaxial repeated load conditions with and without shear stress reversals. Partial unloading and sequential application of repeated loads were also considered. It was found that the resilient moduli values for full unloading of compressive vertical stresses could be correlated to the maximum bulk stress on the sample. Either the log-log or an arithmetic formulation could be used to relate the compressive resilient Young's modulus to the maximum bulk stress. For partial unloadings, however, the resilient modulus was higher than that measured under full unloading, and was not uniquely related to the maximum bulk stress on the sample.

The results from the shear stress reversal repeated load testing showed that the resilient moduli from extension and compression stress states were quite different. The extensional resilient moduli values were smaller than the compressional moduli values under comparable stress conditions. When the vertical stresses were cycled between compression and extension states, the total resilient moduli values fell between the extensional and compressive values. This is believed to more closely represent actual track conditions than prior techniques, which did not include shear stress reversals.

A comparison of the resilient moduli of all the field site ballasts also leads to the conclusion that the moduli values were not significantly dependent upon ballast type.

The inelastic behavior of the ballast was investigated using the repeated load triaxial tests and a box-type testing device. The permanent strain behavior of single-staged, constant-amplitude tests without shear stress reversal could be defined by the first cycle strain, ε_1, and the material constant, C. This constant was independent of stress conditions for a particular ballast, but was not the same for all ballasts.

Staged tests on the ballast were done involving sequential application of variable magnitude repeated loads. For these tests, the total permanent strain developed in a ballast sample was controlled by the maximum past load and was independent of the loading sequence, so long as the number of load repetitions

at each stress level was the same for each of the tests. This means that the heaviest wheel loads, generally produced by impacts from wheel tread irregularities, cause most of the settlement. Subsequent applications of reduced load as well as partial unloadings resulted in negligible increases in permanent strain.

When the repeated loads in the triaxial tests were cycled between extension and compression, the permanent strains developed at rates significantly greater than the rates for one-way loading. The increased permanent strain development was dependent upon both the compressive failure ratio and the ratio of cyclic shear stress to the maximum shear stress resulting from compression loading.

The permanent deformation accumulation in the ballast box tests, which were intended to simulate field behavior, was a logarithmic function of the number of load cycles, the compaction state, and the first cycle deformations. The trends in inelastic behavior were similar to those in the triaxial tests. The relationship between permanent deformation and the log of the number of cycles was similar to the trend of permanent deformation observed at FAST.

The box tests also showed that relatively large horizontal residual stresses can build up in the ballast as a result of cyclic loadings. These residual stresses can develop not only under the tie, but also in the crib areas. This may be a mechanism in the phenomenon of tie migration or skewing. The horizontal stress measurements made in the ballast box suggested that the ballast layer in track is subjected to extreme variations in cyclic stresses. The unloaded stress states may be close to the limiting passive failure stress conditions.

Measurements of vertical track modulus were made before and after the revenue site maintenance operations. The major factors contributing to the magnitude of vertical track modulus were ballast depth and subgrade stiffness. Track modulus measurements made in the track sections at Leeds having wood ties spaced at 19.5 in. and concrete ties spaced at 24 in. were not significantly different. The field measurements did not indicate significant changes in the magnitude of track modulus due to maintenance. Since the ballast is always stiff relative to the subgrade and since the relative contribution of the ballast deformation to the overall elastic track deflection is small, this result may be expected.

The field measurements did show, however, that the uniformity of the support along the track was not improved as a result of the surfacings. Although the property of the ballast under individual ties was made more uniform because of the raising and tamping, as reflected by the plate load tests, the uniformity of contact between the ties and the ballast surface may not be improved.

The GEOTRACK model, with the stress-dependent ballast modulus formulation and constant subgrade moduli determined for each of the sites, was used to predict track deflections and track moduli. The 6- to 30-kip wheel load intervals were used for the comparisons since the field measurements showed some initial slack in the tracks. The model predictions of vertical track deflection agreed well with, although they tended to underestimate, the field measurements.

The original use of track modulus was to enable track designers and engineers to determine the load-carrying capacity of track in a reliable manner. With structural components such as concrete crossties and flexible tie pads of selectable stiffness, the value of the calculated track modulus may not be useful as a performance indicator if the assessment is based only on the

average magnitude of track modulus. The variability of track modulus between tie locations would be a more useful standard of track quality, since the variability would be a direct measure of the uniformity of the track support, which is very important.

The measured dynamic track loadings were used to characterize the mixed loading conditions for each of the field sites. The dynamic wheel load measurements and static wheel loads obtained from consist data showed that the mean static and dynamic loads were approximately equal for a given field site. The distribution of these loads was, however, quite different. The dynamic loads below the 10 percent level of exceedance were not significantly different from the static loads. However, above this level, the dynamic loads were much greater than the static loads for a given percent exceedance due to the impacts resulting from wheel tread irregularities.

At the 0.1 percent exceedance levels, the dynamic wheel loads at Leeds, Lorraine, and FAST were similar, averaging 45.5 kips, with a maximum difference of only 4.5 kips. However, the 0.1 percent exceedance load at Aberdeen was 75 kips. The very high dynamic loads measured at the Aberdeen section were 3 to 5 times greater than the mean dynamic load. These high wheel loads are the result of a combined effect of wheel tread irregularities and the high speeds of passenger trains.

The loading environment at FAST was much more uniform that at the revenue sites, because of the controlled nature of the FAST experiments. While both the mean dynamic and static loads at FAST were on the order of 1.5 to 2 times the average values measured at the revenue sites, the low probability, large loads were 0.5 to 0.8 times the comparable loads at the revenue sites.

A method was developed to convert MGT into an equivalent number of load cycles for the ballast and subgrade. The equivalent number of load cycles per MGT for the ballast ranged from 27,000 to 31,000 at the revenue sites and was about 17,000 at FAST. For the subgrade, the corresponding numbers of cycles per MGT are one-half the numbers in the ballast.

Field measurements of vertical track settlement were made by BCL at each of the revenue sites. These measurements were made using optical survey techniques. The survey data from the Aberdeen site were supplemented by inductance-type strain coils installed in the ballast layer. Measurements of track settlement at FAST were obtained from both optical surveys and embedded instrumentation. Estimates of initial settlement at the Leeds wood and concrete tie sections were necessary to account for the effects of about 0.5 MGT of traffic having passed over the newly surfaced test sections prior to the initial baseline surveys. The ballast strain coils at the Aberdeen site allowed an accurate correction to be applied to the baseline survey at that site.

Permanent ballast strain data acquired using the inductance coils indicated that the total track vertical deformations at Aberdeen could be accounted for by the upper ballast deformation alone, even though only minimal disturbance of the ballast occurred there. This leads to the conclusion that the zone of ballast that was disturbed by the maintenance operation was the primary source of track settlement, and that the subgrade contribution could be neglected.

The settlements at the Lorraine and Aberdeen sites continued to develop at what appeared to be a steady rate throughout the period of the measurements, after the initial traffic following maintenance. Although the total vertical settlements at all of the revenue sites continued to increase as MGT accumulated, the roughness of the track profiles did not increase.

The ballast deformations at FAST were found to be similar for both wood and concrete tie sections. This was true for the ballast measurements obtained during the initial FAST experiments and for the ballast deformations following the 1979 rebuild. The measurements of total track settlement and ballast layer deformations in FAST section 22 tended to support the conclusion that the subgrade contributions to the track settlement could be neglected.

The methodology to predict the inelastic or permanent settlement of the field track sections used GEOTRACK nonlinear stress analyses of the field site track sections with stress-dependent ballast properties, representative subgrade moduli, and multiple-axle combinations of the measured dynamic wheel loads. The predicted stresses from the computer analyses for each particular field site and loading condition were used, along with the permanent deformation behavior of the ballasts from laboratory tests to estimate the resulting ballast strains.

The mixed dynamic field loading conditions were accounted for by a formulation similar to Miner's rule for fatigue analysis. The type of strain superposition was justified based upon the results of the staged-test laboratory experiments. The settlement caused by the ballast was then determined as the product of the ballast strain and the depth of ballast disturbed by maintenance. The disturbed ballast depth was taken to be only 6 to 8 in. below the bottom of the tie for the maintained track sections. The contributions of the subgrade to the total track settlement were neglected.

Although the general magnitudes of the predicted deformations agreed with the measured values, the shapes of the deformation versus MGT predicted results did not agree as well. This was particularly true for the revenue sites. Considering all of the sites, the settlement predictions made for FAST section 22 agreed best with the field measurements. This was probably a result of the more controlled track loading and test conditions present at FAST.

The method used to determine the ballast strains incorporated two alternative types of stress paths, one that matched the peak shear stresses and one that matched both the peak shear stresses and mean stress of a typical roadbed point. There were no distinct trends to indicate that either of the assumed stress paths based on the GEOTRACK calculations led to more consistent agreement between measured and predicted response.

Uncertainties in both the first cycle strains and the representative stress paths could account for some of the differences between measured and predicted settlements. The results from the box test experiments indicated very small or negligible horizontal stress increases from load application, even in the top few inches of the ballast layer. Stress paths derived from these conditions would predict failure stress states in the ballast layer. In contrast, the high K_o values assigned to the ballast and the substantial increases in horizontal stresses in the upper ballast predicted by the GEO-TRACK model resulted in very different stress paths and non-failure conditions. Such uncertainties in the actual ballast stress path make accurate determination of the first cycle strains difficult. The actual representative stress paths for the track ballast layers may be intermediate to the bounds created using the box test and GEOTRACK results.

Deviations between measured and predicted track settlements could have resulted from other factors not considered in the methodology. One of the most important factors not included is thought to be settlement induced by vibrations transmitted through the track superstructure to the ballast, as well as the extremely low probability, large loads encountered in revenue track.

Other factors that can have varying degrees of influence on track settlement and performance include ballast degradation, environmental effects and sub-grade responses. Although these last three factors did not appear significant for the monitoring periods at the field sites investigated during this study, they could well be significant at other sites.

REFERENCES

1. Harrison, H.D., Dean, F.E., Selig, E.T. and Steward, H.E., Correlation of Concrete Tie Track Perfomrance in Revenue Service and at the Facility for Accelerated Service Testing, Federal Railroad Administration, Office of Research and Development, 1984, Report No. DOT/FRA/84/02.1.

2. McMahon, D.R. and Selig, E.T., "Subsurface Investigation Report – Streator, Illinois Wood Tie Section," Department of Civil Engineering, University of Massachusetts, at Amherst, Report No. FRA80-254I, Subcontract from Battelle-Columbus Laboratories for Federal Railroad Administration, November 1980.

3. McMahon, D.R. and Selig, E.T., "Subsurface Investigation Report – Streator, Illinois, Concrete Tie Section," Dept. of Civil Engrg., UMass at Amherst, Report No. FRA80-255I, Subcontract from BCL for FRA, November 1980.

4. McMahon, D.R. and Selig, E.T., "Subsurface Investigation Report – Lorraine, Virginia, Concrete Tie Section," Dept. of Civil Engrg., UMass at Amherst, Report No. FRA80-256I, Subcontract from BCL for FRA, November 1980.

5. McMahon, D.R. and Selig, E.T., "Subsurface Investigation Report – Aberdeen, Maryland, Concrete Tie Section," Dept. of Civil Engrg., UMass at Amherst, Report No. FRA80-257I, Subcontract from BCL for FRA, November 1980.

6. "Documentation of Ballast and Subgrade Aspects of the 1979 Rebuild of FAST Sections 3, 17 and 22," Prepared by Haley and Aldrich, Inc. for U.S. Department of Transportation, Transportation Systems Center, Cambridge, MA., June 1980.

7. Yoo, T.S., Chen, H.M. and Selig, E.T., "Railroad Ballast Density Measurement," Geotechnical Testing Journal, American Society for Testing and Materials, Vol. 1, No. 1, March 1978, pp. 41-54.

8. Selig, E.T., Yoo, T.S. and Panuccio, C.M., Mechanics of Ballast Compaction – Volume 2: Field Methods for Ballast Physical State Measurement, Department of Transportation, Federal Railroad Administration, 1982, Report No. FRA/ORD-81/16.2

9. Panuccio, C.M., Wayne, R.C. and Selig, E.T., "Investigation of a Plate Index Test for Railroad Ballast," Geotechnical Testing Journal, ASTM, Vol. 1, No. 4, December 1978, pp. 213-222.

10. Panuccio, C.M., Dorwart, B.D. and Selig, E.T., "Apparatus and Procedures for Railroad Ballast Plate Index Test," Geotechnical Testing Journal, ASTM, Vol. 1, No. 4, December 1978, pp. 223-227.

11. Kalcheff, I.V. and Hicks, R.G., "A Test Procedure for Determining the Resilient Properties of Granular Materials," Journal of Testing and Evaluation, ASTM, Vol. 1, No. 6, November 1973, pp. 472-479.

12. Brown, S.F., "Repeated Load Testing of a Granular Material," Journal of the Geotechnical Engineering Division, American Society of Civil Engineers, Vol. 100, No. GT7, July 1974, pp. 825-841.

13. Morgan, J.R., "The Response of Granular Materials to Repeated Loading," Proceedings, Third Conference of the Australian Road Research Board, Sydney, Australia, 1966, pp. 1178-1192.

14. Hicks, R.G., "Factors Influencing the Resilient Properties of Granular Materials," Ph.D. Dissertation, University of California at Berkeley, Institute of Transportation and Traffic Engineering, May 1970.

15. Pell, P.S. and Brown, S.F., "The Characteristics of Materials for the Design of Flexible Pavement Structures," Proceedings, Third International Conference on Structural Design of Asphalt Pavements, London, England, 1972, pp. 326-342.

16. Seed, H.B., Mitry, F.G., Monismith, C.L. and Chan, C.K., "Factors Influencing the Resilient Deformations of Untreated Aggregate Base in Two-Layer Pavements Subjected to Repeated Loadings," Highway Research Board, Record No. 190, 1967, pp. 19-57.

17. Thompson, M.R., FAST Ballast and Subgrade Materials Evaluation, Ballast and Foundation Materials Research Program, University of Illinois at Urbana-Champaign, U.S. DOT, FRA, 1977, Report No. FRA/ORD-77/32.

18. May, R.W. and Witczak, M.W., "Effective Granular Modulus to Model Pavement Responses," Transportation Research Board, Record No. 810, Washington, D.C., 1981, pp. 1-9.

19. Rada, G. and Witczak, M.W., "Comprehensive Evaluation of Laboratory Resilient Moduli Results for Granular Material," TRB, Record No. 810, Washington, D.C., 1981, pp. 23-33.

20. Robnett, Q.L., Thompson, M.R., Knutson, R.M. and Tayabji, S.D., "Development of a Structural Model and Materials Evaluation Procedures," Ballast and Foundation Materials Research Program, University of Illinois at Urbana-Champaign, Report No. FRA-OR&D-76-255, July 1976.

21. Knutson, R.M., "Factors Influencing the Repeated Load Behavior of Railway Ballast," Ph.D. Dissertation, U. of Illinois at Urbana-Champaign, Dept. of Civil Engrg., 1976.

22. Alva-Hurtado, J.E., "A Methodology to Predict the Elastic and Inelastic Behavior of Railroad Ballast," Ph.D. Dissertation, UMass at Amherst, Dept. of Civil Engrg., Report No. OUR80-245D, May, 1980.

23. Raad, L. and Figueroa, J.L., "Load Response of Transportation Support Systems," Journal of the Transportation Engineering Division, ASCE, Vol. 106, No. TE1, January, 1980, pp. 111-128.

24. Allen, J.J., "The Effects of Non-Constant Lateral Pressures on the Resilient Response of Granular Materials," Ph.D. Dissertation, U. of Ill. at Urbana-Champaign, Dept. of Civil Engrg., May 1973.

25. Alva-Hurtado, J.E., McMahon, D.R. and Stewart, H.E., "Apparatus and Techniques for Static Triaxial Testing of Ballast," Laboratory Shear Strength of Soils, ASTM STP 740, R.N. Yong and F.C. Townsend, Editors, ASTM, Philadelphia, Penna., 1981, pp. 94-113.

26. Siller, T.J., "Properties of Railroad Ballast and Subballast for Track Performance Prediction," M.S. Project Report, Report No. FRA80-261P, UMass at Amherst, Dept. of Civil Engrg., December 1980.

27. Shenton, M.J., "Deformation of Railway Ballast Under Repeated Loading Triaxial Tests," Report RP5, Soil Mechanics Section, British Railways Research Department, Derby, England, 1974.

28. "Stresses in the Rails, the Ballast and the Formation Resulting from Traffic Loads," Question D71, Report No. 10, Vols. 1 and 2, International Union of Railways, Office of Research and Experiments, Utrecht, The Netherlands, 1970.

29. Raymond, G.P. and Williams, D.R., "Repeated Load Triaxial Tests on a Dolomite Ballast," Journal of the Geotechnical Engineering Division, ASCE, Vol. 104, No. GT7, Proc. Paper 13905, July 1978, pp. 1013-1029.

30. Brown, S.F. and Hyde, A.F.L., "Significance of Cyclic Confining Stress in Repeated-Load Triaxial Testing of a Granular Material," Transportation Research Board Record No. 537, Washington, D.C., 1975, pp. 49-57.

31. Norman, G.M., "Laboratory Tests for Evaluating Ballast Field Performance," M.S. Project Report, Report No. FRA82-291P, UMass at Amherst, Dept. of Civil Engrg., March 1982.

32. Holubec, I., "Cyclic Creep of Granular Materials," Ontario Joint Highway Research Programme, D.H.O. Report No. RR147, Ontario, Canada, June 1969.

33. Campanella, R.G. and Vaid, Y.P., "A Simple K_o-Triaxial Cell," Canadian Geotechnical Journal, Vol. 9, No. 3, 1972, pp. 249-260.

34. Bukoski, R.F., "Railroad Subgrade Soil Characterization for Track Performance," M.S. Project Report, Report No. FRA81-263P, UMass at Amherst, Dept. of Civil Engrg., February 1981.

35. Bukoski, R.F. and Selig, E.T., "Investigation of Railroad Subgrade Properties," Proceedings, Cone Penetration-Testing and Experience, ASCE, St. Louis, Missouri, October 1981.

36. Ladd, R.S., "Preparing Test Specimens Using Undercompaction," Geotechnical Testing Journal, ASTM, Vol. 1, No. 1, March, 1978, pp. 16-23.

37. Stewart, H.E., "Index and Property Testing of FAST Subgrade," Internal Report No. OUR80-240I, UMass at Amherst, Dept. of Civil Engrg., March 1980.

38. ASCE-AREA Special Committee on Stresses in Railroad Track, <u>Bulletin</u> of AREA, First Progress Report, Vol. 19, 1918, Second Progress Report, Vol. 21, 1920.

39. Zarembski, A.M. and Choros, J., "On the Measurement and Calculation of Vertical Track Modulus," AREA <u>Bulletin</u> 675, November-December 1979, pp. 156-173.

40. Chang, C.S., Adegoke, C.W. and Selig, E.T., "The GEOTRACK Model for Railroad Track Performance," <u>Journal of the Geotechnical Engineering Division</u>, ASCE, Vol. 106, No. GT11, Proceedings Paper 15819, November, 1980, pp. 1201-1218.

41. Stewart, H.E. and Selig, E.T., "Predicted and Measured Resilient Response of Track," Accepted for Publication in <u>Journal of the Geotechnical Engineering Division</u>, ASCE, April 1982.

42. Stewart, H.E., "The Prediction of Track Performance Under Dynamic Traffic Loading," Ph.D. Dissertation, UMass at Amherst, Dept. of Civil Engrg., Report No. FRA82-292D, May 1982.

43. Dean, F.E., et al. <u>Measurement and Correlation Analysis Plan for Concrete Tie and Fastener Performance Analysis</u>. U.S. Department of Transportation, Federal Railroad Administration, 1979, Report No. FRA/ORD-79/51 (NTIS: PB 80 183882)

44. Dean, F.E., Harrison, H.D., Prause, R.N., Selig, E.T. and McMahon, D.R., "Measurement and Correlation Analysis Plan for Concrete Tie and Fastener Performance Evaluation," Report No. FRA/ORD-79/51, U.S. DOT, Federal Railroad Administration, Washington, D.C., November 1979.

45. Benjamin, J.R. and Cornell, C.A., <u>Probability, Statistics and Decision for Civil Engineers</u>, McGraw-Hill Book Company, New York, 1970.

46. Selig, E.T., Yoo, T.S., Adegoke, C.W. and Stewart, H.E., "Status Report - Ballast Experiments, Intermediate (175 MGT) Substructure Stress and Strain Data," Interim Report No. FRA/TTC/Dr-10 (IR), Prepared for FAST Program, Transportation Systems Center, Cambridge, Mass., Submitted September 1979.

47. Brown, S.F. and Bell, C.A., "The Validity of Design Procedures for the Permanent Deformation of Asphalt Pavement," <u>Proceedings</u>, 4th International Conference on the Structural Design of Asphalt Pavements, Vol. 1, Ann Arbor, Michigan, 1977, pp. 467-482.

48. Barksdale, R.D., "Laboratory Evaluation of Rutting in Base Course Materials," <u>Proceedings</u>, 3rd International Conference on the Structural Design of Asphalt Pavements, Vol. 1, Ann Arbor, Michigan, 1972, pp. 161-174.

49. Monismith, C.L., "Rutting Prediction in Asphalt Concrete Pavements," Transportation Research Board <u>Record</u> No. 616, Washington, D.C., 1976, pp. 2-8.

50. Pell, P.S., "Characterization of Fatigue Behavior," Highway Research Board, Special Report 140, Washington, D.C., 1973, pp. 49-65.

51. Van deLoo, P.J., "A Practical Approach to the Prediction of Rutting in Asphalt Pavements, the Shell Method," Koninklijke/Shell-Laboratorium, Amsterdam, The Netherlands (Shell Research B.V.), 1976.

52. Selig, E.T., "Soil Strain Measurement Using Inductance Coil Method," Performance Monitoring for Geotechnical Construction, ASTM STP 584, Philadelphia, Penna., 1975, pp. 141-158.

53. Selig, E.T., "FAST Substructure Static Strain and Deflection Measurements from 175 to 422 MGT," UMass at Amherst, Dept. of Civil Engrg., Report No. TSC81-269I, Prepared for U.S. DOT, Transportation Systems Ctr., Cambridge, Mass., April 1981.

54. "Documentation Report for Ballast and Subgrade Instrumentation, 1979 Rebuild, FAST Section 22," Report Prepared by Haley and Aldrich, Inc. for U.S. DOT/TSC, Cambridge, Mass., March 1980.

55. Yang, C.W. and Gong, Y.L., "Vibrations and Dynamic Stresses in Railway Formation under Traffic Loads," Research Institute of Railway Construction, Peoples Republic of China, 1962.

56. Morgan, J.G.D., "The Influence of Vibration on the Load Bearing Stability of Railway Ballast," Ph.D. Dissertation, University of Wales, Dept. of Mechanical Engrg., Cardiff, March 1975.